REALIZATION OF ACTIVE FILTERS USING OPERATIONAL TRANSCONDUCTANCE AMPLIFIER (OTA)

Prasant K. Mahapatra, Manjeet Singh and Neelesh Kumar
Central Scientific Instruments Organization, Sector-30C, Chandigarh, India

ABSTRACT

The performance of filters designed by the use of passive components degrades at audio frequencies and the required resistances and inductances values calculated from the mathematical expression are very difficult to meet from the market. To find a solution to this problem we have performed a study to realize Passive Filters into Active Filters using Operational Transconductance Amplifier (OTA). By controlling the Voltage Gain of OTA, one can change its transconductance, which is very useful in the designing the first order and second order active filters. In this article we have confined our discussions only to the design of first order low pass filters using OTA. It is concluded that the new approach gives us a wide range of tunable cutoff frequencies. Basic properties of OTA are discussed.

1. INTRODUCTION

This paper describes the usefulness of OTA [3, 5] over the conventional Op-Amp in the design of both first order & second order active filters as an active element. OTA is a differential voltage controlled current source (VCCS) where the output current is controlled by an applied input voltage signal. To achieve any required cutoff frequency in passive filter, we require different values of resistors & inductors as calculated from mathematical expression; which mayor may not be available in the market. To solve this problem, we can use OT As. We achieve the required resistance and inductance values by varying its *gm*. What follows describes the use of OTAs as basic building blocks [I, 2] in the design of low pass active filters.

Electric filter [1, 3] can be defined as a frequency selective electrical circuit that passes electrical signals of specified band of frequencies and attenuates> the signals of frequencies outside, the band. Passive components are generally the basic building blocks of filters, which work normally on high frequencies; but at audio frequencies inductor causes problem. Inductor size increases ,at audio frequency and become bulky & expensive. At low frequencies inductor requires more number of turns which adds series resistances and degrades inductor's performance because of its low quality factor (Q), which results in high power dissipation. Using OTA the above mentioned problems are solved.

For Low pass filter [1] the general first order transfer function can be written as:

$$T(s) = \frac{H_o \omega_o}{s + \omega_o}$$

Where H_o = DC gain, ω_o = resonant frequency or cutoff frequency.

The current section has described the fundamental problems in general filter design, the second section gives the general description of OT A, third section describes the basic building blocks of +R, -R, Grounded Inductor, Floating Resistor, Floating Inductor, and in the fourth section we have confined discussions for the derivations of OT A -C (active) filters from first order passive filters. Last section gives the concluding remarks.

2. OTA FUNDAMENTALS

The OTA is a transconductance device in which the input voltage controls the output current. The transconductance *gm* makes the OTA as voltage controlled current source; where as the op-amps are voltage controlled voltage source. An ideal OTA [12] is defined by $I_O = g_m (V^+ - V)$. Where input & output impedances are infinite. The transconductace g_m is directly proportional to control bias current I_b.

Characteristics of Ideal OTA [15] can be summarized as follows

Input impedance $(Z_{in}) = \infty$

Output Impedance $(Z_0) = \infty$

Inverting input current I_0^- = Non-inverting input current I_0^+

Bandwidth $= \infty$

The Figures I & 2 shows the basic schematic and equivalent circuit of OTA.
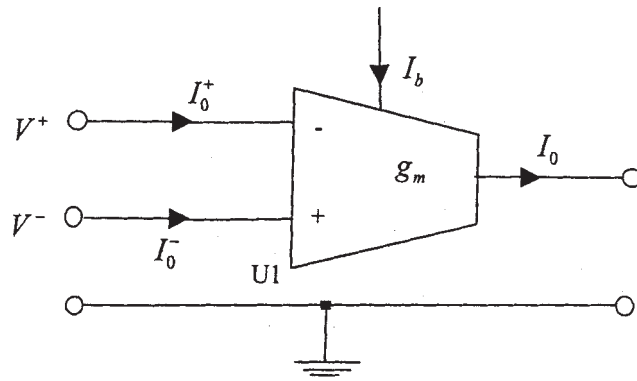

Fig.1. Circuit symbol of OTA [1]
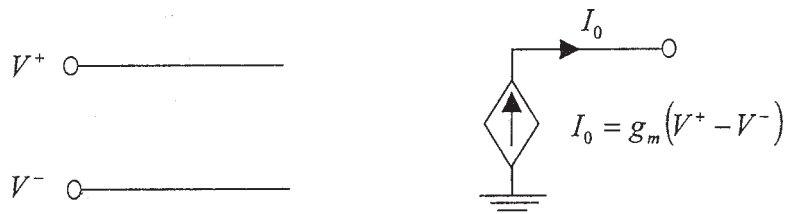
Fig.2. Small signal equivalent circuit of OTA [1]

3. BASIC BUILDING BLOCKS USING OTA

Grounded Resistor (+R)

Consider fig.3. which simulates grounded resistor (+ R) using OTA. Applying KCL at Node A gives us $I_{in} + I_0 = 0$ $\qquad$ (1)

where $I_0 = -Vm \times gm$ $\qquad$ (2)

Substituting the value of I_0 from equation (2) in equitation (1) we have,

$$Z_m = \frac{I}{g_m} \qquad (3)$$
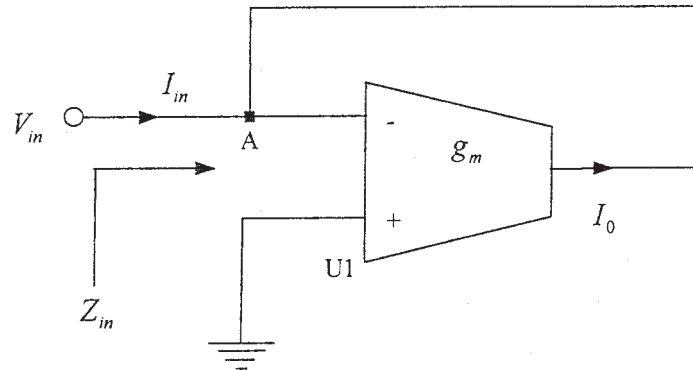
Fig.3. Circuit for simulating a grounded resistor (+ R) [12]

Grounded Resistor (-R)

Consider fig.4 below, which visualizes the simulation of grounded resistor (– R). Applying KCL at node A, we have $I_0 = g_m V_m$ $\qquad$ (4)

Substituting equation (4) in equation (1) we have $Z_{in} = - \dfrac{1}{g_m}$ $\qquad$ (5)
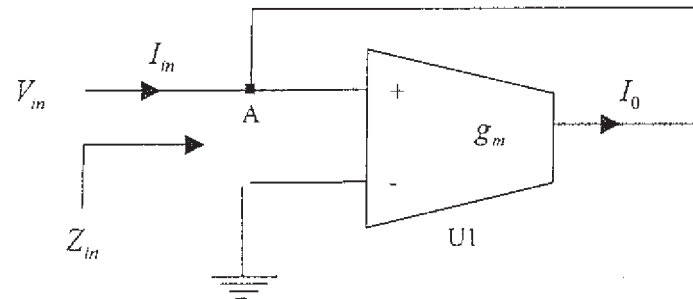

Fig.4. Circuit for simulating a grounded resistor (-R) [12]

Floating Resistor

After analyzing figures 5 & 6 we have

$$I_{01} = g_{m1} \ (V_2 - V_1) \tag{6}$$

$$I_{02} = g_{m2} \ (V_1 - V_2) \tag{7}$$

But $I_{01} = -I_1$ and $I_{02} = -I_2$

Thus from equation (6) and (7) if $g_{m1} = g_{m2} = g_m$ we have $I_1 = -I_2$

Grounded Inductor

Fig. 7 shows the resulting circuit for grounded inductor if we choose $Z_L = \dfrac{1}{(SC)}$

Here it can be concluded that $I_{01} = g_{m1}V_1 \tag{8}$
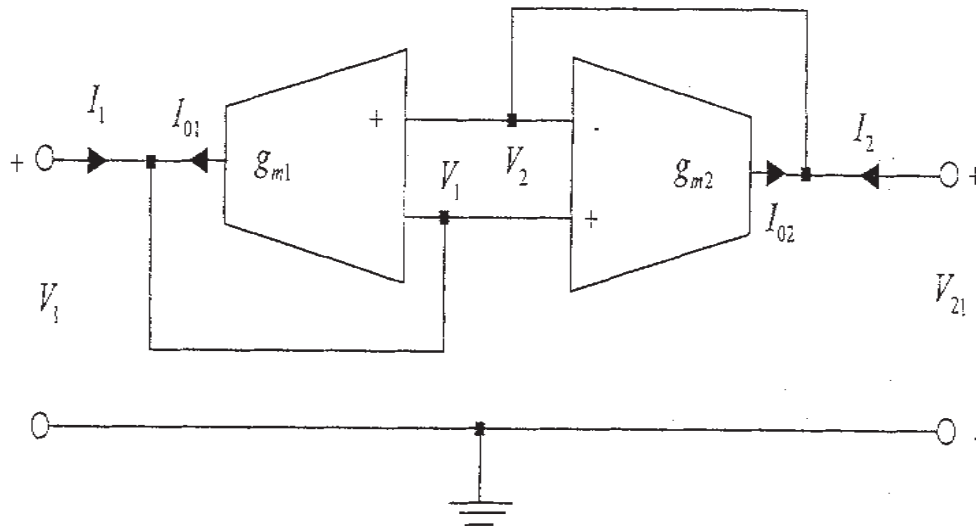

Fig.5. Floating resistor $R = 1/g_m$ for $g_{m1} = gm_2 = g_m$ [15]
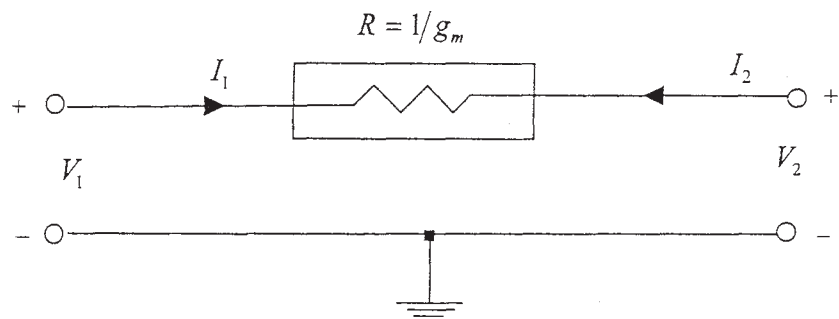

Fig.6. Equivalent circuit of floating resistor [12]

and $I_{01} = I_2^- + I_c$. This expression reduces to $I_{01} = I_c$ (9)

as $(I_2^- = 0)$. By substituting value of I_{01} in (8) we have $I_c = g_{m1}V_1$

But we know that $V_c = I_c \times \dfrac{1}{(SC)}$ (10)

So we can say that $Z_{in} = \dfrac{SC}{g_{m1}g_{m2}}$ (11)

The standard form of representing inductive reactance is $Z_{in} = SL_{eq}$; Hence we have

$$L_{eq} = \dfrac{C}{g_{m1}g_{m2}}$$ (12)

This inductor is electronically tunable by varying g_{m1} where $i = 1, 2$ & Matched.
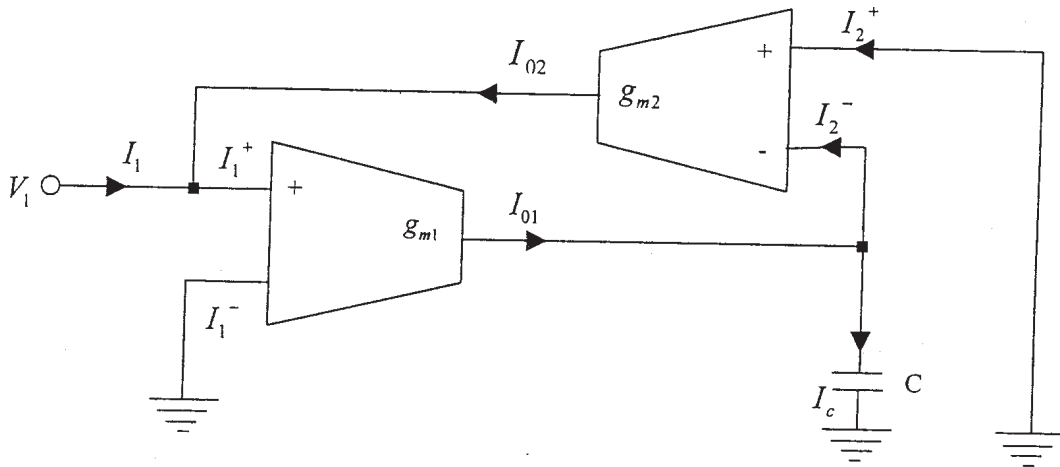
Fig.7. Simulation of grounded inductor [12]

Floating Inductor

From fig. 8 we have $I_1 = \dfrac{g_{m1}g_{m2}}{SC}(V_1 - V_2)$ and $I_2 = \dfrac{g_{m1}g_{m3}}{SC}(V_1 - V_2)$ for $g_{m2} = g_{m3} = g_m$

Floating inductor of value : $L = C / g_{m1}g_m$ has been simulated.

Floating inductors which are difficult to simulate with op-amps are very easy to be simulated by the use of OTA. The only task is to lift the inverting gm1 terminal of fig. 7 off the ground and devise a circuit that generates $I_2 = I_1$ at the second impedance terminal. Fig. 8 shows a simple method, which needs only one additional OTA.
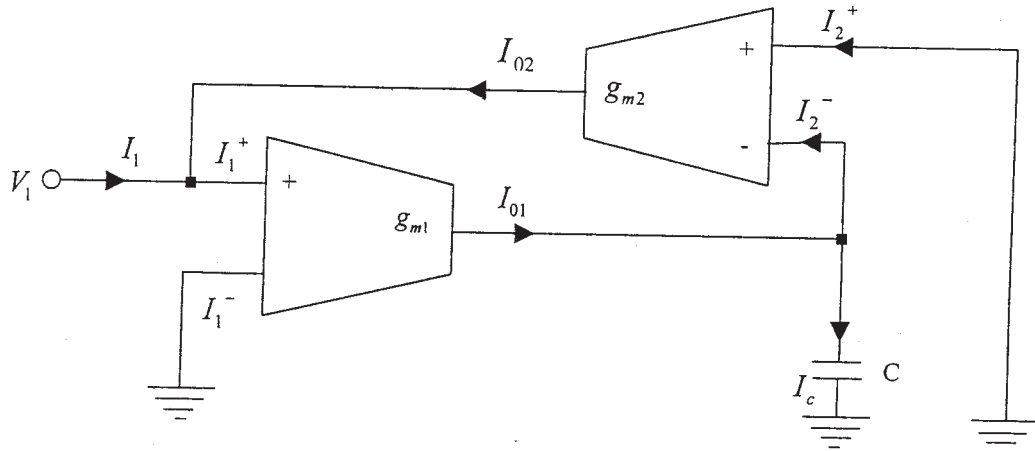
Fig.8. Simulation of floating inductor [12]

4. DERIVATION OF OTA-C FILTERS FROM PASSIVE FILTERS

We have considered two cases to visualize our design methodology.

First order low pass filter

1. Passive Filter

Consider a first order low pass filter as shown in fig. 9 below.
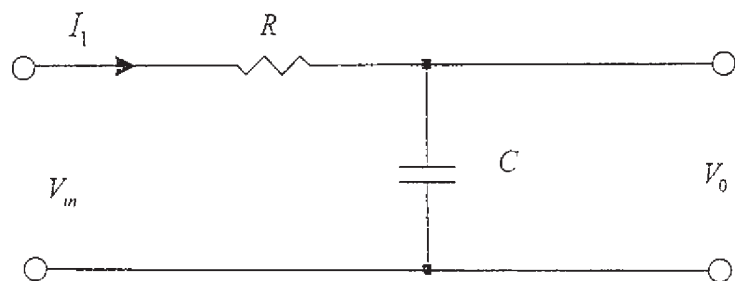
Fig.9. First order low pass filter (passive filter) [1]

Here $V_{in} = I_1 \left[R + \dfrac{1}{SC} \right]$

And $V_0 = \dfrac{I_1}{SC}$ (14)

After substituting the value of I_1 from equation (14) into equation (1), we have

$$\frac{V_0}{V_m} \quad T(s) = \frac{1/CR}{S + 1/CR} \tag{15}$$

Realization using OTAs

From fig. 10 we get $I_1 = g_m (V_{in} - V_0)$ (16)

From equation (16) and equation (14), the transfer function for considered filter is

$$T_{(s)} = \frac{g_m/C}{S + g_m/C} \tag{17}$$
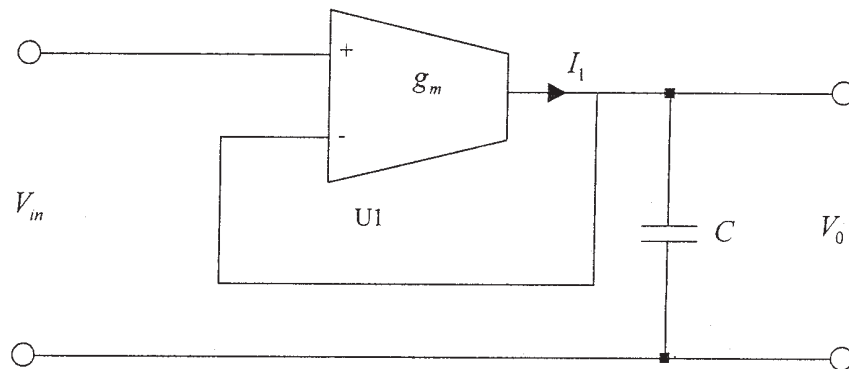
Fig.10. First order low pass filter (active filter)

Passive filter

Now consider a low pass filter of fig. 11. Here $V_{in} = I(SL + R)$ (18)

and $V_O = IR$ (19)

Solution of equation (18) and equation (19) gives us transfer function

$$T(s) = \frac{R/L}{S + R/L} \tag{20}$$
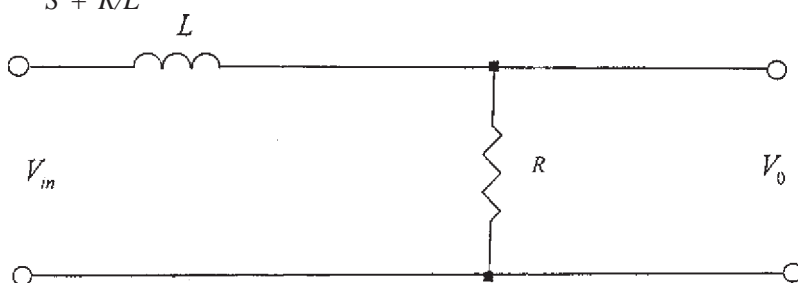
Fig.11. First order passive low pass filter (second method) [1]

Realization using OTAs

From fig. 12 it can be inferred that

$$V_3 = I_2/SC \tag{21}$$

$$I_2 = (V_{in} - V_0)\, g_{m2} \tag{22}$$

Solving equation (21) and (22) we have $\quad V_3 = \dfrac{(V_{in} - V_o)\, g_{m2}}{SC}$ (23)

$$I_4 = -g_m V_o \tag{24}$$

$$I_3 = -V_3 g_{m1} \tag{25}$$

But we see that $\quad I_3 + I_4 = 0$ (26)

Solution of equations (24), (25) and (26) gives the transfer function of the designed filter a

$$\frac{V_0}{V_{in}} = T(s) = \frac{g_{m1}g_{m2}\,/\,Cg_m}{S + (g_{m1}g_{m2}/Cg_m)} \tag{27}$$
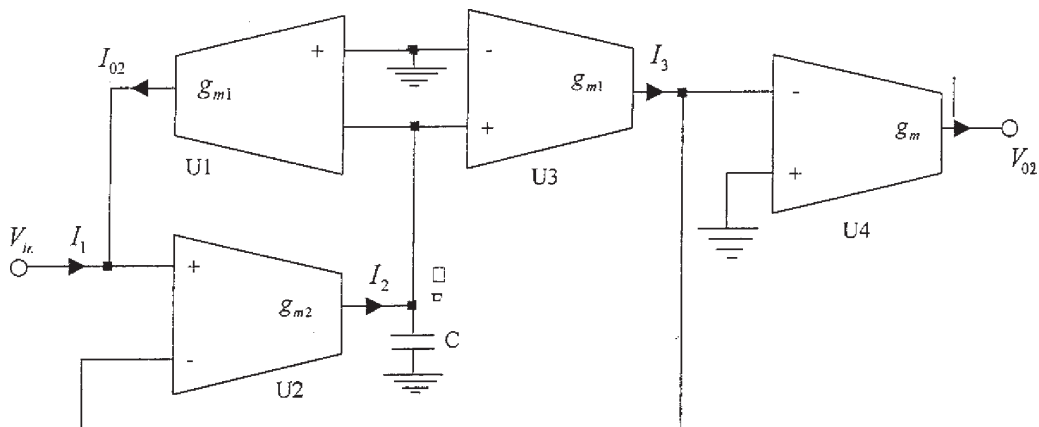
Fig.12. First order active low pass filter (second method)

5. CONCLUSIONS

The above discussion concludes that we can achieve a tunable range of cut off frequency. And for low pass filter we can change cut-off frequency by changing only one parameter g_m. The advantage of using first method can be summarized as follows:

1. Number of OTA used is only one.

2. We can change cut-off frequency by changing *gm* but the degree of freedom for changing g_m is only one.

In case of second method, cut-off frequency can be changed by tuning g_{m1}, g_{m2} or g_m separately or in combination. So we have a larger tunable than the first one. A number of different OTAs are available in market from various manufacturers. With the use the CA 3080 OT A it is possible to achieve extremely linear transconductance characteristic with respect to amplifier bias current. Readers who are interested in making active low pass filter, can try out this design idea and discussions are cordially invited.

REFERENCES :

1. Adel S. Sedra & Kenneth C. Smith, "Microelectronic Circuits", 4th Edition, New Oxford, Oxford University Press, 1998.

2. Vasudev K. Aatre, "Network Theory & Filter Design", 2nd Edition, New Age International (P) Ltd., 1980.

3. Schaumann et. Al., "Design of Analog Filters Passive, Active RC and Switched Capacitor", Prentice Hall, Englewood Cliff, New Jersy, 1990.

4. Louis Weinberg, "Network Analysis & Synthesis", McGraw Hill Book Company Inc., 1962.

5. S. Franco, "Use of Transconductance Amplifier to make programmable active filters", Electronic Design, Vol. 24 pp 98-101, Sep. 1976.

6. A.M Soliman, "A Grounded Inductance Simulation Using the DVCCS/DVCVS", Proc. IEEE, Vol. 66 pp 1089-1091, Sep 1978.

7. H.S. Malvar, "Electronically Controlled Active Filters with Operational Transconductance Amplifier", IEEE Tarns. Circuits Syst., Vol. CAS 29, pp 333-336, May 1982.

8. K. Fukahori, "A Bipolar Voltage Controlled Tunable Filter", IEEE J. Solid State Circuits, SC 16, pp 729-737, Dec. 1981.

9. V.W. Burgger, B.J. Hosticka and G.S. Moschytz, "A Comparison of Semiconductor Controlled Sources for The Design of Active RC Impedances", Int. J of Circuit Theory and Appl., Vol. 10, pp 27-42, 1982.

10. National Semiconductor, Application Note, LM 13600 Dual Operational Transconductance Amplifiers with Linearizing Diodes and Buffers", Feb. 1995.

11. W.R. Grise, "Application of the Operational Transconductance Amplifier to Voltage Controlled Amplifiers and Active Filters", TECHNOLOGY INTREFACE: The Electronic Journal for Engg. Technology, Vol. 2, #2, Winter, s98. URL : http://et.nmsu.edu/~etti.

12. M. Bialco & R.W. Newcomb, "Generation of All finite Linear circuits using the Integrated DVCCS" IEEE Trans on circuit theory, vol. CT-18, pp 733-736, Nov. 1971.

13. Linear Integrated ICs by Roy Chowdary

14. Sclof, Sidney, Design and application of Analog Integrated Circuits, Chapter 9.3, Prentice Hall, Inc. Englewood Cliffs N.J. 1991.

15. Geiger, R.L and Sanchez, Edgar, "Active Filter Design using Operational transconductance Amplifier: a tutorial, IEEE Circuits and Devices Magazine, Vol. 1, Number 2, pp, 20-32, March, 1985.

16. C.F. Wheatley and H.A. Wittinger, OTA Obsoletes OPAMP, P Nat. Econ. Conf. pp. 152-157, Dec. 1969.

GRAPHICAL PROGRAMMING APPLICATIONS TO DATA ACQUISITION AND ANALYSIS OF LONGWALL POWERED SUPPORTS BEHAVIOR IN REAL TIME

Srinivasulu Tadisetty[1], Kikuo Matsui[2] and R.N. Gupta[1]
[1]National Institute of Rock Mechanics, Kolar Gold Fields, India
[2]Faculty of Engineering, Kyushu University, Japan

ABSTRACT

Indian mining operations are day-to-day becoming more and more difficult as mining has extended to deeper horizons resulting in more adverse geo-mining conditions. This situation obviously demands more and more sophisticated and advanced instrumental checking for monitoring of the strata and supports behavior. Therefore, the authors were successfully developed a real time system indigenously for improving efficiency of longwall operations. However, this paper will discuss the innovations in user friendly menus of RT system.

LabVIEW is a graphical programming language that uses icons instead of line of text to create applications. The software was successfully developed on LabVIEW environment for data acquisition and analysis. The software programs were incorporated in Real Time System for acquiring data from underground sensors. The PXI real time system was successfully commissioned in one of the Indian coal mines for continuous monitoring and analysis of longwall powered supports behavior in real time. First time the RT system was successfully developed and applied to Indian mining applications. This paper will discuss various software menus developed under LabVIEW programming environment to facilitate user friendly operations for effective data acquisition and analysis

1. INTRODUCTION

The tremendous potential of longwall mining can be realized only if adequate ground control is maintained (Barczak & Oyler, 1991). Longwall mining technology very much proven world wide could not be very well established in India. Longwall powered supports leg pressure changes as a function of time and distance with longwall face advancement. A loading peak (intensity) is related to the occurrence of severe roof movement when a crack is propagating in the main roof. A strong and thick overhang corresponds to a large overhang and high loading peak by the time the overhang reaches its maximum length. Most of the longwall mines contain multiple layers in the main roof, resulting in a complex loading history due to the combined effect of individual layer. The variation of loading history over a considerable period of time

and inhibits the analysis for trends and correlations with loading events. It is rather difficult to interpret the monitored data using traditional conventional data analysis techniques, but recent technological development in the area of instrumentation provides a great opportunity to solve complex problems. Microcomputers have made it practical to install a high-speed acquisition to collect data from longwall face in near real time (Jiang et al., 1996). This paper will highlight the innovative LabVIEW menus, which were incorporated in the RT system for better user interface.

2. GRAPHICAL PROGRAMMING ENVIRONMENT

LabVIEW (Laboratory Virtual Instrument Engineering Workbench) is a graphical programming environment that uses icons instead of lines of text to create applications. In contrast to text based programming languages, where instructions determine program execution. LabVIEW is a program development environment, much like modern C or Basic development environment. It is a general purpose programming system with extensive libraries of functions for any programming task. LabVIEW gives the flexibility and performance of a powerful programming language without the associated difficulty and complexity. It can reduce system development and increase productivity. LabVIEW programs are called virtual instruments or VIs (virtual instruments) because their appearance and operation imitate physical instruments. VIs are hierarchical and modular. It can be used to top-level programming or subprograms within other programs. The VI comprises the following three components:

Front panel: The front panel is the user interface of the VI and has controls and indicators, which are interactive input and output terminals of the VI respectively. Controls are knobs, pushbuttons, dials and other input devices and supply data to the block diagram of the VI. Indicators will simulate instrument output devices and display data.

Block diagram: After building the front panel, add code using graphical representations of functions to control the front panel objects. The block diagram is contains this graphical source code. Front panel objects appear as terminals on the block diagram. Additionally the block diagram comprises of functions and structures from built in LabVIEW VI libraries. Wires are connected each of the nodes on the block diagram, including control and indicator terminals, functions, and structures.

Palettes: LabVIEW palette gives the options need to create and edit the front panel and block diagram. Palettes are of two types. They are tools and controls palette.

Tools palette: The tools palette is available on the front panel and the block diagram. A tool is a special operating mode of the mouse cursor. When tool is selected, the cursor icon changes to the tool icon. The tools are used to operate and modify front panel and block diagram objects.

Controls palette: The controls palette is available only on the front panel. The controls palette contains the controls and indicators to create the front panel.

Functions palette: The functions palette is available only on the block diagram. The functions palette contains the VIs and functions to build the block diagram. All the palettes can be placed anywhere on the screen.

3. LABVIEW MENUS

Only three software menus are required for implementing real time operations. These menus also called real time menus. Three menus were developed on LabVIEW programming environment. They are main menu, configuration menu and processing menu as shown in Figures1 to 3. All these menus were successfully incorporated in RT system. These menus were facilitated the user friendly operations and improved user interface for better operations.
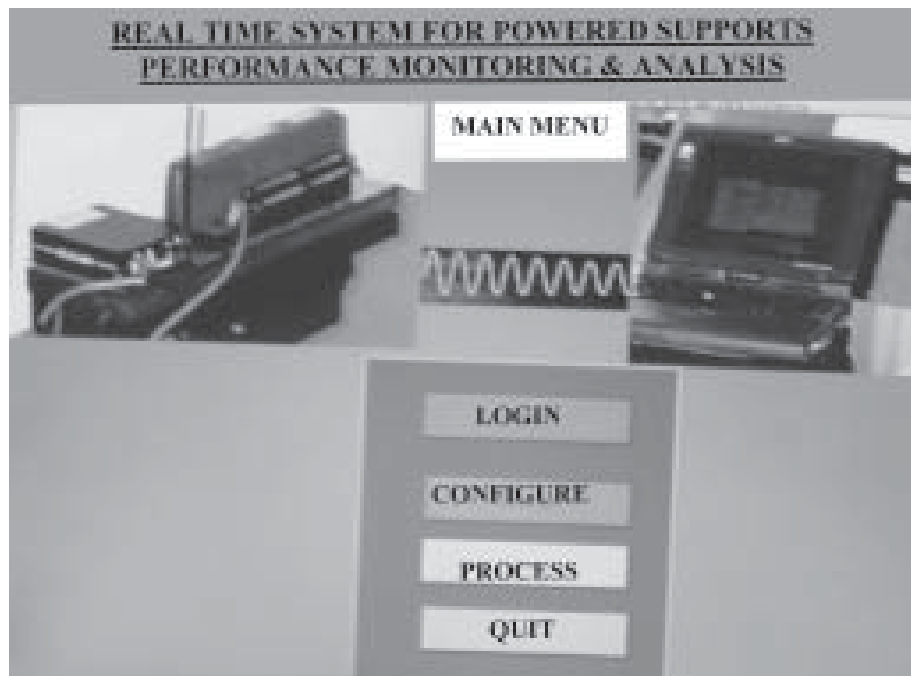
Fig.1. Main Menu

Figure 1 shows the main menu of the Real Time (RT) system developed on virtual environment (graphical programming). The main menu has four pull up menus (sub menus). They are LOGIN, CONFIGURE, PROCESS and QUIT as shown in Figure 1. The main menu was needed a valid password id (identification) to LOGIN for entering into other menus. Therefore the software operations of RT system were protected from unauthorized operations.

Figure 2 shows configuration menu of the RT system. The configuration menu also needs a valid password id for working on this menu. The configuration menu was played a major role in data acquisition and analysis. The configuration menu was facilitated to configure various underground sensors from remote surface RT system. The configuration of various sensors was includes location of sensors in underground along with chock number, type, units, date of installation, date of replaced, initial readings, data acquisition rate, warning limits, name of the data file, and number of sensors as shown in Fig.2. Each Field Point (FP-I) module of data acquisition system was interfaced to 8 sensors (Figure 2 and 3). Therefore this configuration menu can support to configure 40 sensors. The capacity of the configuration menu can be extendable. The data processing menu (Figure 3) was followed the configuration

menu to produce results. Consequently, the configuration menu was a very important menu in successful real time operations.
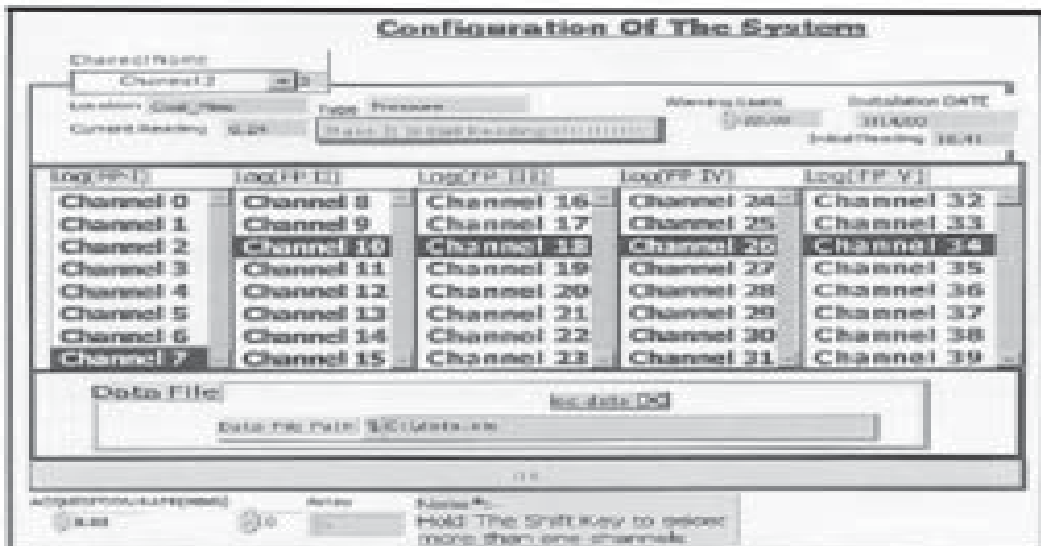
Fig.2. Configuration Menu
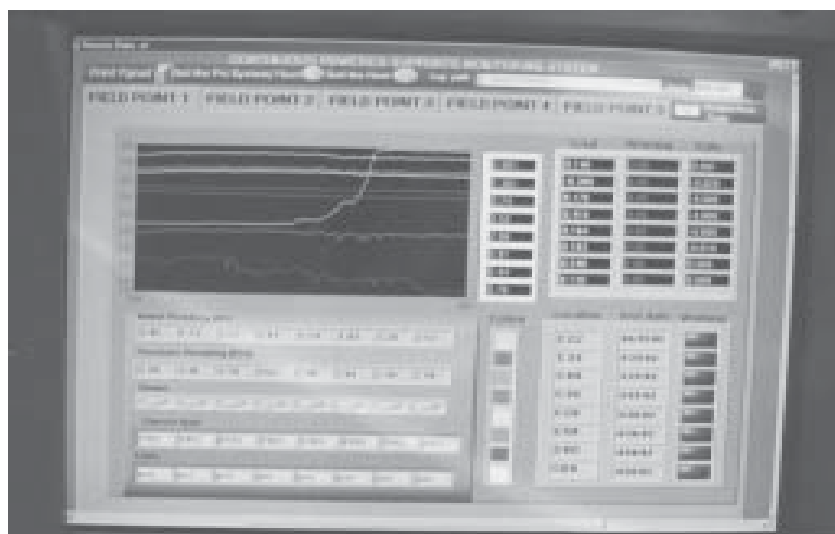
Fig.3. Data Processing Menu

Figure 3 shows the data processing menu of the RT system. The data processing menu was output display of RT system as shown in Figure 3 and 6. The data processing menu is also called real time display. The RT system was executed the various software routines as per the instructions of configuration menu for acquiring data from underground sensors and

displayed on data processing menu after analysis. The various features of the data processing menu are shown in Figure 6. The data processing menu cannot accept user instructions directly. However, it follows the instructions of the configuration menu. Thus the configuration menu is controlling the data processing menu.

4. FLOW OF RT OPERATIONS
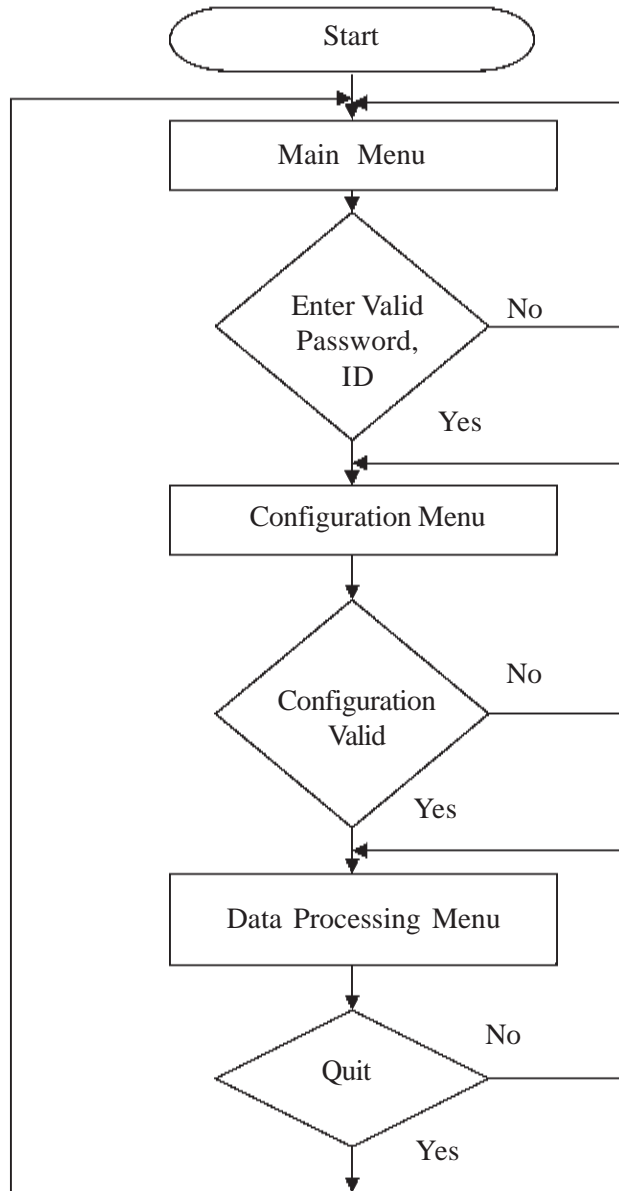
Fig. 4 : Flow of major real time operations

The major software flow of real time operations is shown in Figure 4. The operator (user) is required a valid password and ID for operating. Moreover, he should be familiar with systematic programming of configuration menu. Otherwise, he will not be allowed to modify or program the system operations. Therefore, the RT system operations were fully protected from unauthorized operations. Thus, the system operations are reliable and accurate.

5. APPLICATION OF REAL TIME SYSTEM

5.1 Experimental mine

The problematic longwall mine was selected at Ramagundem area II. The longwall panel No.4 was prepared in one seam bottom section leaving the 3m clay/shale coal in the roof at GDK (Godavarikhani) 10A, SCCL (Singareni Collieries Company Limited) Ramagundem. Depth of the panel varies from 247 to 297m. The compressive strength of the stone roof is 13.6 MPa. The overlying strata was highly water bearing. Longwall retreat was 4 to 5 m per day. An average daily production was 2000 t. The panel and face length were of 940 and 116 m respectively. The panel working height was 3.0 m. This panel was equipped with 80 chock shields of capacity 4X800 t. The seam thickness was 6.40 m with a 0.30 m clay band and an average gradient of 1 in 6 towards N73^0 E. The strata overlying in the coal seam was composed of coarse to medium grained ferruginous sandstone, coarse grained kaolinised felspathic massive sandstone with clay and gray shale's.

5.2 Instrumentation Layout

Figure 5 shows instrumentation layout of over and under ground. All the systems and modules were controlled by RT system. The wireless data acquisition system was mainly comprises of wireless transmitting antenna and radio modem. The pressure and leg closure
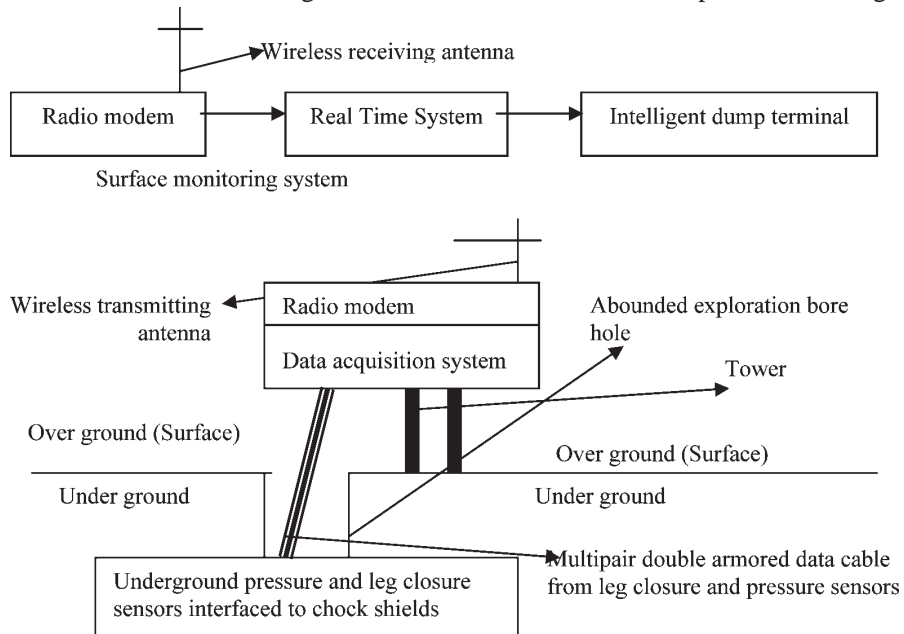
Fig. 5 : Instrumentation layout of over and underground

sensors interfaced to the surface data acquisition system (Figure 5). The output of data acquisition system was interfaced to radio modem. The output of radio modem interfaced to the wireless transmitter as shown in Figure5. The surface monitoring system (Figure 6) was mainly comprises of radio modem with wireless receiver, RT system and intelligent dump terminal. The wireless receiver was received data from wireless transmitter. The RT system was received data from wireless radio modem. The RT system was executed in-built data analysis software routines. The result of the analysis was sent to intelligent dump terminal. Intelligent dump terminal has in-built display. This display also called as a real time display. Therefore the received data was displayed on real time display as shown in Figure 6.

5.3 Real Time System

The RT system was developed on advanced virtual instrumentation environment (Tadisetty et al., 2002). Therefore software plays a vital role in this innovative new system. The RT system was an economically viable and reliable system. Since the system developed on virtual environment, the system capacity can be extended as and when required. The RT system was successfully commissioned at one of the longwall mine, GDK (Godavarikhani) 10A, SCCL Ramagundem, India for continuous monitoring and analysis of longwall strata behavior and supports performance to effective mining operations.

The RT system was interfaced to wireless receiver and intelligent dump terminal as shown in Figure 6. The RT system was commissioned on the surface around 25 km away from wireless transmitter (Tadisetty et al., 2003). The line of sight was maintained for effective data transmissions. The RT system was acquired underground sensors data from wireless receiver and displayed on real time monitor after analysis as shown in Figure 6. The detailed discussion on wireless system was reported by the same authors (March, 2003) in same journal. Therefore, the more discussions on wireless data transmissions are restricted.

All the underground powered supports (chock shields) leg closure and pressure sensors were configured on configuration menu of the RT system. The data acquisition time selected was one minute. The warning limit selected for chock shields was 400 bars. The RT system was initiated inbuilt warning modules whenever the support pressure crosses warning limit (threshold). The real time display was updated for every minute with the latest information of strata and supports. This information was facilitated to management for taking prompt decisions for implementing precautionary measures to effective mining operations.

The real time display was includes cluster of various informations like underground sensors and strata and supports behavior as shown in Figure 6. The underground sensor display information was includes type, location, units, calibration, date of commissioned and date of replaced. The chock shields display information was includes setting pressure, yield pressure, supply pressure, hydraulic circuit failures, influence of shearer cutting, influence of adjacent shield advancement and dynamic loading in graphically and numerically as shown in Figure 6. Further, the numerical display was indicates the rate of change in parameters. The display of strata behavior was includes caving of immediate and main roof, face spalling, stress levels in face and cavities. All the aforesaid information was continuously updated for every minute promptly after detailed analysis on real time. The RT system was initiated warning modules during adverse behavior of strata and supports for implementing necessary precautionary measures to avoid safety and productivity loss. The RT system was successfully recorded behavior of strata and supports in standard format for easy and quick access. The data continuity and reliability was maintained due to in built reliable wireless operations.
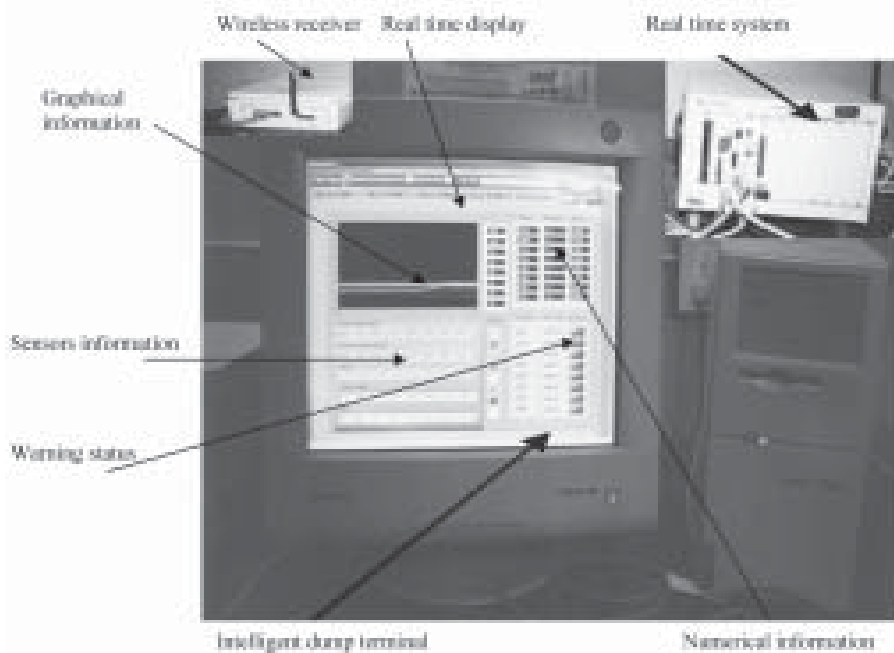
Fig. 6 : Real Time System interfaced to Wireless Receiver and intelligent dump terminal

5.4. REAL TIME ANALYSIS AND INTERPRETATION OF FIELD DATA

The real time data analysis and interpretation of selected data records of RT system are as follows: Chock shield C64 setting pressure was 250 bars initially at 20.23 hrs on 26th April 2002 as shown in Figure 7. The chock shield pressure increased in steps to 278 bars from 20.23 to 22.53 hrs due to face operations. The support pressure reduced to 262 bars at 23.00 hrs due to fall in the goal. The chock shield was near the tailgate. The RT system was successfully recorded and forewarned the adverse shield behavior for implementing necessary precautionary measures during fall in the goal at 23.00 hrs. The RT system was successfully recorded the behavior of C64 chock shield as discussed above.
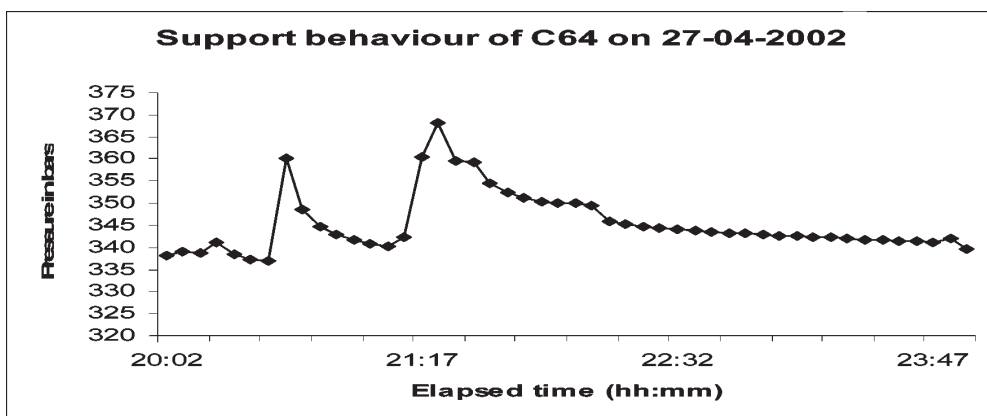
Fig. 7 : Chock shields C64 behavior on 26th April 2002

Chock shield C64 setting pressure was 338 bars initially at 20.02 hrs on 27th April 2002 as shown in Figure 8. The pressure suddenly increased and then decreased and again increased and decreased between 20.32 to 22.00 hrs due to periodic falls in the goal behind the support. The chock shield pressure returns back to setting pressure at 23.09 hrs. The chock shield was near the tailgate. The RT system was successfully evaluated the chock shield performance and initiated warning module during the periodic falls.
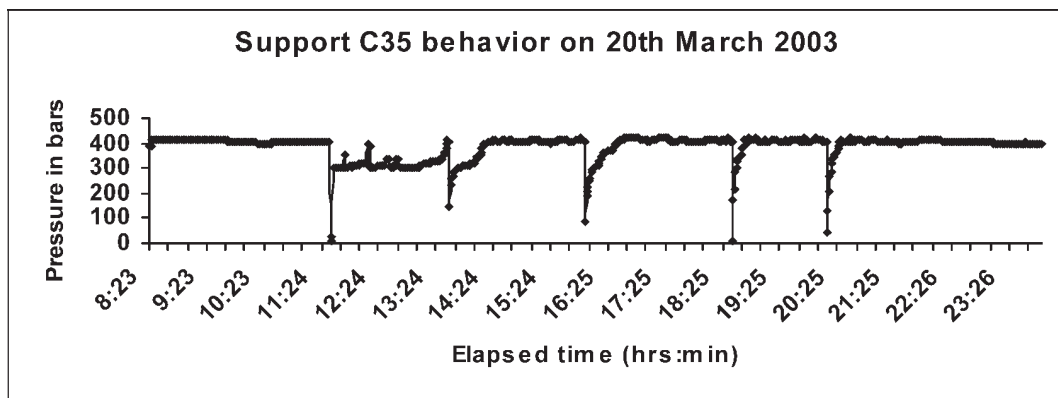
Fig. 8 : Chock sheld C64 behavior on 27th April 2002
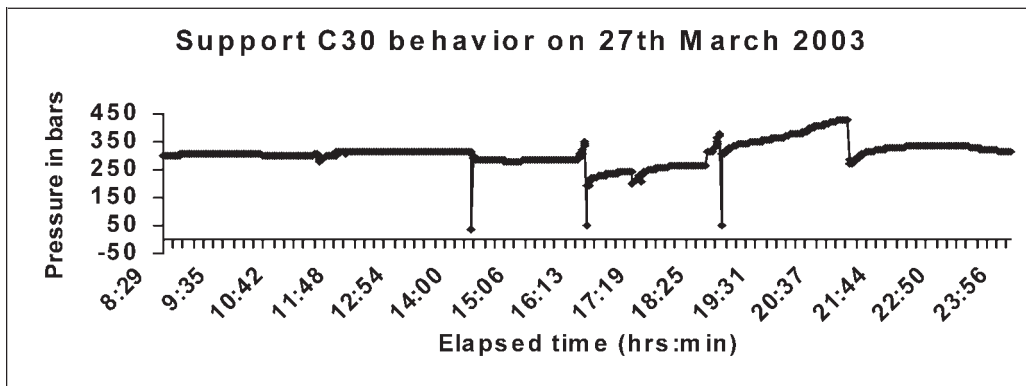
Fig. 9 : Chock sield C64 behavior on 27th April 2002

The setting pressure of C35 chock shield was 380 bars at 8.23 hrs on 20th March 2003 as shown in Figure 9. It was advanced at 12.24, 16.25, 19.25 and 20.25 hrs. The support pressure was reduced to 150 bars at 14.24 hrs due to face (hydraulic) leakage. Support pressure was yielding from 15.24 to 21.25 hrs due to periodic weight. The support was in the centre of the panel. The RT system was successfully forecasted the hydraulic leakages and periodic weightings as per above discussions.

The setting pressure of C30 chock shield was 300 bars at 8.29 hrs on 27th March 2003 as shown in Figure 10. The support was advanced at 15.00, 16.13, and 19.31 hrs. The support pressure was increased to 400 bars at 21.00 hrs due to onset of periodic weighting. The support pressure was reduced to 250 bars at 21.44 hrs due to face (hydraulic) leakage. The support was in the centre of the panel. The RT system was successfully recorded chock shield C30 behavior as per above discussions.

5. CONCLUSIONS

Software menus were successfully developed on LabVIEW programming environment and incorporated in the RT system for user friendly operations. The graphical programming environment was successfully explored for developing compatible software menus to mining applications with password id protection. In Indian mines security of the systems and software is very important due to most expensive mining systems and machinery. In addition, the productivity and safety of mining operations are also very important. Therefore compatible software with required security was successfully developed and implemented. The RT system was successfully recorded and forecasted various failures of mining machinery and adverse strata behavior as per real time analysis to effective mining operations. First time the RT system was successfully developed indigenously and applied to Indian mining applications to effective and efficient longwall operations.

ACKNOWLEDGEMENTS

REFERENCES

1. Y.M. Jiang, D-W Park, D. Deb and R.L. Sanford, "Development of on-line evaluation of longwall roof behavior using neural networks and fuzzy sets", Journal of society for mining, metallurgy and exploration, 1996

2. Srinivasulu Tadisetty, Kikuo Matsui and Gupta R.N, "Virtual instrumentation for real time analysis of supports behavior", Journal of mines, metals and fuels, special issue on annual review 2002, December 2002

3. Srinivasulu Tadisetty, Kikuo Matsui and Gupta R.N, "Frequency hopping techniques for reliable geomechanical data transmission", Journal of the instrument society of India, Vol.33, No.1, 15th March 2003

4. Thomas M Barczak and David C Oyler, "A model of shield-strata interaction and its implications for active shield setting requirements", USBM RI 9394, 1991.

DESIGN AND DEVELOPMENT OF WATER COOLED PROBES TO MEASURE PRESSURE AND TEMPERATURE IN HIGH TEMPERATURE, HIGH PRESSURE ENVIRONMENT

K. Anil Kumar, S.A.Vasudev and Meera Kaushal

Gas Turbine Research Establishment, Bangalore - 560 093

ABSTRACT

The measurement of total pressure and total temperature of gas at the inlet of a turbine cascade is essential during the testing of the cooling configuration of turbine blade. A Water cooled probe was designed and developed to operate in a high pressure high temperature environment to measure the gas parameters in the order of pressure 25 bar, temp 1700 K, and velocity up to 150 m/sec. The pressure calibration of probe was carried out in the Calibration lab of GTRE at Mach numbers in the range of 0.3 -0.6. The temperature calibration to find out recovery factor was not carried out due to lack of a suitable facility, but a comparative study was carried out in Heat transfer rig of GTRE with a similar uncooled probe. The total estimated uncertainty in pressure and temperature calibration is in the range of 2% - 4%.

1. INTRODUCTION

In Heat Transfer rig, the turbine blade (HPT NGV) is housed in a sectorial test section immediately after a combustor as shown in fig (1). The aerodynamic flow parameters of gas i.e. Total pressure and total temperature, to be measured between the combustor exit and HPTNGV in a restricted area, but in the same time any insertion in the gas flow path should not create wake effect at the entrance of stator blade, which may affect the cooling effectiveness of turbine blade. To measure the gas temperature profile at the exit of combustor needs more points of measurements in radial direction for accurate assessing. The mounting hole available on test section is just 13mm in diameter. The use of any uncooled probe is restricted up to 900°C gas temperature. Having considered all the above problems, rig testing at high pressures and temperatures of 30 bar and 1500°C demands a complex test vehicle (probe) that must be water cooled to maintain the properties.

Two types of Water cooled probes viz Temperature probe and Combination probe were designed, fabricated and calibrated against the Master probe. Temperature probe has three calibrated shielded R-type (Pt 13%Rh) thermocouples at 3 radial locations, and Combination probe has two temperature points and one pressure point at different radial locations. This
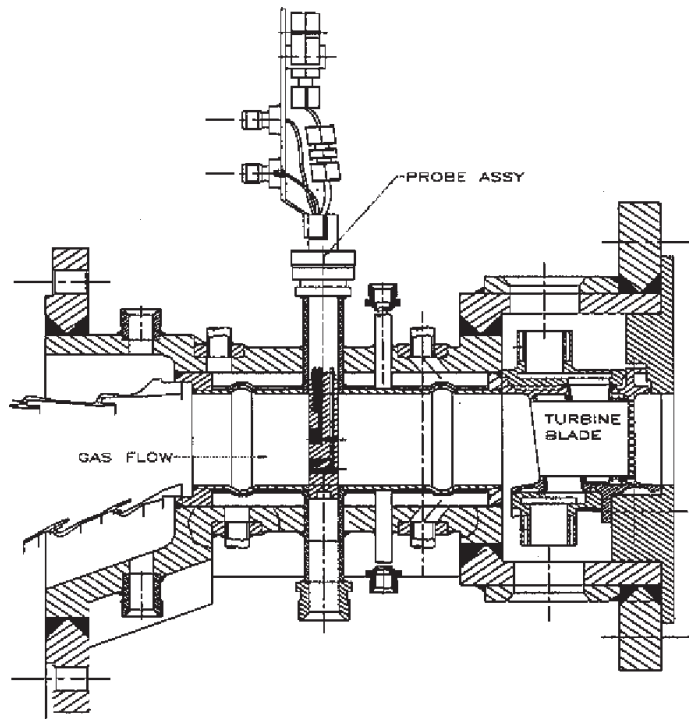
Fig.1. Test Section

paper describes design considerations, errors and calibration details involved in probe development.

2. DESIGN CONSIDERATION FOR MEASUREMENT FOR PRESSURE AND TEMPERATURE

2.1. Temperature measurement

Care must be taken to minimise errors in gas temperature measurement when a thermocouple is inserted into a fluid. The total temperature of a fluid at a velocity V is equal to the thermodynamic temp of a fluid, when this fluid is stopped in an adiabatic manner. The relation between Static temperature (the temperature, when probe moves along at the velocity V of the flow) and Total temperature is,

$$T_T = Ts + \frac{(1+\gamma-1)}{2} *M^2$$

The most important aerodynamic and thermodynamic factors affecting thermocouple design are,

2.1.1. Velocity error

In a probe, the gas is not brought to rest adiabatically, the velocity error caused by incomplete kinetic energy recovery is defined as,

$$\Delta T = (1 - r)\frac{\dfrac{\gamma - 1}{2}M_J{}^2}{1 + \dfrac{\gamma - 1}{2}M_J{}^2}T_T \qquad\qquad r = \frac{T_J - T_S}{T_T - T_S}$$

The velocity error can be minimised by decreasing Mach no MJ at the thermocouple junction by means of a stagnation tube.

2.1.2. Conduction error

The error caused by the heat conduction along the thermocouple wire is quantified as,

$$\Delta T = \frac{T_T - T_M}{\cosh L\left(\dfrac{4h_c}{D.k}\right)^{1/2}}$$

2.1.3. Radiation error

Radiation error is caused by radiation from thermocouple junction to the enclosure (Wall).

$$\Delta T = T_T - T_J = \frac{\sigma.\varepsilon}{h_c}\left(T_J{}^4 - T_w{}^4\right)$$

2.2. Pressure measurement

In a flowing gas, the static pressure can be measured through a hole in a wall If the fluid is brought to rest by an isentropic process, the pressure to a maximum value called Total pressure.

Total pressure = Static pr(Ps) + Dynamic pr ($\rho\ V^2/2$)

Fig.2. Probe Assembly
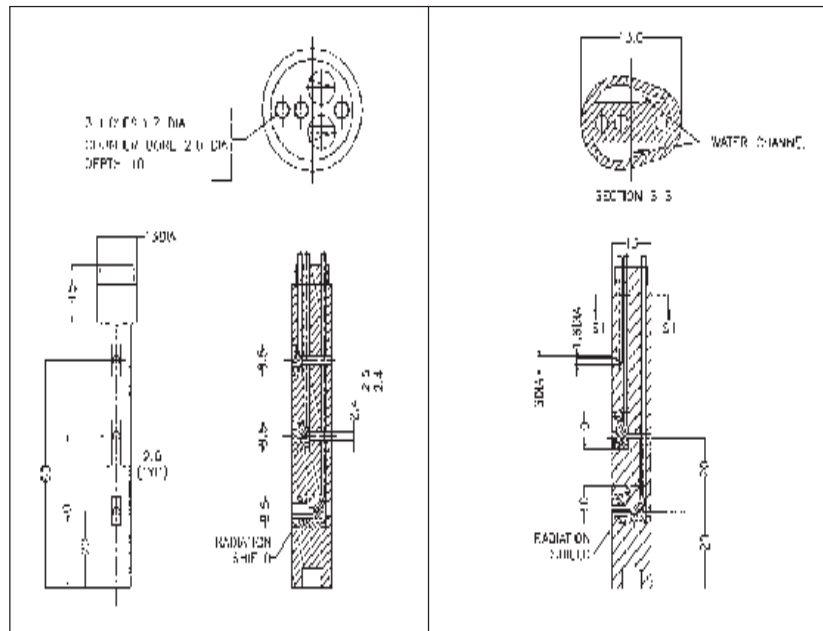
Fig.2a. Temperature Probe   Fig.2b. Combination Probe

3. PROBE DESIGN

The variety of physical and aerodynamic conditions of gas flowing through the test section needs close attention while deciding the geometric design of probe. Two types of Water cooled probes were designed as shown in Fig (2a) viz Temperature rake which measure Total temperature and Fig (2b) viz Combination probe which measure Total pressure and Total temperature both.

The probe stem was made with Nickel based super alloy. The required water flow rate for cooling the entire probe when subjected to maximum operating condition is estimated as 2.5 ltrs/min and the actual flow measured is in safer side. Though the probe was first made with Nickel based super alloy, the usage of low cost SS material is also possible as sufficient water flows through the probe to maintain its properties. The aerodynamic shape allows the probe to eliminate the wake effect to a great extent. The SS tubes are used inside the probe to route thermocouple as well as pressure line out of the probe stem.

The wall thickness between the water and gas side in the probe was crucial because of space constraint in the probe. But in actual use, water pressure is maintained equal to gas pressure during all rig operating conditions thus maintaining the structural integrity of the probe.

During the testing of probes, one of the main areas of concern was temperature measurement. The hot junction of thermocouple is surrounded by cooled walls of probe stem and exposed to gas through an opening. It was not possible to provide a Kiel type sensor because of space constraint. The error observed during the test was 50 to 70°C as radiation and conduction losses were too much. Later a metallic shield was incorporated surrounding

the hot junction and that helped to reduce the error. But the use of metallic shield is restricted as there is a chance of melting. Finally a radiation shield made out of cemented carbide was used. The thermocouple can be inserted into the probe as a replaceable unit. Provisions are made to bleed the air through tube to ambient with high velocity, which increases the coefficient of convective heat transfer, but up to a level of the maximum allowable velocity error. The loss because of conduction and radiation can be minimised by having high velocity through stagnation tube.

4. CALIBRATION AND ERROR ESTIMATION

4.1. Pressure measurement

Probes are fabricated and assembled after undergoing various manufacturing process, brazing, and welding. So precision in the pressure measurement depends on the final geometrical dimensions of probe. In order to achieve the precision in pressure measurement, the probe was calibrated against a master probe. Pressure calibration is carried out in calibration facility, GTRE. A master probe (Wedge shaped) supplied by M/s Rotodata, was used as reference probe, which was calibrated with tracebility to National standard by a third party.

A dedicated data acquisition system by M/s Scanivalve is used for this purpose. The calibration of test probe was carried out for a Mach no range of 0.3 to 0.67. The different set points and percentage error obtained during the calibration is given in Table (1). Fig (3a) and Fig (3b) shows the typical graph of recovery factor vs. Mach number and %error vs. Mach number.

4.2. Temperature measurement

The various errors estimated as follows

4.2.1 Velocity error

The velocity error estimated for Mach number 0.15 is 3.33 °C

Set No	Mach No	Master Probe Pressure, Po (psi)	Test probe pressure, P (psi)	Dynamic pr, q (psi)	Recovery factor (P/Po)	% Error (P-Po)/q
1	0.3328	13.609	13.596	0.996	0.9990	-1.30
2	0.3508	13.669	13.662	1.106	0.9994	-0.63
3	0.4007	13.787	13.771	1.436	0.9988	-1.1
4	0.4608	13.967	13.963	1.884	0.9997	-0.21
5	0.4933	14.106	14.103	2.154	0.9997	-0.13
6	0.5462	14.401	14.369	2.636	0.9977	-1.21
7	0.6183	14.899	14.894	3.379	0.9996	-0.14
8	0.662	15.314	15.305	3.895	0.9994	-0.23
9	0.672	16.586	16.571	4.325	0.9990	-0.34

Table 1. Pressure Calibration report

Mach No. Vs Recovery factor

Fig. 3a

Mach No. Vs % error
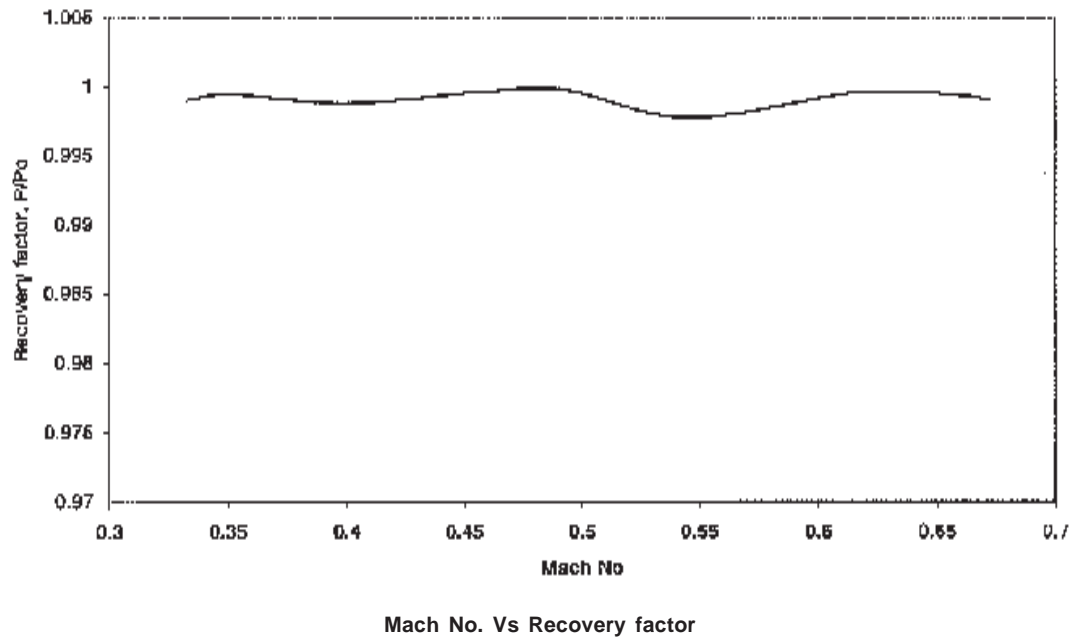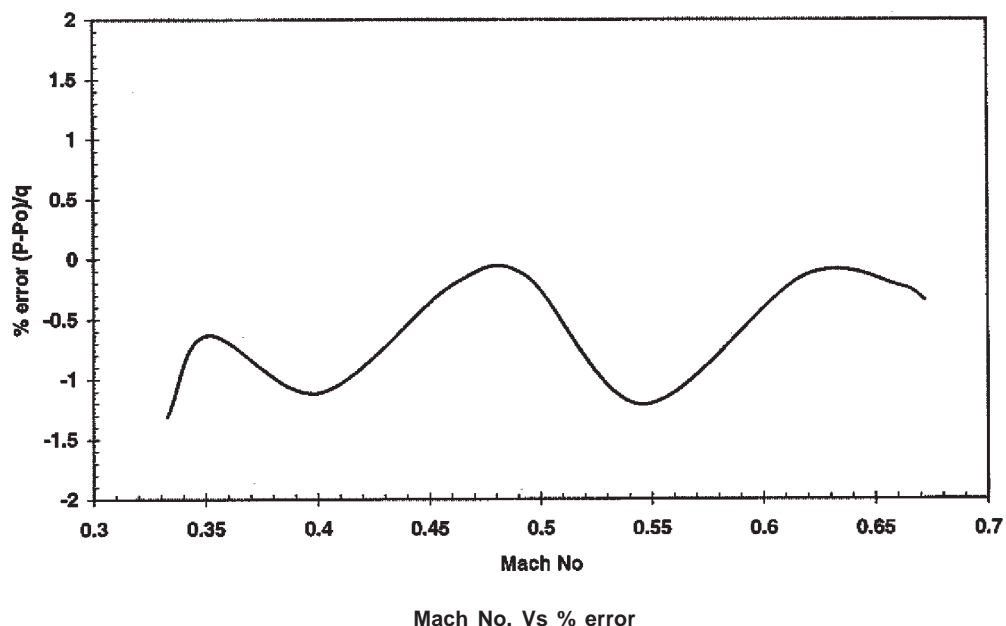
Fig. 3b

4.2.2 Conduction error and Radiation error

The estimated conduction and radiation errors are 3.5 °C and 12.5 °C.

Generally two types of calibration need to be carried out for a stagnation temperature probe as per ASTM procedure.

4.3.1 Normal temperature calibration

A Cavity type black body is used to calibrate test Thermocouple of R Type. Black body cavity is an isothermal cavity, which emits radiation with an emissivity of approx 1.0. The cavity length is sufficient to accommodate the thermocouple enough to reduce the conduction error. The test thermocouple is placed inside the cavity and setting of temperature is done with an accuracy of ± 5°C at 1000°c. A multifunction calibrator (MCX II) of M/s Druck make is used to measure the signal of test thermocouple. The values of temp and emf generated against standard value are given in Table (2). It shows the deviation between calibration value and standard value of R Type test thermocouple is within 0.8 %.

Temp Deg C	Std mv	Test probe mv	% deviation
150	1.041	1.040	0.09606
200	1.469	1.468	0.06807
250	1.923	1.908	0.78003
300	2.401	2.387	0.58309
400	3.408	3.403	0.14671
500	4.471	4.469	0.04473
550	5.021	5.020	0.01992
600	5.583	5.568	0.26867
650	6.157	6.157	0.00000
700	6.743	6.740	0.04449
750	7.34	7.340	0.00000
800	7.95	7.935	0.18868

Table 2. Comparison of standard output with actual thermocouple output
for R Type Thermocouple

4.3.2 Recovery factor calibration

The recovery factor of a stagnation temperature probe should always be known before using it for temperature measurement. Probe calibration for temperature was not carried out, but an experimental comparative study was carried out using an uncooled probe as reference. An Air preheater increases the temperature of compressed air to 555°C and pass through a long duct to settle the temperature uniform and allows passing through a test section where test and uncooled probes are fitted. Temperature of gas is controlled within ± 2°C using a microprocessor based Moore controller. A PLC (Programmable logic controller) based data acquisition system used to acquire the data in every 500 millisec. The system is capable to process the data at a scan rate of 50 samples /sec. The experiment result is given in Table (3).

Set no	Uncooled probe Temp (Deg C)	3 Point Temperature Test probe					
		Hub (Deg C)	% Deviation	Mean (Deg C)	% Deviation	Tip (Deg C)	% Deviation
1	555	553	0.36036	552	0.540541	555	0
2	556	554	0.359712	552	0.719424	555	0.179856
3	555	552	0.540541	552	0.540541	555	0
4	555	553	0.36036	552	0.540541	554	0.18018
5	555	552	0.540541	552	0.540541	553	0.36036
6	555	553	0.36036	552	0.540541	552	0.540541

Table 3. Comparison of water cooled probe readings with uncooled probe readings

5. RESULTS AND DISCUSSIONS

The pressure probe calibration was carried out from 0.33 to 0.672 Mach numbers. Total 9 readings were taken and duration of each reading was approximately 60 mins. The probe has shown the error within ± 1.5% of the dynamic head.

The temperature probe checking was carried at 0.15 Mach number. The gas flow maintained in a steady state condition for a period of 30 mins and numbers of readings were taken at the rate of 2 data per second. The deviation observed during thermocouple calibration is within ± 0.7% and deviation from uncooled probe reading is within 0.54%. The probe has successfully used for 100 hrs without failure. Constant modification has been carried out to minimise the error to a great extent.

ACKNOWLEDGEMENT

NOMENCLATURE

HPTNGV - High pressure turbine nozzle guide vane. h_c - Heat transfer coefficient
Tm - Probe stem temperature   D - Diameter of thermocouple
V   - Velocity   k   - Thermal conductivity
Cp - Specific heat at constant pressure   L   - Length of thermocouple
T_S - Static temperature   Tw - Wall temperature
γ   - Specific heat ratio   Ps - Static pressure
M   - Mach number   ρ - Density
ΔT - Temperature difference   P - Test probe total pressure
r   - Recovery factor   q - Dynamic pressure
T_j - Junction temperature (Test probe)   Po - Master probe total pressure
T_T - Total temperature of gas   α - Stefan Boltzman constant

REFERENCES:

1. "Aerodynamics Measurement" by Robert Dean
2. "Agard AR - 245", Year June 1990 - Recommended practice for measurement of gas and temp
3. "Heat transfer and application", Year 1999, Author Kirk. D. Hagen, Published by Prentic -Hall.
4. "Measurements in Flames", Year 1972, Authors J.Chedaille and Y. Braud, Published by Edward Arnold (Publishers) Limited.

DESIGN OF A TDI TRANSFER AND WEIGHING SYSTEM

Arvind Kumar, K.K. Radhakrishnan and V.K. Bhat

High Energy Materials Research Laboratory, Pune - 411 021

ABSTRACT

In the field of Defence and Space, the matrix, that gives the strength to the solid composite propellant, is generally a polyurethane formed by cross-linking of telechelic polymer and toluene diisocyanate (TDI). TDI is widely used all over the globe, for propellant manufacturing and also as a cross-linking agent in polyurethane industry. The use of TDI though may be to the extent of 1% of propellant weight, is observed to be hazardous and causes great discomfort to the workers. Spillage and exposure are observed to be maximum during transfer of required quantity of TDI from big size drums to smaller containers for further processing. Environmental interference due to moisture susceptibility has been found to be a major factor that affects its use as well as quality of the product.

To reduce the risk and hazard in transfer of such toxic compounds attempts for process automation are continuously made in resin and polymer industries. However, many of the indigenous propellant plants still continue with the manual system. A TDI transfer and weighing system has been designed at HEMRL, Pune. In this design remotely operated PLC based SCADA system is incorporated with safety interlocks and logics for transferring TDI with a weighing accuracy of $\pm10g$ in 5 kg. The design and the logics added to the system overrule any accidental spillage and subsequent environmental pollution and thus take care of human safety.

The total scheme uses various electronic field instruments. Selection of instruments and their application has been done in such a way that operation of TDI transfer and weighing becomes more accurate and safe to environment. This can be used for any similar application where hazardous chemicals are to be transferred.

1. INTRODUCTION

In the field of defence and space, the new class of heterogeneous solid composite propellant has come to stay for application in large size boosters and also in small tactical missile propulsion requirements. This class of propellant is heterogeneous in nature and consist of inorganic oxidisers and metallic fuel embedded in a polymeric binder matrix. The matrix, which provides the required structural rigidity to the solid propellant, is generally polyurethane, formed by cross-linking of telechelic polymer and an isocyanate. Toluene diisocyanate (TDI) is widely used in the industry all over the globe, as the isocyanate not only for propellant

manufacturing, but also in most of the polyurethane industries. TDI is reported to cause health hazards even at 0.02 ppm[1] level for 5 min and short and long term effects of TDI on respiratory system are available.

Though the use of TDI may be to the extent of 1 % of propellant weight, it is observed to adversely affect the health and cause great discomfort to the workers during processing. Spillage and exposure is observed to be maximum during transfer/weighing of TDI during propellant processing. Hence design of TDI transfer and weighing system becomes important in propellant processing.

To reduce the risk and hazard in transfer of such toxic compounds attempts to do the process automation is continuous in resin and polymer industries. However, many of the indigenous propellant plants still continue with the manual system. Present paper describes a TDI transfer and weighing system designed at HEMRL, Pune for using in propellant processing.

2. BASIC REQUIREMENTS OF TRANSFER SYSTEM

Three aspects of the process requirement are considered in designing the transfer & weighing system.

2.1. Accurate measurement

TDI is a critical component in the polymer reactions and accurate quantity has to be incorporated to get repeatable mechanical properties. Any deviations can affect the product quality and may lead to major process problems.

2.2. Moisture effect

TDI is highly moisture sensitive and can react with trace moisture[2, 3] and form impurities deteriorating the product quality and also liberate gases to the environment. In addition, on prolonged storage can form dimers, which are solids and lead to scale formation. Hence frequent exposure to atmosphere during transfer is highly detrimental.

2.3. Health hazard

Exposure to TDI affects the respiratory system leading to irritation and breathing problem and in extreme cases requiring hospitalisation even for short exposure. TDI is also carcinogenic[4] in nature.

3. GENERAL TRANSFER SYSTEM FOR HAZARDOUS CHEMICALS

Two types of system are generally followed for transfer of hazardous liquid chemicals in the industry.

a) Manual

b) Semi automatic

In the manual system, drums are tilted manually and material poured into a can for weighing. Disadvantages of adopting this system are too many and high exposure is expected to persons handling the transfer as accurate weighing necessitates repeated handling. Also tilting of drums is risky and involves inherent hazards. In this method TDI exposed to moisture in the atmosphere, forming dimers and affect the quality of TDI.

In semiautomatic system, pedallistic stroke pump/ diaphragm pumps/ vertical pumps are used to transfer material from drum to measuring can. In such a system, pumps can be operated through control panel. However, because of pump discharge pressure, such transfer involves more risk involving gland/seal leakage from pumps. Also another disadvantage is that pump has to be stopped manually and any error may cause disastrous consequences. Besides this, contamination due to moisture and consequent formation of impurities will be the same as in case of manual transfer.

4. DESIGN APPROACH

In the present design remotely operated PLC (Programmable Logic Controller) based SCADA (Supervisory Control & Data Acquisition) system is incorporated with safety interlocks and logics for transferring TDI with a weighing accuracy of ±10 gm in 5 kg. The design and the logics added to the system overrule any accidental spillage and subsequent environmental pollution and thus take care of human safety.

In the present transfer system, set point only has to be entered on control screen and if all the safety interlocks are checked and found okay, then only transfer of material will start and automatically stop at desired set point. Consequently, accuracy and repeatability is expected to be of high order. The transfer mechanism is a combination of vacuum and gravity flow and as such, risk and hazards involved will be reduced to a large extent. Because of PLC & SCADA all the necessary safety interlock and effective control can be given in this type of transfer system. Along with these aspects, contamination due to moisture will also be negligible as exposure to atmospheric moisture is minimized.

4.1. Design description

The selection of instruments and interlocks in the present design is to ensure accurate weighing of clear liquid TDI received from trade in drums without any normal impurities as detailed in the earlier paragraph. As such, in the present system TDI is initially transferred from drums to intermediate storage tank by vacuum through a trap vessel so no TDI vapour escape into the atmosphere through vacuum pump. Intermediate vessel is used as storage vessel for TDI and is positioned at a height so that gravity head can be used in subsequent transfer processes. The required quantity is transferred to the measuring vessel by gravity through seal pot so that no air from atmosphere come in contact and contaminates the TDI inside the system. Measuring vessel is found necessary as. storage capacity of intermediate vessel is 300ltr and transfer of 1 - 5 kg per batch, can not be directly controlled with ±10gm accuracy. A P & I diagram is given in figure-I. The logic and design step details are given below under different sub sections.

4.1.1. Main storage to intermediate tank

The steps involved are as follows: -

a)   System to check whether level is up to mark or not in the trap vessel and if it is okay then only the vacuum pump will start.

b)   Check the level of TDI intermediate tank level, and only if level is up to the mark vacuum ball valve will open

c)   Drain valve of intermediate to be kept closed. TDI storage drum to be kept at the position and dip rod inserted manually into it. After this, valve in transferring line

Transfer & Weighing System for Toluene Diisocyanate
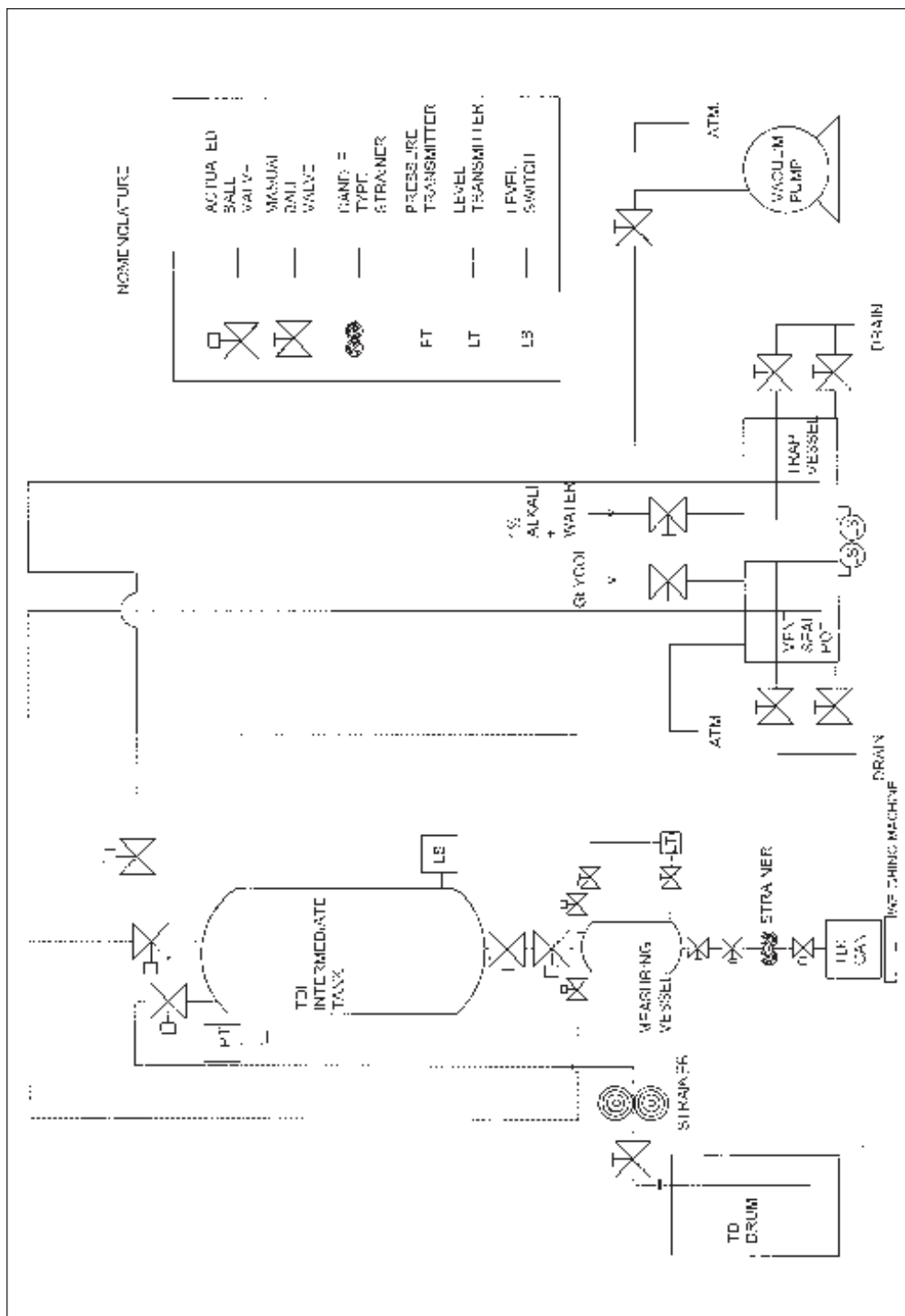
from storage drum to intermediate tank is to open and the valve to close when level in TDI intermediate tank reaches the desired level.

d)   Vacuum valve to close when vacuum in intermediate tank reaches to desired level and to open again when it falls below set point.

e)   All these operations to takes place automatically in auto mode by just clicking the start transfer button in SCADA. In manual mode these operation is to be done manually. If any interlock is not fulfilling during operation then that interlock will display in SCADA.

4.1.2. Intermediate tank to measuring vessel by gravity / vacuum flow

a)   System to check the level of trap vessel & vent seal pot. If levels of both tanks are found okay then further operation to start.

b)   In case of TDI transfer by vacuum, start the vacuum pump and open vacuum valve of measuring vessel, provided the level of measuring vessel is not high. In case of gravity transfer, vacuum pump and valve will not operate and vent valve of measuring vessel will open.

c)   Vent valve of intermediate tank to open.

d)   Feeding valve to intermediate tank to be closed.

e)   If level of measuring vessel shows low level then bottom valve of intermediate tank to open.

f)   As level in measuring vessel reaches to set point, ball valve to measuring vessel to close.

4.1.3. Filling & weighing of TDI in container

a)   System to check the readiness of vent seal pot.

b)   Weight of TDI to be filled in container has to be entered in SCADA and place the container on the weighing machine.

c)   Vent valve of measuring vessel to open.

d)   Ball valve to container open only after the measuring vessel bottom control valve gradually open and filling starts. The control valve gradually closes as weight of filling container approaches to its set point. Ball valve and control valve both close as the required weight of TDI is filled in the container.

5. EQUIPMENT AND INSTRUMENT SELECTION IN THIS SYSTEM

5.1 Control valves

Leakage from control valve is one of the major bottlenecks in manufacturing process and as TDI is carcinogenic in nature even in low concentration, control valve used in this system has to be selected with utmost caution. Leakage from globe type valve is from the stuffing box. However in bellow seal type valves bellow element act as a protective cover for valve stem and no liquid or gas will be in touch with valve stem. Hence there is no possibility of leakage of fluid through stuffing box. Control valve used in this system is of air to open type, so that in fail-safe condition it will be in closed condition.

5.2 Actuators

Actuators used for ball valves in transfer & weighing system are spring return[6, 7] types so that if power or air fail these valve will close in fail-safe condition.

5.3 Interlocks and Logics

Interlocks[8] & logics for operation are made for each and every operation and redundancy is given in control logic so that even in case of one of the instrument malfunctioning other instrument will take care. As an example, in case of Level transmitter malfunctioning the weighing machine will take care of safe operation as only exact quantity will be filled in the container and no liquid spillage is ensured.

For operating this system PLC[9] & SCADA system is used to make environment user friendly and to improve process control. In the present case as I/Os are not many, PLC works out less costly and is used instead of DCS (Distributed Control System).

Instrument used are of smart type transmitter[10] with HART protocol. Calibration of these transmitters is easier than analogue transmitters. Smart transmitters have built in diagnostic and hence will be easy to diagnose in case of any malfunctioning of instruments.

6. TEST RESULTS

Trial run using toluene was undertaken to validate the design. The functioning was found with an accuracy of ±10gm for weighing up to 5kg. The equipment was adopted to TDI after fine Pill tuning of control valve with actual run of TDI. The effectiveness of filter was also tested by deliberate inclusion of solid dimer in TDI liquid. The weighed out material was found to be clear TDI liquid with ±10gm accuracy.

7. CONCLUSIONS

The transfer and weighing system designed is incorporating the control logic with safety interlocks for transfer and weighing of hazardous liquid like Toluene diisocyanate and is found useful in reducing the health hazards associated with such chemicals. The scheme can be adapted to other similar liquid transfer systems where in automatic control on accuracy and non-exposure is required.

REFERENCES

1. G. Weirs, 'Hazardous Chemical data book' second edition.
2. Ullmann, 'Ullmann's Encyclopedia of Industrial Chemistry'.
3. D.J. Davis, J.A. Davis, G.T. Cristianson, 'Fire Fighter's Hazardous material', 2nd edition.
4. Jeffrey W. Vincoli, 'Risk seal valves for hazardous chemicals'.
5. Rajesh Salins, 'Bellow seal valves for hazardous applications', *J.* Chemical Industry Digest, Pumps & Valves Special Issue, 77 (1993).
6. Vinod C. Bhasin, 'Actuator Selection', *J.* Chemical Engineering, 140 (Nov. 1990).
7. S. Ram Mohan, 'Valves Actuator Sizing and Selection', *J.* Chemical Industry Digest. Pumps & Valves Special Issue, 81 (1993).
8. Christopher Read, 'Start to Improve Batch Operations' *J.* Chemical ENgineering Progress, 69 (Jan 2000).
9. Joseph La Fauci, 'Choose the Right Control System' *J.* Chemical Engineering Progress, 55 (March 1998).
10. Cecil L. Smith, 'Process Engineers: Take Control!', *J.* Chemical Engineering Progress, 19 (Aug 2000).

DESIGN OF DECODER FOR IRIG-B TIME CODE

A.K. Hanjura

National Physical Laboratory, Dr. K.S. Krishnan Marg, New Delhi - 110 012

ABSTRACT

Among the Inter Range Instrumentation Group (IRIG) time codes, IRIG-B is most popular worldwide. Most of the digital clocks provide this time code as an output. This time code can be transmitted over a long distance, and needs to be decoded and displayed. Transmission can be as potential free contacts or as radio signals. The present paper describes the design of a microprocessor based IRIG-B time code decoder and display unit, designed specially to decode and display time of the day from Standard Time and Frequency Signals (STFS) transmitted from National Physical Laboratory, New Delhi, via INSAT satellite for the hundred odd users all over the country.

1. INTRODUCTION

Inter Range Instrument Group (IRIG) time codes were developed and used extensively during World War II. Out of various IRIG time codes, IRIG-B time code is most widely used. This code carries information on the time of the day (hours, minutes and seconds) and also the day of the year (1 to 365 or 366). Other information in this code is not relevant in the present context.

IRIG-B time code is available as an output in many standard clocks. It is generally in the form of voltage pulses of 5-10 volts. In case, where the code is intended to be transmitted over long distances, it is available as potential free contacts, to be converted into voltage pulses at the other end.

National Physical Laboratory, New Delhi, is transmitting Indian Standard Time via INSAT satellite[1]. The users of this time service usually have a commercial master clock which can get synchronized by IRIG-B time code. For this purpose, we have designed the receiving system of the satellite based time service so as to provide the time in IRIG-B format. Other users, who do not have such a master clock, would like to get the correct time of NPL displayed remotely. For this, it is necessary to decode the IRIG-B time code and to display it. The present design is in that context.

2. IRIG-B FORMAT

The format of IRIG-B serial time code[2] is shown in fig. 1. Each frame of IRIG-B is of one-second duration and comprises a pulses at intervals of 10 ms (a total of 100 pulses). These pulses are either 2 ms or 5 ms or 8 ms wide representing a logical '0' or '1' or a
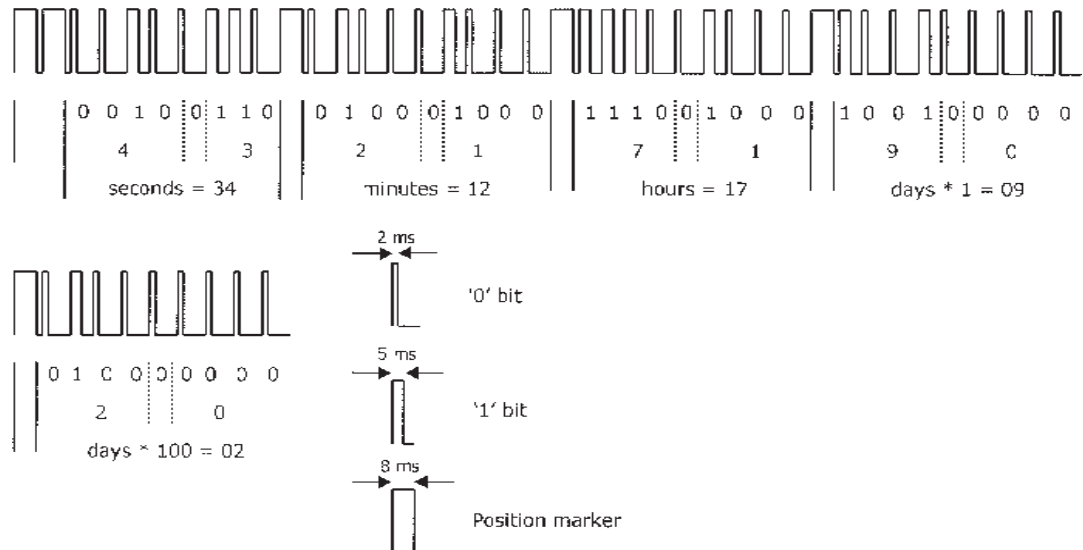
Fig.1. IRIG-B Time Code Format
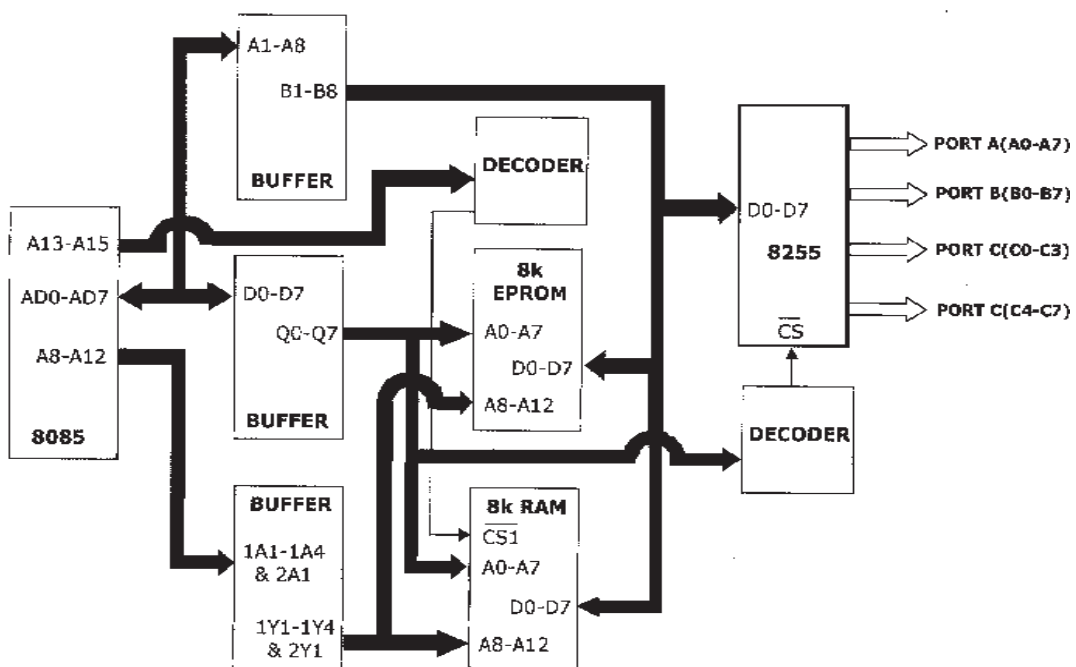
Fig.2. Block Diagram of Microprocessor Card

position marker. The frame is divided into ten sub-frames, each of 10 pulses. First sub-frame starts with two consecutive position markers followed by eight binary bits representing second. Second sub-frame starts with a position marker, followed by 9 data bits representing the minute. Third, fourth and fifth sub-frames are quite similar to the second one and represent the hour, days and hundreds of days.

3. SYSTEM HARDWARE

3.1. Microprocessor Card for Decoding of IRIG-B Time Code

The decoding of the incoming IRIG-B time code is done using INTEL 8085 CPU based card. The block diagram of the card designed for this purpose is shown in fig. 2. It comprises the CPU 8085, a Programmable Peripheral Interface 8255, an 8k RAM 6264, an 8k EPROM 2764, various buffers and decoders. All the input / output lines are terminated on a 64-pin connector.

3.2. Display Card

The block diagram of the display card is shown in fig. 3. A total of ten 7-segment displays are used to display the time and day of the year in the format

HHMMSS DDD

Where HR, MM and SS are hour, minute and second and DDD is the day of the year. The data to be displayed is sent by the microprocessor over B-port followed by an appropriate number at the C-port. The value at C-port is decoded by a 4-to-l0 decoder to generate latch
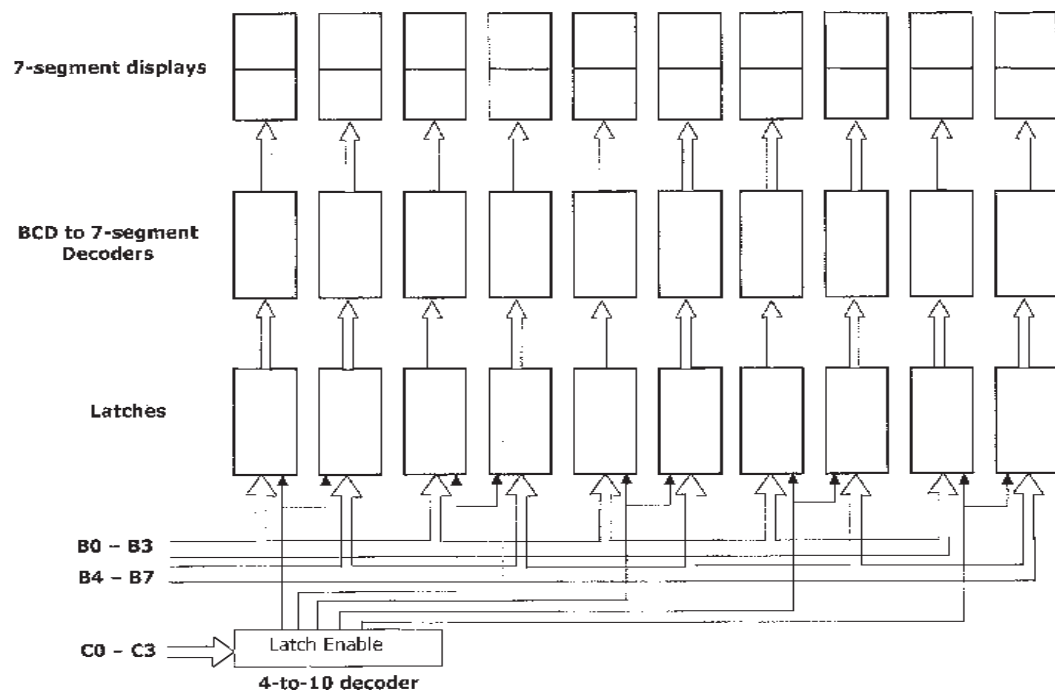
Fig.3. Block Diagram of Display Card

pulse corresponding to the digit where the data is to be displayed. The entire data stream is sent over B-port in quick succession and each byte is followed by the generation of the corresponding latch pulses. This enables the numbers to be displayed.

3.3. Interconnections

The IRIG-B time signal (TTL level) to be decoded is fed to the Serial Input Data (SID) pin as well as to the interrupt pin (RST 7.5) of the CPU (8085). The 8 lines of B-port of 8255 are connected to the data input lines of the display card. The 4 lines of C-port (C0-C3) of the 8255 are connected to the input lines of the 4-to-10 decoder of the display card.

4. SYSTEM SOFTWARE

The assembly language program is written into the EPROM. The instructions for the Main Program and the Interrupt Service Subroutine RST 7.5 when executed, perform the following tasks.

4.1. Main Program

The ports Band C are initialized as output ports. In addition, certain RAM locations used as counters are initialized. These counters are used for:

- Number of times the program has executed the delay loop of 3 ms in order to find out whether the pulse is logical '0' or '1' or a position marker.
- Keeping a count of the pulses in a given sub-frame.
- Identifying two successive position markers.

After this, the program idles in a wait loop until an interrupt pulse is detected at RST 7.5 pin of the CPU. On detection, the program jumps to the location in EPOM where the instructions for RST 7.5 are written, executes them and returns to the wait loop.
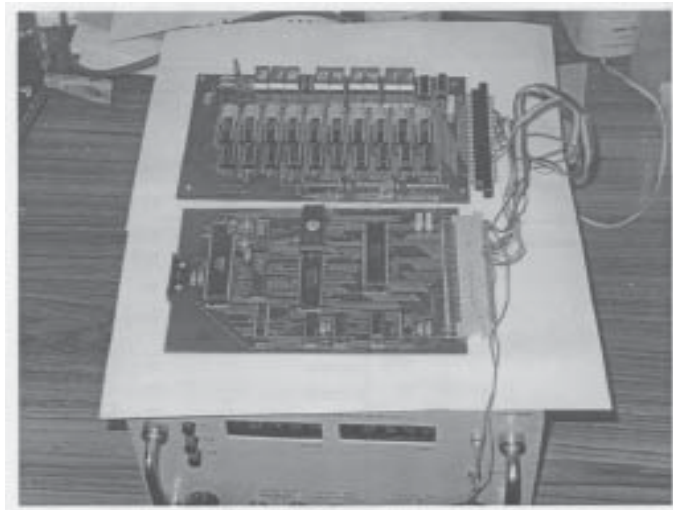
Fig.4. Photograph of the IRIG-B Decoder

4.2. Interrupt Service Subroutine RST 7.5

This subroutine is serviced when the input pulse arrives. This subroutine does the following.

- Executes a 3 ms delay loop till the input level becomes zero. A counter keeps track of the number of times the loop is executed. If the loop is executed only once, it is '0' bit; if executed twice it is '1' bit, otherwise it is a position marker.

- Looks for two successive position markers for the start of a frame.

- Checks the widths of data bits and places them in appropriate places.

- At the end of five sub-frames, it converts the stored data into BCD numbers.

- Runs the display subroutine to display the BCD numbers.

5. CONCLUSION

The decoder based on the above design was developed and operated. The cards designed and the interconnections are photographed as shown in fig. 4.

6. REFERENCES

1. A. Sen Gupta, A.K. Hanjura and B.S. Mathur, 'Satellite Broadcasting of Time and Frequency Signals', Proc. IEEE, Vol 79, No. 7, 973-981 (July 1991).

2. P. Kartaschoff, 'Frequency and Time', Academic Press, 1978.

FUZZY LOGIC pH CONTROLLER IN SUGAR INDUSTRY

**B.T. Jadhav[a], G. G. Tengshe[b], A.B. Kulkarni[c], R. R Mudholkar[d]
and S.R. Sawant[d]**

[a]Department Of Electronics, Yashavantrao Chavan Institute Of Science, Satara (M.S.)
[b]Department Of Electronics, D.Y. Patil College of Engineering, Kolhapur 416004 (M.S.)
[c]Department of Applied Electronics, Gulbarga University,gulbarga~585 105(K.S.)
[d]Department Of Electronics, Shivaji University, Kolhapur 416004 (M.S.)

ABSTRACT

The process of pH control in sugar industry forms an important clarification phase. But no fixed value of pH can be prescribed, however for optimum clarification; the desirable figure varies with the type of juice i.e. with the nature of impurities. Rapid changes in pH are likely to give secondary precipitation in the juice in or after sub siders. Adjustment of pH is necessary to minimize decomposition of sugars in clarification and subsequent boiling house operation. In the narrow limits, of pH, satisfactory removal of impurities from raw juice is practicable. To embed the knowledge of human expert for satisfactory clarity of juice, we propose a fuzzy logic pH control technique to maintain the desired level of pH.

1. HUMAN EXPERTS IN SUGAR PROCESS

Many stages are involved in the process of sugar production. Each stage in turn involves many processes some of which require process controlling for the better end results and yield. After a survey of some sugar mills established in western Maharashtra (India) it has been found that the result of many processes depends largely on human experts. Some sugar industries attempts for the conventional automation but have not given the desired results. As such even today sugar factories heavily rely on the manual control of various processes hence fuzzy logic is used.

1.1: Clarification and pH of juice

For the clarification of raw juice hundreds of materials have been tried. But maximum sugar industries in India use the "lime-defecation" and "sulphitation" processes to get clear juice. The juice becomes clear after defecation and sulphitation where it is at neutral level i.e. its pH is about 7. The raw juice pH leaving the mills is generally in the neighborhood of 5.1 to 5.5[1-2].

Defecation Procedures

- Cold liming: Lime is added to a pH of 7.2 to 8.3 and then heated.
- Hot liming: First heated and then lime is added to a pH about 7.8.
- Fractional liming with double heating: Liming to a pH 6.2 to 6.4 then heated up to boiling and re-liming to a pH 7.6 to 8.2 and reheating for settling.
- Liming while boiling:After boiling juice sample is cooled then pH is observed.
- Pre-liming separations and mixing: Pre-liming below neutral and part of juice is heated and remaining part limed upto 9.3 pH and mixing for clarity.
- Compound clarification: the dear juice pH is about 6.8 to 7.1.

Sulphitation Procedures

- Cold sulphitation: Sulphitation - liming - heating process. The clear juice pH is about 6.9 to 7.0.
- Hot sulphitation: Heating -1iming-sulphitation-reheating-settling process. Sulphitation upto pH of 7.2.
- Fractional liming and sulphitation: Heating-pre-liming- sulphitation- final liming-reheating process. The final liming to pH of 7.4. In some sugar industries liming before sulphitation is 'carried out while in others sulphitation before liming is done.

1.2 pH control

Manual or Automatic controllers are used for this purpose[3-6]

i) Manually or

ii) Automatically

Manual control

Different ways are used in the manual pH control. One of them is an operator maintain the juice flow (Mt/h) and SO_2 gas flow (compressor air pressure in kg/cm^2) rates constant and by adjusting the lime control valve, he get the desired value of pH. By using the mechanical valve the diameter of the outlet pipe of lime milk tank is changed. If the incoming juice flow rates are 85 and 115 Mt/h then the diameter of the pipe is 15 and 17 mm respectively. In this case raw juice temperature is kept constant. The pH value of clear juice is laying in-between 6.9 to 7.2. This adjustment is based on the operator experience. Such type of technique is used in the. Damaji Co-Operative Sugar Mill Ltd. Mangalwedha (M.S.).

Auto control

In auto control different types controller's used to maintain the desired pH values. Some sugar industries use the electronic controller to control the pH to the required value by adjusting the lime flow & SO_2 gas flow rates simultaneously and the raw juice flow rate is kept constant. Here only one pH sensor is used to observe the pH value. This type of controller is utilized in the Ajinkyatara Co-Operative sugar Mill Ltd. Satara (M.S.).

In Kumbhi-Kasari Co-Operative Sugar Mill Ltd. Kuditre, Kolhapur (M.S.); pH value of clear juice is maintained to the desired level by adjusting the lime flow rate but in this case SO_2 gas and raw juice flow rates are constants. In this microprocessor based control system

two pH sensors are used to sense the limed juice pH and clear juice pH. The chemist decides these pH values. The stepper motor is used for valve adjustment of lime flow.

In another auto controller raw juice and SO_2 gas flow rates are kept constant. Only clear juice pH is sensed and maintain by varying the lime flow rate using stepper motor valve adjustment technique.

Some sugar factories initially keep the raw juice flow rate constant and adjust the lime flow rate to get the pH up to 9.6 to 10.5 for alkalinity. Then SO_2 gas is bubbled to reduce the limed juice pH value about 7. The SO_2 gas flow rate is adjusted by varying the airflow to the compressor using the potentiometer and stepper motor auto arrangement. Here also two pH sensors are used. Such controller is used in Jawahar Sugar Ltd. Hupari, Kolhapur (M.S.). For lime flow variation, valve is adjusted using stepper motor.

Whatever may be the way of control the pH, the target is get the clear juice. To embed the practical knowledge of human operator in the conventional controller to control the pH, we propose fuzzy logic based pH controller by keeping the raw juice and SO_2 gas flow rates constant and controlling the lime flow by varying the valve opening diameter (mm). The variations of pH values with respect to the lime-flow-valve-opening-diameter (LFVOD) (mm) are given in the Table 1.

PH Values	6.71	6.83	7.10	7.17	7.21	7.33	6.91
LFPVOD (mm)	18	17	16	15	14	13	12

Table 1 : pH Variation with lime flow

2. DEVELOPMENT OF FUZZY LOGIC PH CONTROL SYSTEM

The complete set-up of fuzzy logic based pH control system is shown in **Fig.1.** The combined glass pH electrode is calibrated with the ELICO based pH meter. This electrode is
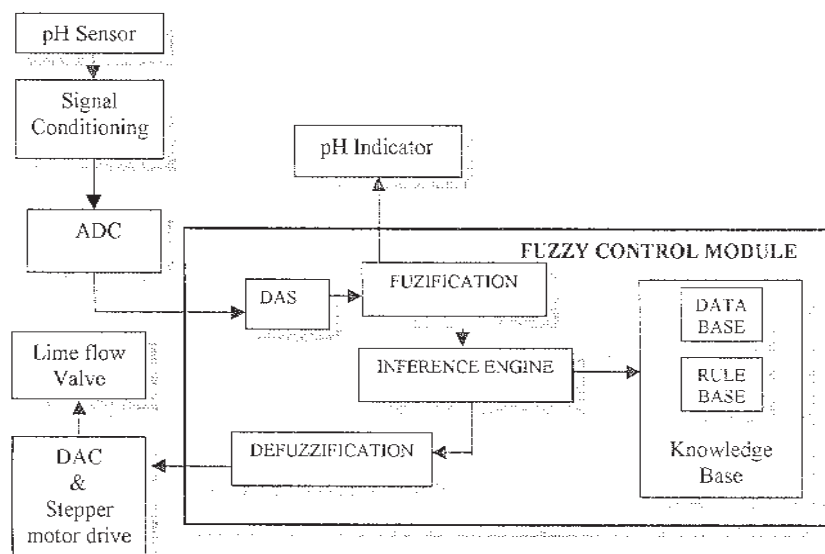
Fig.1. Block diagram of Fuzzy pH Control system

easily available in the market. The IC's LF 356, LM 324 and Transistor BC 109 are useful for signal conditioning. The eight channels ADC IC 0809 is suitable to convert the data in the digital form. The DAS (Data Acquisition System) stores the data coming from the sensor. The output of defuzzifier is read by the DAC IC 0808 and drives the stepper motor using the driver circuitry. The stepper motor arrangement is' essential for the opening and closing of the valve. at the required diameter. Immediately after the measurement of pH the Fuzzy Control takes control of lime-milk regulation. This involves the following steps[7,8,12,13]

- Fuzzification
- Knowledge Representation
- Inference Process
- Defuzzification

2.I. Fuzzification

The input variable "pH" and output variable "Lime-Flow-Valve-Opening-Diameter" (mm) are selected for fuzzification. Based on the on-line observations the operating ranges are decided and variables are assigned using meaningful linguistic values. Fuzzification is carry out by using appropriate membership functions over practical ranges[7,9]. The fuzzy sets so obtained are then labeled using the term set

$$T = \{NL, N, NM, SP, SD, PM, P, PH\}$$

NL = Negative Large, N = Negative, NM = Negative Medium, SP = Set pH, SD = Set Diameter, PM = Positive Medium, P = Positive, PH = Positive High. The membership functions are shown in Fig.2.
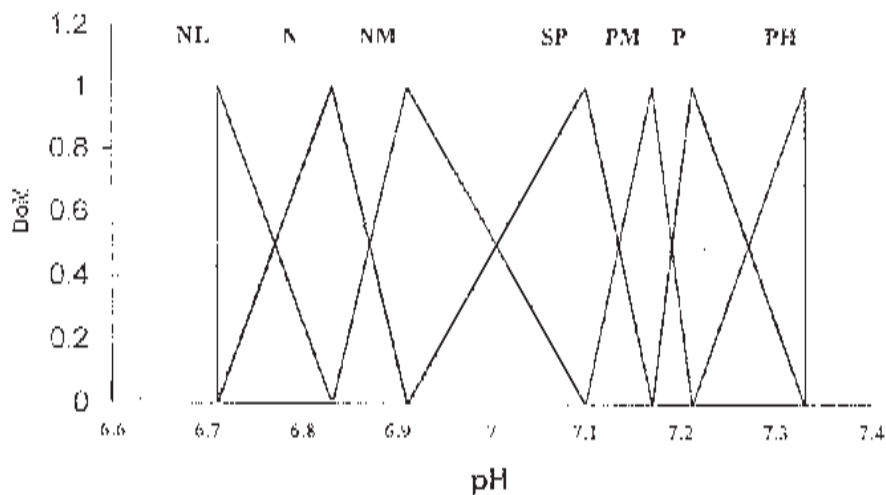

*Fig. 2a : Membership Functions of pH*
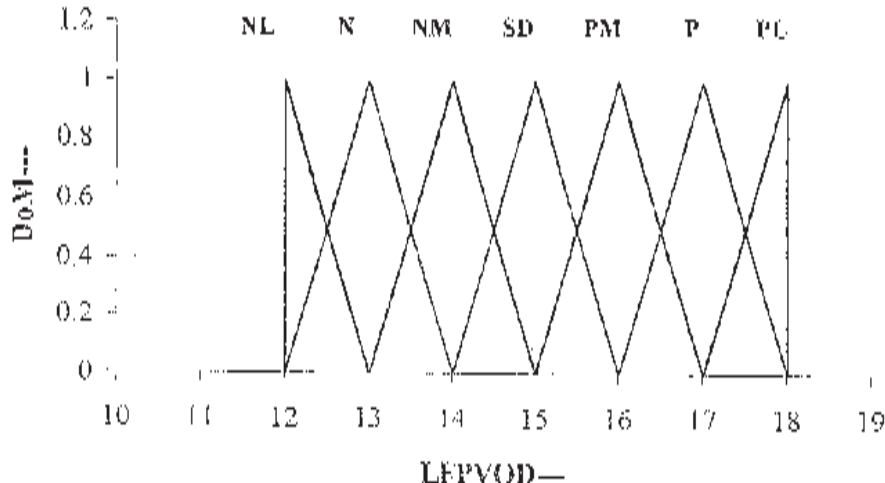
Fig. 2b. Membership Functions

2.2. Knowledge Representation

The knowledge pertaining to the pH control strategy is structurally formulated in terms of situation based action rules. These refer to the required information from database. The knowledge base is thus composed of rule-base and database[7,9-11].

2.2.1. Data-Base

'The database provides the required infqrmation kept in data-files to Fuzzification, Inference Engine and Defuzzification modules. This includes

- Membership functions representing the meaning of linguistic values of pH and Lime-Flow -Pipe-Valve-Opening (LFPVO) in mm.

- Labels of fuzzy sets representing linguistic variables.

- Operating ranges (Universe of Discourse) of linguistic variables.

Typical membership functions for pH are defined as follows[8,12,13]-

μ_{NL} (pH) = L(6.71,6.83); $\qquad$ μ_{N} (pH) = Λ(6.71,6.83,6.91);

μ_{NM} (pH)= Λ(6.83,6.91,7.10); $\qquad$ μ_{SP} (pH) = Λ(6.91,7.10,7.17)

μ_{PM} (pH) = Λ(7.10,7.17,7.21); $\qquad$ μ_{P}(pH) = Λ(7.17,7.21,7.33)

μ_{PL} (pH) = Γ(7.21,7.33)

Typical membership functions for Lime-Flow-Pipe-Valve-Opening (mm) are defined as follows-

μ_{NL} (LF) = L (12,13); $\qquad$ μ_{N}(LF) = Λ(12, 13, 14);

μ_{NM}(LF) = Λ(13,14,15); $\qquad$ μSD(LF) = Λ(14, 15, 16);

$\mu_{PM}(LF) = \Lambda(15, 16, 17);$ $Jlp (LF) = \Lambda(16, 17, 18);$

$\mu_{PL}(LF) = \Gamma(I7, 18)$

User can carry out the tuning of membership functions to suit well to his control policy.

2.2.2. Rule-Base

The control policy of pH control is formulated in terms of fuzzy inference rules[7-10,14,15]. These rules are either gathered from experienced buman operator or careful study of existing pH control systems. The rule-base thus represents the control strategy employed in the pH control. Typical set of rules is given in the Table-II. User can modify the rule-base to suit well to his control policy.
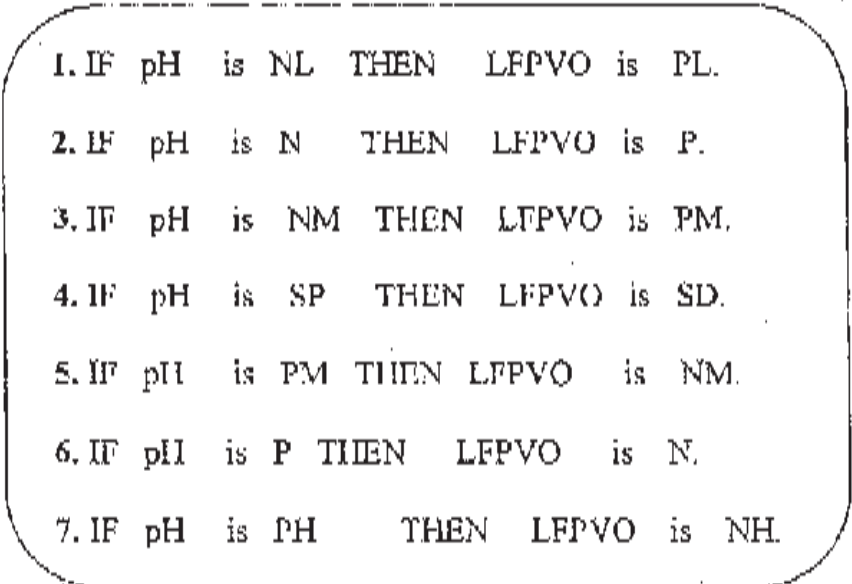
1. IF pH is NL THEN   LFPVO is PL.

2. IF pH is N   THEN LFPVO is P.

3. IF pH is NM THEN LFPVO is PM.

4. IF pH is SP   THEN LFPVO is SD.

5. IF pH is PM THEN LFPVO   is NM.

6. IF pH is P THEN   LFPVO   is N.

7. IF pH is PH   THEN   LFPVO is NH.

Table 2 : Set of Fuzzy action rules

The incoming pH-value from sensor fires the rules from rule-base, system then enter into the fuzzy inference process.

2.2.3. lnference- Engine

The inference scheme employed in pH control is based on individual rule firing of Mamadani type. In this scheme contribution of each rule is evaluated and overall decision is derived[7,8,10].

During inference process each rule is individually fired by a crisp value of pH coming from sensor and fuzzification module determines degrees of satisfaction of rules: This generates clipped fuzzy sets (CFS) representing opening of the valve for lime flow. The process of inference is illustrated in Fig.3.

2.2.4. Defuzzification

Defuzzification of clipped fuzzy sets generated in the fuzzy process yields the single crisp value of Lime-Flow-Pipe-Valve-Opening (mm) that represents the overall fuzzy outcome. Many defuzzification methods are available, however Height Defuzzification (HD) being computationally simple and fast is employed here[7-10,14,15]. The crisp rate of lime flow pipe valve opening is given by equation(*)[7,8].

$$
\textbf{LFPVO (mm)} = \frac{\sum\limits_{r=1}^{q} Pm^{(r)}, h^{(r)}}{\sum\limits_{r=1}^{q} h^{(r)}} \quad \text{--------------------} \quad (*)
$$

Where, $P_m^{(r)}$ = peak value of rth clipped fuzzy set, $h^{(r)}$ = height of rth clipped fuzzy set and q = number of fuzzy rules fired.

The process of HD is shown is illustrated in Fig.3. Defuzzified value of LFPVO works to keep the pH value of sugar juice to a target value.
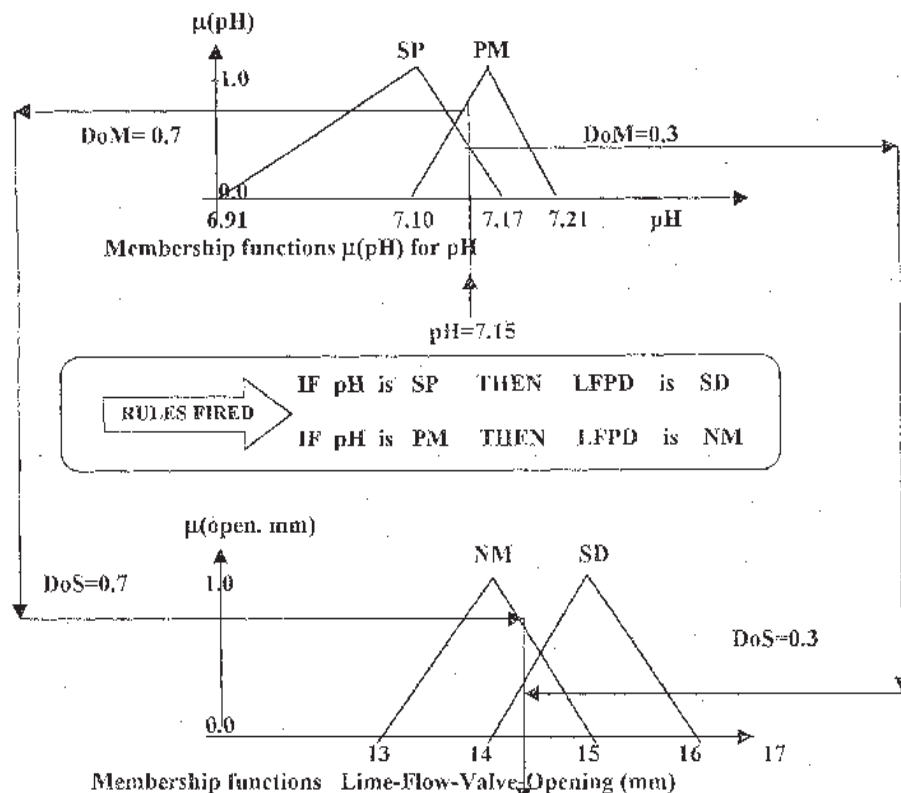

Fig.3. Inference Process and Defuzzification

3. SAMPLE RESULTS

Sample results are highlighted in Table-III. The modulation. of pH value adjusted by pipe valve opening diameter carrying the lime juice is shown in the Table-IV, followed by graphical variation of pH in the Fig 4. The loop of pH variation continuous till pH reaches to set value hence the control becomes smooth & robust. The main advantage of fuzzy pH control is that it doesn't required detailed mathematical model of pH controlling process to make stability. The results are good & it is expected to be better than those of conventional control method.

Parameter	Parameter values
1. Target pH	7.10
2. pH from Sensor	7.15
3. Rules fires	IF pH is SP THEN LFPVO IS SD with DoM = 0.3 IF pH is PM THEN LFPVO is NM with DoM 0.7
4. Defuzzified LFPVO	LFPVO = 14.3 mm
5. The New pH attained	7.13

Table 3. Sample results

No. of Iteration	Current pH	Modulated pH
1	6.80	7.31
2	7.31	6.81
3	6.81	7.27
4	7.27	6.95
5	6.95	7.05
6	7.05	6.98
7	6.98	7.09
8	7.09	7.10
9	7.10	7.10

*Table 4. pH modulation through Iteration*
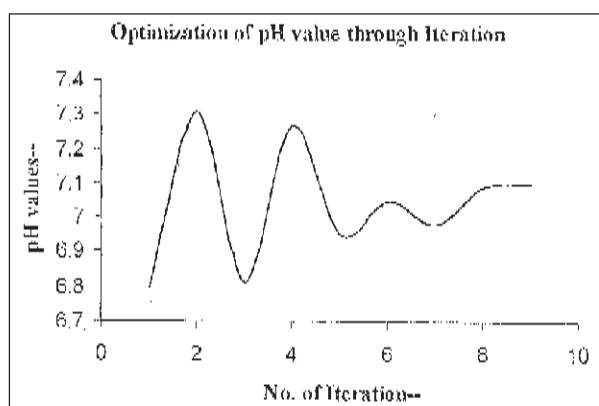
Fig.4 : Optimization of pH value through Iteration

REFERENCES

1. E. Hugot, "Handbook of Cane Sugar Engineering", (1972), Elsevier Publishing Company, New York, ch. 25, pp. 407-408.

2. P. Honing, "Principles of Sugar Technology", (1953), Volume-I,2, Elsevier Publishing Company, New York.

3. L. Foullay, S. Galichet, "Fuzzy Sensors For Fuzzy Control", Vol.2, No.1 (1994), 55-66.'

4. Editorial Staff, "Developments in process control and instrumentation in sugar in dustry", INT.SUGAR JNL., 2000, Vol. 102, No.1222.

5. M. Benn, B.Grondin-Perez, J.-D.Lan-Sun-Luk and J.P. Chabriat, "Modelling Cane Sugar vaporation and Crystallisation", J .of Indian Sugar,June,2000,pp.141-146

6. G. Eggleeston, "Hot and Cold lime clarification in raw sugar manufacture II: Lime addition and settling behaviour", INT.SUGARJNL., 2000, VOL. 102, NO. 122!.

7. G.J. Klir and B.Yuan, "Fuzzy Sets and Fuzzy Logic", (1997), Prentice-Hall of India, New Delhi, Ch.1, 12, pp.1-29, 327-339.

8. D. Driankov, H. Hellendoom and M. Reinfrank, "An Introduction to Fuzzy Control," (1996), Narosa Publishing House, New Delhi, Ch.I-3, pp.1-144.

9. K.Tanaka (Translated by T.Tiimira), "An Introduction to Fuzzy Logic for Practical Applications", (1996), Springer-Verlag, NewYork, Ch. l, 4, 5, pp.1-13, 81-86, 121-130.

10. R.R.Yager & D.P. Pilev, "Essentials of Fuzzy Modeling and Control", (1994), A Wiley-Interscience Publications, New York, ch.4, pp.109-148.

11. Parvati C.S. & Prahlad V., "Fuzzy Controller For A Separately Excited DC Motor", (1993), Proceedings of National Science Conference, IIT, Kanpur, India, pp.202-207.

12. K.C. Cheok, K. Kobayashi, S. Scaccia and G. Scaccia, (1996), "A Fuzzy Logic-Based Smart Automatic Windshield Wiper," IEEE Control Systems, pp.28-33.

13. R.R. Mudholkar, S.R. Sawant, G.G. Tengshe and AB.Bagwan, "Fuzzy Logic Transformer Design Algorithm (FLTDA)", (1999), Active and Passive Elec. Comp., Overseas Publishers Association. N.V., Vo1.22, pp.17-29.

14. E. Cox, "The Fuzzy Systems Handbook - A Practitioners Guide to building, using and maintaining Fuzzy Systems", (1998) AP-Professional, Boston, Ch.3,7,9, pp.45-469.

15. T. Terano, K. Asai and M. Sugeno, "Applied Fuzzy Systems," (1997), AP Professional, London, chap. 1, pp.1-7, ch.2,3, pp. 26-49, 51-56.

ANN CONTROLLERS FOR INDUSTRIAL TEMPERATURE CONTROL SYSTEMS

A.K. Goel, Manoj Kumar Sharma and Neeraj Gill
GZS College of Engg. & Tech., Bathinda - 151 001

ABSTRACT

Temperature control systems play an important role in the process industry. In this paper, Artificial Neural Network (ANN) controllers using multilayer perceptrons (MLPs) are designed for a simple water bath system and a Continually Stirred Tank Heater. Their performance is compared with the conventional feedback controllers (CFC) " with respect to set-point regulation, the effect of unknown disturbances and variable time delay in the systems. On comparison, the performance of neural network controller (NNC) is found better in tracking the reference than the CFC. From simulation results, it is concluded that the NNC outperform the CFC and offer a large scope in further advancement in the field of intelligent instrumentation.

I. INTRODUCTION

The conventional feedback controllers find wide applications in the process industry as they can be implemented very easily. However, to compensate for plant parameter variations and set-point changes etc., such fixed-gain feedback controllers are insufficient and need to be retuned. The massive parallel processing, nonlinear mapping and self-learning abilities of neural networks have been motivating factors for development of intelligent control systems[1]. The back propagation neural network based on the generalized delta learning rule, a gradient descent search technique, has been widely used. Yabuta and Yamada[2] proposed a neural control learning scheme where a neural network is trained to implement a non-linear optimum regulator by minimizing a quadratic cost function. Psaltis, Sideris, and Yamamura[3] designed a neural network controller using MLP. Narendra and Parthasarathi proposed an indirect inverse dynamics model learning approach.

The process control systems often exhibit some non-linearity and variations in their parameters due to noise, disturbances and *other* environmental factors making them difficult to control accurately. In this paper, two temperature control systems have been considered, namely; Water Bath Temperature Control System[5] and' Continually Stirred Tank Heater (CSTH)[6]. Neural Network Controllers (NNC) using MLPs are designed for both the systems and their performance is compared with the Conventional Feedback Controllers (CFC) with respect to set point regulation, the effect of unknown load disturbance and variable dead time in the system.

This paper is organized as follows: Section II includes a brief description of the water bath temperature control system and its CFC and NNC implementation. The CSTH and its NNC and CFC are described in Section III. The results obtained are then discussed in Section IV. Finally, the conclusions are drawn in Section V.
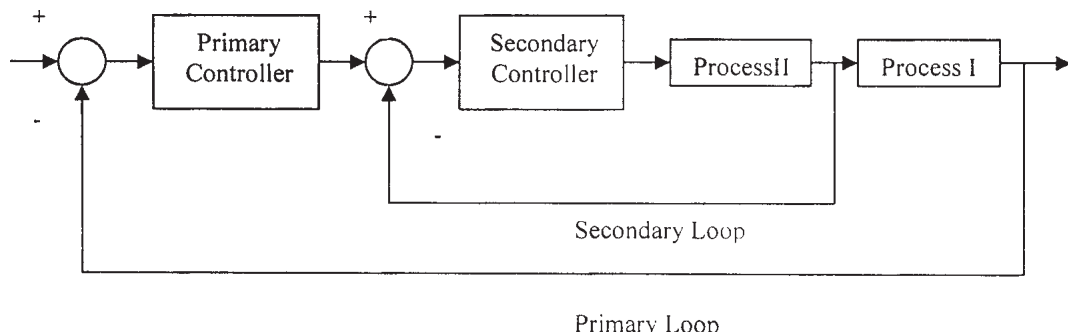

Fig.1. General Block Diagram of Cascade Control Scheme

2. WATER BATH TEMPERATURE CONTROL SYSTEM

The water bath system consists of a water tank in which cold water is entering from one side and heated water is leaving from the other. The capacity of water tank used is 12 liters. The water in the tank is heated by a 2500W base heater. A stirrer rotating at 120 rpm is used to ensure even temperature distribution. A transport delay 30 sec has been incorporated into the mathematical model of the system. The inlet water temperature is taken as 25°C. The volume of water is assumed to be constant and therefore, the inlet flow rate is equal to outlet flow rate and is maintained at 1 liter/min. It is further assumed that there is no change of state. The set point for output tank water temperature is equal to 40°C.

The equation defining the system is given below:

$$\frac{dT}{dt} = \frac{F}{V} * (Ti - T) + \frac{Q}{V * \rho * c_p} \tag{1}$$

where T and Ti are tank temp. and inlet temp., F is the water flow rate, V is the volume of the tank, Q is heat input, p and cp are the density and heat capacity of water respectively.

The CFC was implemented using MA TLAB and SIMULINK. The sampling time of 30 sec was used in the simulation. The initial values of K_p, K_i and K_d, the proportional, integral and derivative gain parameters of the CFC were calculated using Ziegler Nichols method[7] and were further tuned using hit and trial method. The final tuned values of K_p, K_i and K_d are equal to 1.5, 0.01 and 3.0 respectively.

For the NNC, thirty-five random combinations of plant inputs were generated and the response of the system was obtained for each combination. Eight samples at regular time intervals were taken from each response. Thus, a total of 280 training samples were generated to train the NNC.

A three-layered MLP was used to implement the NNe. The input layer consisted of 4 neurons, which account for the F, Ti, reference tank temperature and the delayed plant output. Ten neurons were employed in the hidden layer. One output neuron accounted for the lone output. Backpropagation learning algorithm was used to train the NNC8. The training was stopped once the sum squared error goal of 0.001 was achieved. The trained NNC was then configured as a direct controller to control the process.

3. CSTH TEMPERATURE CONTROL SYSTEM

The CSTH system consists of stirred tank heater, where the tank inlet stream is received from another process unit. The objective is to raise the temperature of the inlet stream to a desired value. A heat transfer fluid is circulated through a jacket to heat the fluid in the tank. It is assumed that there is no change of phase in either the tank fluid or the jacket fluid. The volume of water in the tank and the jacket is assumed to be constant. Therefore, the inlet and outlet flow rates are same. The tank and the jacket inlet temperatures are equal to $10^\circ C$ and $90^\circ C$ respectively. The objective is to attain the output tank temperature at $50^\circ C$.

The two equations for this system are obtained as:

$$\frac{dT}{dt} = \frac{F}{V} * (T_i - T) + UA * \frac{(T_j - T)}{(V * \rho * C_p)}$$

$$\frac{dT_j}{dt} = \frac{F_j}{V_j} * (T_{ji} - T_j) - UA * \frac{(T_j - T)}{(V_j * \rho * C_{pj})}$$

where T and Tj are tank and jacket temperatures, F and Fj are tank and jacket flow rates, Ti and Tji are the tank and jacket inlet temperatures, U is the overall heat transfer coefficient and A is the area for heat transfer, C_p and C_{pj} are the tank and the jacket heat capacities, ρ and ρ_j are the tank and jacket fluid density, Y and Yj are the tank and jacket volumes and t is time.

For this system, cascade control scheme, as shown in fig. I is used. In the control scheme, two PI controllers are used in cascade. The primary controller is used to set the reference point, Tj, for the secondary controller. The objective of the secondary controller is to attain the set Tj by manipulating Fj in the range 0 to 60 It./min. The cascade control scheme was implemented in MATLAB and SIMULINK. The sampling time of 6 sec was used in the simulation. The transfer functions used were obtained by linearizing the equations 2&3. The primary and secondary controllers were tuned by hit and trial method. The gain parameters for the two PI controllers thus obtained were as: primary controller $K_p = 2.3$ and $K_i = 0.0001$, secondary controller $K_p = 0.46$ and $K_i = 0.008$.

The NNC was implemented using the direct inverse model of the CSTH process. The equations of CSTH were solved using Runga-Kutta 4th order method. Thirty-five random combinations of plant inputs were generated and the system response was obtained for each combination using the numerical solution. Eleven samples at regular time intervals were taken from each response. Thus, 386 training samples were generated to train the NNC.
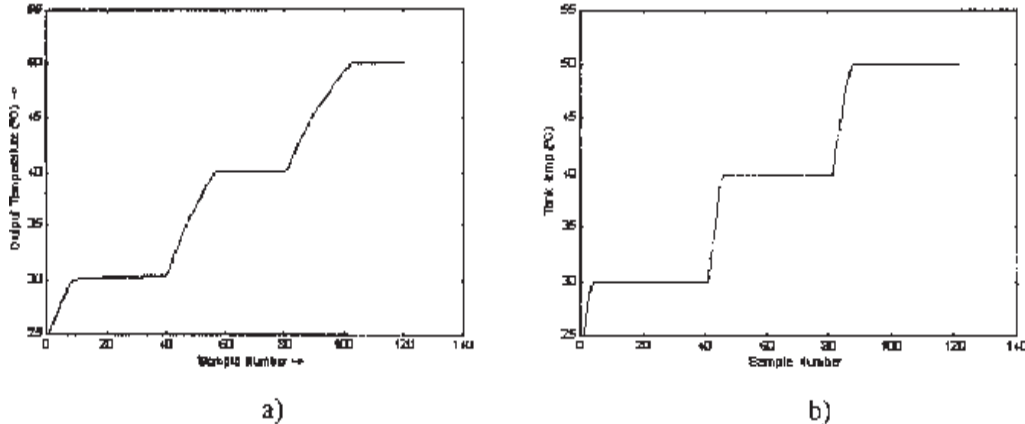
Fig.2. Multistep Tracking Performance a) CFC and b) NNC for Water Bath System

A three-layered neural network having 10 hidden neurons and two output neuron was used. The input layer consisted of 6 neurons to account for the inputs: F, Ti, Tji, tank reference temperature and previous tank and jacket temperatures. The backpropagation algorithm was used for training the controller. The learning rate was fixed at 0.0 I. The training was stopped once the sum squared error goal 0.001 was obtained. Then the NNC was configured as a direct controller to control the CSTH.

4. RESULTS AND DISCUSSION

Three sets of experiments were conducted on the processes. A multi-step reference was used to test the ability of the two controllers with respect to set point regulation. The ability of the controllers to withstand load disturbance was also tested. The last set of experiments was used to evaluate the performance of the two controllers with respect to variable dead time. It is pertinent to add that neither the NNC was re-trained nor the CFC was retuned for their performance comparison experiments.
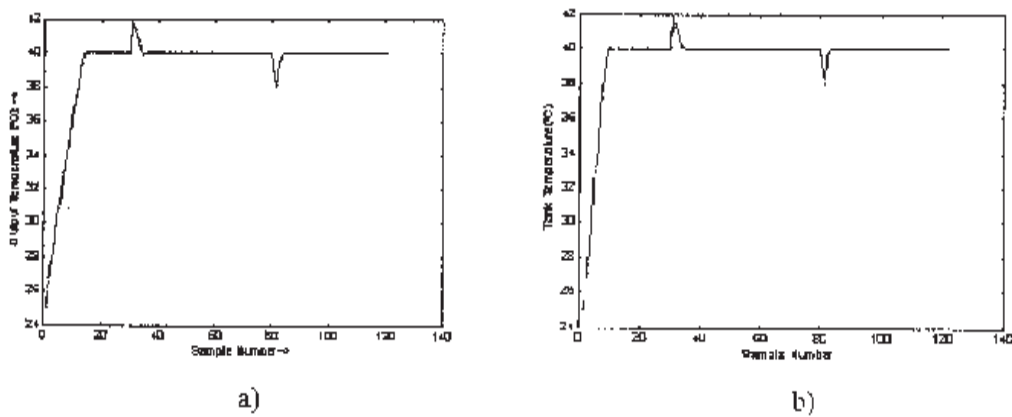

Fig.3. Disturbance Rejection Performance a) CFC and b) NNC for Water Bath System

a)   b)
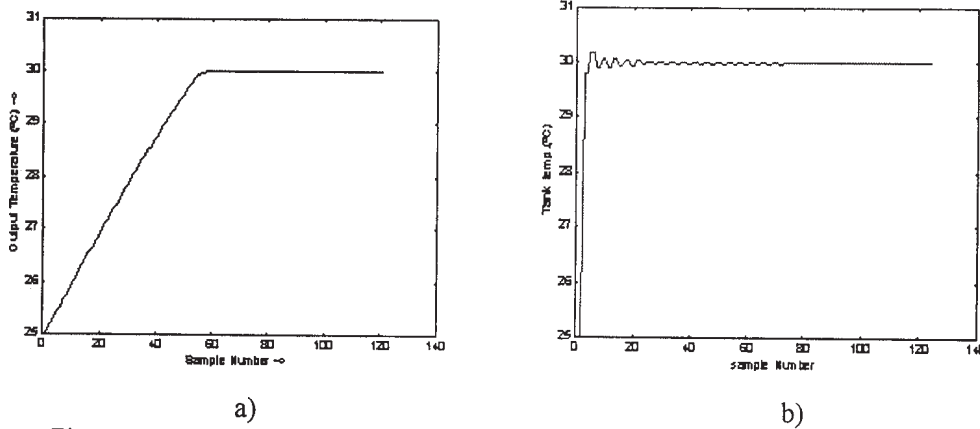
Fig.4. Variable Time Delay Performance a) CFC and b) NNC for Water Bath System

4.1. Water Bath Temperature Control System

The multi-step reference tank temperature was given over 120 samples; 30°C, 40°C and 50°C for 40 samples each. The tracking performance for CFC and NNC is shown in the fig.2a and 2b respectively. For disturbance rejection test, disturbances of 2°C and -2°C were added to the output at the 40th and 80th sampling instants resp. The response of both the controllers is shown in the fig.3a and 3b respectively. In the third set of experiments, a delay of two samples was incorporated. The response obtained for the CFC and NNC is shown in the fig. 4a and 4b respectively.

4.2. CSTH Temperature Control System

The multi-step reference tank temperature was given over 600 samples; 40°C, 45°C and 50°C for 200 samples each. The tracking performance for CFC and NNC is shown in the fig. 5a & 5b resp. For disturbance rejection test, disturbances of 2°C and -2°C were added to the output at the 150th and 350th sampling instants resp. The response of both the controllers is shown in the fig.6a & 6b resp. In the third set *qf* experiments, a delay of two samples was incorporated. The response obtained for the CFC and NNC is shown in the fig. 7a & 7b respectively.

It can be observed that the NNCs performed better for all the three sets of experiments. The NNC tracked the reference temperature and the rise time is considerably less as compared to CEC. The CFC performs poorly for the first set point in case of water bath temperature control system (figure 2). The CSTH PI controller tracks the last set point very well but fails badly in tracking first and the second set points (figure 5). The CFC actually needs to be retuned. The NNC once trained, does not require to be trained again. The NNC and CFC showed comparable performance in load disturbance rejection in Water Bath System (figure 3) but for CSTH (figure 6), the NNC outplays the CFC. The CFC performed poorly. The performance comparison with respect to variable delay also re-affirms the superiority of the NNC over the CFC (figure 4 and 7).

5. CONCLUSION

Two control systems for temperature regulations of Water Bath and Continually Stirred Tank Heater (CSTH) have been implemented. The CFC scheme is found to be simple to implement but performs poorly with respect to set-point regulation, disturbance rejection and variable time delays. Neural Network based controller performed far better and therefore it is concluded that they offer a large scope in further advancement in the field of intelligent instrumentation.

ACKNOWLEDGEMENT

REFERENCES

1. White, D.A. and D.A. Sofge. 'Handbook of intelligent control', Van Nostrand Reinhold, New York, (1992).

2. T. Yabuta and T. Yamata, 'Learning control using neural networks', *proc.* 1991 *IEEE Int. Conf. Robotics Automation,* Sacramento, CA, (1991).

3. D. Psaltis, A. Sideris, and A. Yamamura, 'A multilayered neural network controller', *IEEE control Syst. Mag.,* **10***,* no.3, 44-48, (1989).

4. K.S. Narendra and K. Parthasarathy, 'Identification and control of dynamical systems using neural networks', *IEEE Trans, Neural Networks,* **1,** 4-27, (1990).

5. Sigeru Omatu, Marzuki Khalid and Rubiyah Yusof, 'Neuro-Control and its Applications', Springer-Verlag London' Limited (1996).

6. A.K. Goel and Surekha Bhanot, 'Modeling of Continually Stirred Tank Heater with ANNs using Successive Over-Relaxation Back propagation Algorithm', *Asian Control Conference ASCC 2002,* Singapore, 614-617, (2002).

7. Ogata, K., 'Modem Control Systems', Third Edition, Prentice-Hall, Englewood Cliffs New Jersey, (1998).

8. A.K. Goel and Surekha Bhanot, 'Successive Overrelaxation Back Propagation Algorithm for ANN Training: A Simulation Study', *Int. Conf. on Computer Applications in Electrical Engg., IIT Rorkee,* 245-249, (2002).

A DIGITAL MICROMANOMETER FOR VERY LOW PRESSURE MEASUREMENT

Achanta Ramakrishna Rao

Dept of Civil Engg, Indian Institute of Science, Bangalore - 560 012

ABSTRACT

A highly sensitive micromanometer to measure low differential pressure heads is developed. It works on capacitance principle by which it measures the air gap, up to 2mm with an accuracy of 0.001 mm, between either a mercury meniscus or a metallic float and a sensing element with an accuracy of 0.00l mm. The movement of mercury meniscus or a metallic float is due to the applied differential pressure in the manometer circuit. It has a digital display and can be connected to a computer through a data acquisition system for continuous recording of data. It can be used either for water or air as experimental fluids. Also, it is easy to operate and maintain as well as reasonably very economical too; and ideally suited for Indian conditions. It has applications in hydraulic and aerodynamic laboratories, especially useful in the measurement of water surface elevations in open-channels and velocity profiles in boundary layers. Four models with different measurement accuracies of pressure head are presented which show that the measurement accuracy of the pressure head can be achieved from 0.0011mm to 0.0175mm and cover the ranges up to 2.2mm to 35 mm of water head.

1. INTRODUCTION

In experimental investigations either in hydraulic or aerodynamic laboratories measurement of small pressure variations with high accuracy is extremely important. For example the measurement of water surface elevations along the flow direction in an open-channel and the measurement of local velocities along the flow depth or boundary layer thickness as well as the measurement of relatively small pressure drops over a pipe flow are some of the challenging tasks in laboratories. Generally the magnitude of water surface slopes could be in the order of about 10^{-4}, thus the water surface drop over a distance of a meter length is only one-tenth of a millimeter. Many times the local or point velocities along the flow depth in an open channel or even in pipes are to be measured at least with an accuracy of $v = 1$ cm/s and this is to say that the velocity head ($v^2/2g$) could be about 0.005 mm of water. Hence such measurements demand very high accuracy. Thus, while investigating the fluid flow behavior either in open channels, pipes or wind tunnels, micro-manometers are essential to measure such small pressure heads with high accuracy. The author of this paper has faced such a serious problem in his experimental research, which had prompted him to develop couple of micro-manometers to meet such measuring requirements.

Such low differential pressures are often measured with a V-tube using suitable manometric liquids, whose density is very close to that of the working or experimental fluid. Micromanometers using two manometric liquids, which are immiscible and whose densities are close to each other (Brow & Schwertz, 1947; Streeter & Wylie, 1979) are often used for such measurements. To improve the sensitivity of the manometers, inclined manometers are often preferred to vertical limb manometers although these manometers have their own limitations in use. For instance, even a small change in the difference of densities of the manometric liquids is likely to cause significant variation in the measurement of head in differential liquid density manometers. Also, it is experienced that the response of such manometers are slow and sluggish. Inclined manometers cannot be effectively used below about 10° of inclination to the horizontal plane because of difficulties in reading and of possible errors due to the alignment of the manometric tube itself.

Many types of other sensitive manometers given in literature are often delicate, difficult to make and maintain. A highly sensitive tilting gauge capable of reading 2.5×10^{-4} cm of water called Chattock tilting gauge was in use and it was later modified by Duncan (1927), Ower and Pankhurst (1966) and Pankhurst and Holder (1968). Other types of sensitive manometers with zero adjustment of the indicator, were developed by various investigators. They generally consist of a reservoir with a plunger, an inclined sight tube and a vernier arrangement. A manometer developed by Hodgson (1929) with such an arrangement was found to be ten times more accurate than the Chattock gauge. Later, Macmillan (1954) and Smith & Murphy (1955) also developed similar manometers with certain improvements. The manometer showed an accuracy of $\pm 2 \times 10^{-4}$ inch ($\pm$ 0.005 mm) of water for differential pressures of less than 0.8 inch (20 mm) of water. Stalhane (1934) developed yet another null-type manometer using two different-sized horizontally kept cylindrical vessels containing alcohol. The smaller vessel contains an air bubble (which is like an air bubble in spirit level), which is used as an indicator. This manometer was designed for field use and it has an accuracy of 0.01 mm of water. Some others used flexible bellows in the manometer, whose sensitivity was comparable to the Chattock gauge.

While reviewing the various types of sensitive micro-manometers one may come to a conclusion that they still have certain limitations. A major limitation in a null-type manometer is its cost particularly because of the accessories attached to it. For example, in the Chattock gauge one needs a powerful microscope and a fine wheel vernier to keep the oil film back to the zero position. When a microscope is used, however, there appears to be of no need for a tilting arrangement or even the oil film because the traveling microscope attached with a fine vernier can itself measure small differential heads directly on a simple V-tube manometer or a piezometer. The Chattock gauge has certain serious limitations that the oil film may break during its operation and restoring the film is a tedious job; also, it has a delicate glass work and also the maintenance required like cleaning etc. is not easy. The modified Chattock gauge looks attractive due to the mobility of the air bubble, which was used as an indicator (with xylol as the manometric fluid), instead of the middle cup or bulb of the Chattock gauge. However the other limitations are not avoided also the flow past the air bubble is possible particularly when there are fluctuations in applied pressures because the air bubble is easily susceptible to change of shape.

Most of the manometers mentioned above find their best use with air as the working fluid. For measurements with water, however, several problems may arise when these manometers are used. F or example, in open channel flow experiments, it is likely that the water (working or experimental fluid) used may not always be pure and may slowly contaminate the whole manometric system. Also these manometers are either too rigid or too delicate to facilitate day-today operation and maintenance.

It is therefore essential to have a manometer which is highly sensitive, simple in operation and maintenance, and easy in fabrication. Keeping these in view, a high sensitive liquid bubble manometer for measuring low differential heads, primarily intended for use in open channel flow, has been developed by Rao (1979). It can also be seen in reference, Rao and Vedula (1981). It has a built-in calibration facility and can be used to measure differential pressure heads up to a maximum of 20 mm with an accuracy of 0.0-1 mm of water. The liquid bubble consists of two miscible liquids, viz. benzaldehyde and normal hexane (each of which is immiscible in water) in such a proportion that the bubble density is very close to that of water density. The liquid bubble, which occupies the full cross sectional area of the glass tube containing the water, traverses in a glass tube in proportion to the differential pressure applied. This too has the following minor limitations: The density of the liquid bubble must be carefully maintained within ±2% of the density of water and the liquid bubble has to be frequently replaced. Water in the manometer should be chemically clean. The major advantage of this manometer is its cost and accuracy in measurement. It hardly costs few hundred Indian rupees at present and easy to fabricate and use, however it has a serious disadvantage of slow in operation as its response to pressure variations is slow and normally takes about 5 minutes time to record a single reading.

Due to the advancements in present day technology, pressure transducers, hot wire/film anemometers, laser Doppler anemometers etc., are extensively used for measuring small pressure/velocity heads. But these instruments are prohibitively expensive for Indian conditions. Hence there appears to be a need to develop a simple economical and quick responsive micro-manometer to satisfy the modern needs. Such a manometer, which works on capacitance measurement principle is developed and presented here. The manometer quickly senses the applied pressures and displays the corresponding reading digitally. It is capable of measuring pressure heads up to a maximum of 2mm of mercury, with a resolution of 0.0-01 mm. It can be attached to a computer through a data logging system for continuous monitoring/recording of the data.

2. DESCRIPTION AND WORKING PRINCIPLE

The micromanometer as a unit consists of three major components, namely: manometer circuit, capacitance transducer and governing equation or working principle. They are described here.

2.1 Manometer Circuit : The micro-manometer consists of four interconnected cylindrical glass sumps, S_1, S_2, S_3 and S_4 as shown in Fig. 1. All the sumps are of uniform cross-sectional areas of A_1, A_2, A_3 and A_4 respectively. The sumps S_1 and S_2 as well as S_4 and S_3 are connected at their bottom where as the sumps S_2 and S_3 are connected at the top as shown in Fig. 1. The sumps S_1 and S_2 and the sumps S_3 and S_4 are filled with heavier liquids
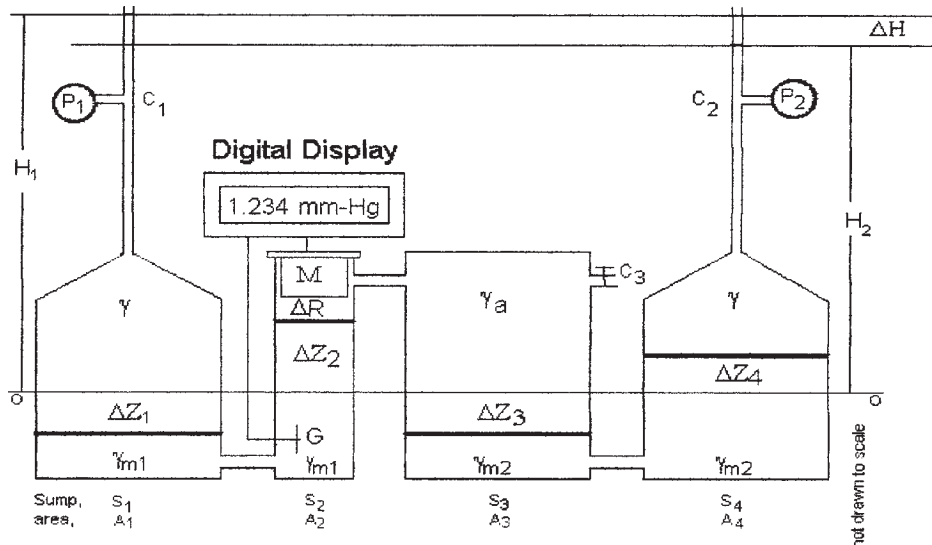
Fig.1. Schematic Diagram of Micromanometer

of unit weights γ_{m1} and γ_{m2} respectively. Air of unit weight γ_a, is trapped on the top of the sumps S_2 and S_3. Let the levels of manometric fluids stand at a datum of 0-0, before the application of differential pressure as shown in Fig. 1. The cocks C_1, C_2 and C_3 can be used appropriately to induct sufficient quantities of manometric fluids and to apply differential pressures as well as to remove any air bubbles in the experimental fluids. The sump S_1 is connected with a higher pressure P_1, where as the sump S_4 is connected with a lower pressure of P_2. Thus the applied differential pressure head is,

$$\Delta H = H_1 - H_2 = (P_1 - P_2)/\gamma \qquad (1)$$

Where, γ is the unit weight of the experimental fluid. The micromanometer is expected to measure and display the differential pressure head, ΔH with highest possible accuracy.

A probe, M, which measures the air gap, ΔR, between the mercury meniscus and itself, is rigidly fixed at the top of the sump S_2 such that there is free communication of pressure through air in the sumps S_2 and S_3. However, sufficient gap is provided between the level 0-0 and the probe M to facilitate a free vertical movement of mercury level as per the applied differential pressure intensity. In the present arrangement the maximum gap provided is 2mm. It may be noted that a metallic float can be used in place of mercury meniscus in sump S_2, the details of which are explained later in this paper.

2.2. Capacitive Transducer : A precise displacement measuring device based on variable capacitance principle with a non-contact type transducer is developed and used to measure the air gap, ΔR in the sump, S_2. The capacitance between two parallel conductive plates in an electrical circuit varies with the distance between the plates in a fixed relation to the change in distance. The main innovations in this component are to make use of either (i) mercury meniscus as a moving plate (grounded through G for the purpose) in capacitance circuit, or (ii) a metallic float as a moving plate in some other occasions (not shown in Fig. 1), with

view to measure accurately and display digitally the air gap, ΔR between a fixed plate (the probe, M) and the movable plate (either a mercury meniscus or a metallic float), which moves because of the applied differential pressure head, ΔH.

The capacitance between the transducer and the mercury is detected and compared with a fixed capacitor in a detector circuit. The output of the detector circuit is fed to an AC-DC converter circuit, and then passes through several filter stages. A stable DC output is obtained at the last stage. This DC voltage is fed to a digital display, which displays the distance between the transducer and mercury meniscus directly in mm. Block schematic diagram of the instrument is shown in Fig. 2. The signal output can be connected to a computer through a data acquisition system for a continuous recording of data. Turbulent fluctuations in the experimental fluid flow are expected to transmit through the manometric circuit and finally in to the signal output. Hence, provisions are made in the circuit to suppress such minor and continuous fluctuations in the signal to get a stable readable display.

Signal Input	Detector	AC-DC converter	Filter Amplifier	Output
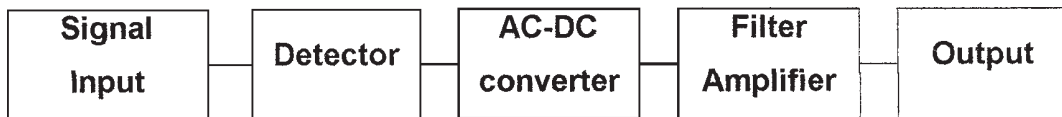
Fig.2. Block Schematic Diagram of Signal Processing

The capacitive transducer thus developed has a range of up to 2 mm and a resolution of 0.001 mm. It may be noted that the range of measurement can be increased by increasing the cross sectional area of the probe M, as well as the cross-sectional area of the sump, S_2 according to capacitance principle. The operating range of temperature is 8$^{\text{o}}$C to 40°C.

2.3 Working Principle : Due to the application of differential pressure, the level of manometric fluid (of unit weight γ_{m1}) in sump S_1 lowers by a distance of ΔZ_1 where as its level in sump S_2 rises by ΔZ_2 compared the datum O-O. As a consequence, the levels of the manometric fluid (of unit weight γ_{m2}) in sumps S_3 and S_4 have to under go a similar change such that it lowers by ΔZ_3 and rises by ΔZ_4 in the respective sumps. By assuming all the manometric fluids including air are incompressible, the volumetric displacement in each of the sumps is the same, hence the following expression is valid.

$$A_1\Delta Z_1 = A_2\Delta Z_2 = A_3\Delta Z_3 = A_4\Delta Z_4 = \text{a constant} \qquad (2)$$

Where, A_1, A_2, A_3 and are the cross-sectional areas of the sumps S_1, S_2, S_3 and S_4 respectively. The following general expression or governing equation can be derived for the differential pressure head, ΔH in terms of water, while balancing the pressures at various levels in the manometer circuit.

$$\Delta H = \Delta Z_2 \left[(\gamma_{m1}-\gamma_a)/\gamma_w+(A_2/A_1)(\gamma_{m1}-\gamma)/\gamma_w+(A_2/A_3)(\gamma_{m2}-\gamma_a)/\gamma_w+(A_2/A_4)(\gamma_{m2}-\gamma)/\gamma_w\right] \quad (3)$$

Where, γ_w is the unit weight of water. (One may prefer to express the differential pressure head, ΔH in terms of mercury then unit weight of mercury, Ym, has to be used in place of γ_w). The value of terms inside the square brackets is called as the 'manometer constant', C_M and hence Eq.3 can be expressed as follows:

$$\Delta H = C_M\Delta Z_2 \qquad (3a)$$

The probe M measures the air gap, AR, between the mercury meniscus and itself, as shown in Fig. 1. It may be noted that as ΔR reduces there is an increase in ΔZ_2 and vice versa and thus there exists a direct relation between ΔZ_2 and ΔR. Therefore, one may say that the capacitive transducer measures indirectly the relative changes in ΔZ_2 with an accuracy of 0.00 1mm for a range up to 2mm.

3. MODELS OF MICROMANOMETERS

It may be appropriate to mention here that: lesser the value of C_M then the measurement accuracy of ΔH is higher, however the range of ΔH is reduced; the reverse is also true such that the range of ΔH can be increased by increasing the value of C_M however the accuracy of ΔH measurement decreases. Above Eq.3 is the general or governing equation of the micro-manometer as shown in Fig.l and such an equation can be used to develop several models of micro-manometers with different values of CM with certain relative technical and economic advantages. Four of such models are discussed here under the common conditions of $A_1 = A_3 = A_4 = A$, $A_2 = a$, a/A = 0.l; and ΔZ_2 is measured with an accuracy of 0.00l mm and its range is up to 2mm.

3.1. First Model : In this model mercury is used as manometric liquid in all the sumps, thus $\gamma_{ml} = \gamma_{m2} = \gamma_m$, the unit weight of mercury. Also the cross-sectional areas of the sumps S_1, S_3 and S_4 are equal to A i.e., $A_1 = A_3 = A_4 = A$, where as the sump S_2, containing the probe M, is of a relatively smaller cross sectional area, $A_2 = a$. The unit weight of air in sump S_2 and S_3, at their top, is Ya. In this model both water and air can be used as experimental or working fluid. If water is taken as the experimental fluid (then $\gamma = \gamma_w$, unit weight of water), and a governing equation for this model can be deduced from Eq. 3, as

$$\Delta H = \Delta Z_2 \ [(l+a/A)(\gamma_m-\gamma_a)/\gamma_w + (2a/A)(\gamma_m/\gamma_w-1)] \tag{4}$$

The usefulness of the above equation can best be illustrated by using certain numerical values. Thus, by taking values of a/A=1/10, γ_m=13.6 gmf/cm^3, γ_w=1 gmf/cm^3 and γ_a = 1.2x10^{-3} gmt/cm^3, the value of manometer constant, C_M = 17.48, which is the value of the terms inside the square brackets of Eq.4. As ΔH_2 is measured with an accuracy of 0.00l mm, the differential head, ΔH can be measured with an accuracy of 0.01748 mm of water head, or about 1. 69 micro bar. This is reasonably a sufficient accuracy of measurement for most problems (with low pressure heads) in pipe and open-channel flow experiments. As the design value of ΔZ_2 is up to a maximum of 2mm, the range of the differential head ΔH that can be measured in this model is up to 35 mm of water head with an accuracy of 0.01748 mm. In general, the measurement accuracy of ΔH can be increased, by decreasing the value of a/A; where as the range of ΔH decreases.

It may be noted here that air can be used as experimental fluid ($\gamma = \gamma_a$) instead of water. An appropriate equation similar to Eq. 4 can be derived from the general Eq. 3, as

$$\Delta H = \Delta H_2 \ [(1+3a/A)(\gamma_m-\gamma_a)/\gamma_w] \tag{4a}$$

The major advantage of the first model is such that the turbulent fluctuations in the experimental fluid are significantly dampened due to the presence of heavier manometric fluid of mercury in all the four sumps and hence the signal output (as seen in the digital display) is stable. The major disadvantage is the increased cost of the manometer due to large amounts

of expensive mercury in all the four sumps. It may be noted that about 2 to 3 kgf of mercury is required (for a/A = 0.1) for the manometer shown in Fig. 1. It is experienced that the cost of the mercury itself is about 25% of the total cost of manometer in this model. In the next models attempts are made to reduce or totally avoid the use of mercury in the sumps there by reducing the cost of making the micro-manometers.

3.2 Second Model : In this model the usage of mercury is reduced to half when compared to the first model. Here, mercury is avoided in the sumps, S_3 and S_4 by allowing the experimental fluid itself to get filled in those two sumps. Except this change, all are kept identical to the first model. Hence by making use of $\gamma_{ml} = \gamma_m$ and $\gamma_{m2} = \gamma_w$, the following governing equation for this second model is obtained, when water ($\gamma = \gamma_w$) is used as the experimental fluid, as,

$$\Delta H = \Delta Z_2 \ [(1+a/A)(\gamma_m - \gamma_a)/\gamma_w] \tag{5}$$

By taking values of a/A=1/l0, γ_m=13.6 gmf/cm^3, γ_w=1 gmf/cm^3 and γ_a =1.2x10^{-3} gmf/cm^3 the value of manometer constant is, C_M =14.96. The accuracy of ΔH measurement is =0.01496 mm of water head and its range is up to a maximum of about 30mm. The second model is more economical than the first model because of the reduced quantities of mercury. Also there is a slight improvement in the measurement accuracy of ΔH. In this model too air can be used as an experimental fluid ($\gamma = \gamma_a$) instead of water and in such a case the following governing equation, similar to Eq.5, is derived from Eq.3.

$$\Delta H = \Delta Z_2 \ [(I+a/A)(\gamma_m - \gamma_a)/\gamma_w + (2a/A)(\gamma_w - \gamma_a)/\gamma_w] \tag{5a}$$

3.3 Third Model : This is a very interesting model because the mercury is totally avoided in all the sumps. It contains only water and air, and one can consider it as an inverted air manometer, however with a difference that a metallic float is used in Sump S_2. The probe M and the metallic float forms a capacitance in which M is a fixed plate where as the float is a movable plate and its movement is due to the pressure changes. Thus in this model, $\gamma_{ml} = \gamma_{m2} = \gamma = \gamma_w$ and substituting them in Eq. 3, the governing equation for the third model, for water as the experimental fluid, is obtained as follows.

$$\Delta H = \Delta Z_2 \ [(1+a/A)(\gamma_m - \gamma_a)/\gamma_w)] \tag{6}$$

By taking the usual values of a/A = 0.1 and γ_a/γ_w = 1.02x10^{-3}, the manometer constant, C_M = 1.1. Hence the sensitivity of the instrument is 0.0011 mm or 1/909th of mm of water head (because, like in all the models, ΔZ_2 is measured with an accuracy of 0.001 mm.). Even though it has remarkably a very high accuracy but the range of ΔH is limited only to 2.2mm of water head because the maximum range of ΔZ_2 is 2mm. It is of importance to note that, in this model while using water as the experimental fluid, cross-sectional areas of the sumps S_1 and S_4 have no consequence (as they are filled completely with water); however, cross sectional areas of the sumps, S_2 and S_3 can effect significantly the accuracy and range of ΔH measurement. Also, on many times a higher range of ΔH is desirable at the expense of a lower accuracy. This can be achieved by increasing the value of alA i.e., the ratio of cross-sectional areas of sumps S_2 and S_3 such that a>>A (It may be noted that A>>a in the previous models). For an example, if *a/A* = 10, the manometer constant C_M becomes 11 and thus the accuracy of measurement of ΔH is now reduced to 0.0l1mm and its range is increased to

22 mm of water head. This model is the most economical when compared to all other models because mercury is totally avoided. However, pressure fluctuations are relatively more in this model and some special techniques have to be adopted in the manometer -circuit to suppress such fluctuations.

In this model too, air can be used as the experimental fluid instead of water. Hence by making use of the conditions $\gamma_{ml} = \gamma_{m2} = \gamma w$; $\gamma = \gamma_a$ and as usual $A_1 = A_3 = A_4 = A$ and $A_2 = a$ in Eq. 3, the following equation can be obtained for air as the experimental fluid for the third model.

$$\Delta H = \Delta Z_2 \ [(1+3a/A)(1 - \gamma_a/\gamma_w)] \tag{6a}$$

3.4. Fourth Model: In this model the micro-manometer is used as a 'piezometer' to measure a single pressure P_1 only, instead of measuring a differential pressure heads like in the previous three models. This model is useful only when the pressure head, P_1/γ is relatively small. In this model, only the sumps S_1 and S_2 are only used and the remaining two sumps are not needed in the manometer-circuit. However, the sump S_2 (which contains the probe, M) is open to atmosphere. In this model also, either air or water can be used as an experimental fluid. Thus, the governing equation for this model with water as the working fluid can be obtained by making use of the conditions of $\gamma m1 = \gamma m$, $\gamma = \gamma w$ and as usual the geometric conditions $A_1 = A_3 = A_4 = A$ and $A_2 = a$ in Eq. 3, as,

$$\Delta H = \Delta Z_2 \ (\gamma_m/\gamma_w + (a/A)(\gamma_m/\gamma_w-1)] \tag{7}$$

Hence, the manometer constant, CM is about 14.86 when, γ_m=13.6 gmf/cm^3, $\gamma_w = 1$ gmf/cm^3 and a/A = 0.1. As ΔZ_2 is measured with an accuracy of 0.001, the accuracy ΔH measurement is about 0.01486 mm and its range is about 29.72 mm of water head.

The following equation can be obtained if air is used the experimental fluid instead of water in the fourth model.

$$\Delta H = \Delta Z_2 \ [\gamma_m/\gamma_w + (a/A)(\gamma_m-\gamma_a)/\gamma_w] \tag{7a}$$

4. CALIBRATION

The working principle of the micro-manometer is verified with Eq.7 of the fourth model with mercury and water as manometric and experimental fluids respectively by conducting a calibration test. The head H_1 is varied in steps by adding water in to the glass tube of the sump and the corresponding display reading of the capacitance manometer (ΔR in Fig. 1) is noted. The water level in the glass tube from the sump S_1 is noted by using a powerful traveling microscope with a least count of 0.01 mm. Sumps S_1 and S_2 are made out of glass with internal diameters of 63mm and 28 mm respectively. Therefore, a/A = 0.1975 and from Eq.7, C_M=16.09. A plot between the display reading of the manometer and the head All measured by a traveling microscope is shown in Fig. 3. The data points fall on a linear line with a slope of 16.83 suggests that the manometer is working very well as per the principle. However, theory suggests $C_M = 16.09$, where as from calibration it is obtained as 16.83, thus there is a variation in the manometer constant. Such a variation is generally expected and it is attributed mainly due to functioning of the capacitive transducer it self. Also it is due to some variations in unit weights of liquids and variation in the sump diameters as well as their verticality, which

can affect directly the value of a/A. Thus the micromanometer is working very well and serving the purpose of low-pressure measurements.
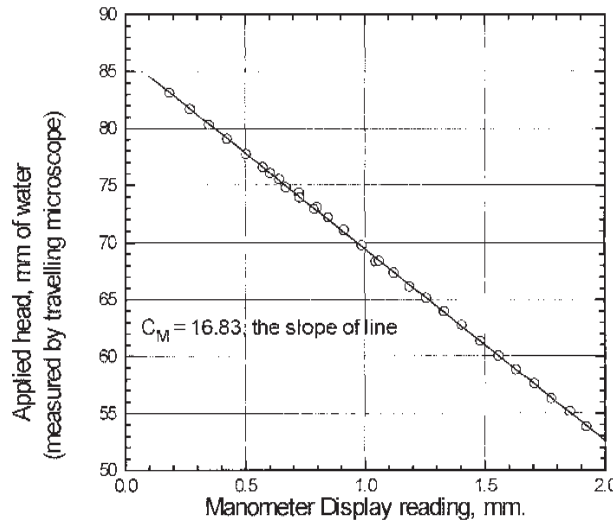

Fig.3. Calibration of Micromanometer

5. RESULTS

A digital micromanometer for low differential pressure heads is developed, as shown schematically in Fig.1. It contains three major components namely: (1) 'manometer circuit' - it is conveniently designed to use either water or air as experimental fluid; (2) 'a capacitive transducer' - the main innovations in this component are either to make use of (i) mercury meniscus as a moving plate in capacitance circuit in some models (1st, 2nd and 4th models), or (ii) a metallic float as a moving plate in some other models (3rd model) with a view to measure accurately and display digitally the air gap, ΔR between the fixed plate (probe, M) and the movable plate (either mercury meniscus or metallic float), which moves because of the applied differential pressure head, ΔH and (3) 'a general equation governing the working principle' as given in Eq.3, connecting the functioning of components (1) and (2).

Several types of micro manometers can be designed from Eq.3, however, for sake of illustration some models are discussed and presented in Table 1 by assuming the following conditions: $A_1 = A_3 = A_4 = A$, $A_2 = a$, and $\Delta R = 0.1$; and ΔR (indirectly the ΔZ_2) is measured by the capacitance circuit with an accuracy of 0.00lmm and its range is up to 2mm.

6. CONCLUSIONS

A micro-manometer, which works on capacitance principle is developed and presented. It has a direct digital display with a provision to monitor continuous monitoring of data. It can be used to measure differential pressures with either air or water as the experimental fluids. Four different models of micromanometer, are presented for use under different conditions along with their economy for a real use. The working principle of the manometer is verified by conducting a calibration study.

Model	Exptl. Fluid	The manometric fluids of unit weights in Fig. 1 are to be replaced by the following			Model Equation	C_M	Measurement of ΔH, mm of water head	
		γ	γ_{m1}	γ_{m2}			Accuracy (mm)	Range (mm)
1A	water	γ_w	γ_m	γ_m	Eq.4	17.48	0.01748	34.96
1B	air	γ_a	γ_m	γ_m	Eq.4a	17.68	0.01768	35.36
2A	water	γ_w	γ_m	γ_w	Eq.5	14.96	0.01496	29.92
2B	air	γ_a	γ_m	γ_w	Eq.5a	15.16	0.01516	30.32
3A	water	γ_w	γ_w	γ_w	Eq.6	1.10	0.00110	2.20
3B	air	γ_a	γ_w	γ_w	Eq.6a	1.30	0.00130	2.60
4A	water	γ_w	γ_m	--	Eq.7	14.86	0.01486	29.72
4B	air	γ_a	γ_m	--	Eq.7a	14.96	0.01496	29.92

Note: The notation: $\gamma_m = 13.6$, $\gamma_w = 1$ and $\gamma_a = 0.0012$ gmf/cm^{3}are unit weights of mercury, water and air respectively: It is assumed that $A_1 = A_3 = A_4 = A$ and $A_2 = a$; $a/A = 0.1$ and ΔR (or ΔZ_2) is measured with an accuracy of 0.001 mm and its range is up to 2mm.

Table 1. Some Models of Micromanometers and their Resolutions/Accuracy, Range of Measurement

NOTE: A patent is pending on the product of digital micromanometers developed and presented in this paper. Those who are interested are advised to contact the author for more details.

REFERENCES

1. Brow, J.E., and Schwertz, F.A, 'A simple micromanometer', *Rev.* Sci. *Instrum.* Vol. 18, pp.183,(1947)

2. Duncan, W.J, 'On a Modification of the Chattock Tilting Pressure Gauge, Designed to Eliminate the Change of the Zero with Temperature', l Sci. Instrum., V. 4, pp. 376. (1927)

3. Hodgson, J.L., 'A Sensitive Micromanometer', J. Sci. Instrum., Vol. 6, pp. 153. (1929)

4. Macmillan, F.A, 'Liquid Manometer with High Sensivity and Small Time-lag', J.Sci. Instrum., Vol. 31, pp. 17. (1954).

5. Ower E and Pankhurst R C *Measurement of Air Flow,* 4th ed., Oxford: Pergamon Press, (1966)

6. Pankhurst, R.C. and Holder D.W., *'Wind Tunnel Technique',* London: Sir Isaac Pitman, (1968)

7. Ramakrishna Rao, A, *'Seepage Effects on the Resistance Characteristics of Sand Bed Channels',* Ph.D. Thesis, Indian Institute of Science, Bangalore. (1979)

8. Ramakrishna Rao, A. and Vedula, S., "Liquid Bubble Manometer for Low Differential Heads", Proceedings, Indian Acad. Sci. (Engg. Sci.,), Vol. 4, pp. 87-94. (1981)

9. Smith, AM.D. and Murphy, J.S., 'Micromanometer for Measuring Boundary Layer Profiles', Rev. of Sci.lnstrum., Vol 26, pp. 775. (1955)

10. Stalhane, O., 'A New Micromanometer', J. Sci. Instrum., Vol. 11, pp. 79. (1934)

11. Streeter V L & Wylie E B *Fluid Mechanics* 7th ed., McGraw-Hill, Kogakusha Tokyo, (1979)

4-WAY POWER DIVIDER-CUM-COMBINER

A.K. Agrawal

Mody College of Engineering and Technology Laxmangarh (Rajasthan) - 332311

ABSTRACT

A 4-way Power Divider-cum-Combiner has been analyzed which uses transmission lines (Instead of Resistors) connected between the various output ports. Unlike resistors (used by Wilkinson), the transmission lines dissipate little power. The lengths of the transmission lines are assumed to be a quarter wavelength at the centre' frequency. The expressions for the coupled power and the power into the isolated arm are derived for a presumed power split k: 1 between the coupled and isolated powers in the power divider, which is matched at the input port. The coresponding power expressions are likewise derived for the power combiner.

1. INTRODUCTION

Wilkinson[1] developed an N-way power divider that would split the input power into N output ports, and also provide isolation between the output ports. The unique feature of the Wilkinson Power divider was the use of resistors connected between the various output ports. When the output ports are terminated in the correct load imped-ances, there is no current in the resistors; so they do not absorb any power. However, if any port is not matched, the reflected power from that port is partly absorbed by the resistor network and partly returned to the input, but no power is wupled into the other output ports as long as they remain properly terminatedz.

But the aforesaid elimination of power dissipation in the resistors is possible only at the centre frequency of the power divider. The resistors do dissipatc.power at other frequencies within the band-width of the divider. So replacing resistors with transmission lines will reduce power dissipation except for the possible mismatch at the ports, which can be taken care of by proper selection of the characteristic impedances of the transmission lines.

In this paper, a 4-way Power Divider-cum-Combiner has been analyzed which uses transmission lines instead of resistors connected between the output ports. The lengths of the lines are taken.to be $\lambda/4$ at the centre frequency. The Power Divider is assumed to be matched at the input port. Also the power fed into the divider is assumed to be split in the ratio k:l between the coupled and isolated ports. With these assumptions the expressions for coupled power and power into the isolated port are derived. The corresponding expressions are like,~ise derived for the Power Combiner.

The structure of Power Divider-cum-Combiner is shown in Fig.t. In the Power Divider, the power from the antenna represented by source Vg_1 with internal impedance Zg_1 is distributed into four 50-ohm loads. In the Power Combiner, the powers from four sources Vg_2 with internal impedances Zg_2 are combined and fed into the antenna at port 1. In the latter case the ports with 50-ohm loads are the isolated ports.

2. THE POWER DIVIDER

For convenience, and due to symmetry, only one arm of the 4-way Power Divider need be considered as shown in Fig.2. The assumed input admittances looking from either side at the four nodes are also shown in the figure. The antenna admittance in each arm will then become $Yg_1/4$, where $Yg_1 = 1/Zg_1$. Similarly the admittance of sources Vg_2 is $Yg_2 = 1/Zg_2$.

Let Yin_4 be the admittance looking leftward into any arm from node-4. Then the total input admittance of the other 3 arms looking outward from anyone arm at node-4 will be

$$Y_4in = 3Yin_4 \tag{1}$$

The electrical lengths of the lines $(Zi, \beta i)$ are assumed to be equal, i.e.,

$$\beta_1 I_1 = \beta_2 I_2 = \beta_3 I_3 = \theta \tag{2}$$

Therefore, for lines of characteristic admittances Y_1, Y_2, and Y_3 (where $Y_1 = 1/Z_1$, $Y_2 = 1/Z_2$ and $Y_3 = 1/Z_3$) we have

$$Yin_2 = Yg_2 + \frac{\dfrac{Yg_1}{4} + jY_1\tan\theta}{Y_1 + jY\dfrac{g_1}{4}\tan\theta} \quad Y_1 = Yg_2 + \frac{4Y_1{}^2}{Yg_1} \qquad \theta = \Pi/2 \tag{3}$$

$$Yin_3 = Y_0 + \frac{Yin_2 + jY_2\tan\theta}{Y_2 + jYin_2\tan\theta} \quad Y_2 = Y_0 + \frac{Y_{12}{}^2}{Yin_2}, \quad \theta = \pi/2 \tag{4}$$

$$Yin_4 = \frac{Yin_3 + jY_3\tan\theta}{Y_3 + jYin_3\tan\theta} \quad Y_2 = Y_0 + \frac{Y_3{}^2}{Yin_3}, \quad \theta = \pi/2 \tag{5}$$

Now using (1), the admittances looking from the left are :

$$Y_{3in} = Y_0 + Y_{34} = Y_0 + \frac{3Yin_4 + jY_3\tan\theta}{Y_3 + j3Yin_4\tan\theta} \quad Y_3 = Y_0 + \frac{Y_3{}^2}{3Yin_4}, \quad \theta = \pi/2 \tag{6}$$

$$Y_{2in} = Yg_2 + \frac{Y_{3in} + jY_2\tan\theta}{Y_2 + jY_{3in}\tan\theta} \quad Y_2 = Yg_2 + \frac{Y_2{}^2}{Y_{3in}}, \quad \theta = \pi/2 \tag{7}$$

$$Y_{1in} = \frac{Y_{2in} + jY_1 \tan\theta}{Y_1 + jY_{2in}\tan\theta} \quad Y_1 = \frac{Y_1^2}{Y_{2in}}, \quad \theta = \pi/2 \tag{8}$$

3. CHARACTERISTIC ADMITTANCES OF TRANSMISSION LINES

It is desirable that the antenna feeds the loads Z_0 with as little power going into Zg as possible, as shown in Fig.2. Hence the following requirements must be met:

(i) For matching between the antenna and Power Divider input

$$Y_{1in} = Yg_1/4 \tag{9}$$

From (3) to (8), Y_1 in is determined and equated to Yg1/4. This gives the following equation:

$$Y_0(16Y_1^4 - Yg_1^2 Yg_2^2) = 2Y_1^2 Y_2^2 Yg_1 + Y_2^2 Yg_1^2 Yg_2 \tag{10}$$

(ii) This is also desirable that the power from the antenna arriving at port 2 is not absorbed in Zg_2.

Let $\quad Y_{2i}n - Yg_2 = kYg_2, \; K > 1 \tag{11}$

Using the equations (3) to (8) we obtain

$$\frac{3Y_2^2}{kYg_2} - 4y_0 = \frac{Y_2^2 Yg_1}{4Y_1^2 + Yg_1 Yg_2} \tag{12}$$

From (11) and (12) Y1 and Y2 are determined as :

$$Y_1 = 1/Z_1 = Yg_1 Yg_2(k+1)/2) \tag{13}$$
$$Y_2 = 1/Z_2 = 2Y_0 Yg_2 k(k+2)/(k+3) \tag{14}$$

(iii) Determination of Y_3 : On substitution of Y_1 and Y_2 into (3), (4) and (5)

$$Yin_4 = Y_3^2 (k+3) / \{(3Y_0 (k+1)\} \tag{15}$$

From (1) the external admittance seen by any one arm at node 4 is

$$Y_{4in} = 3Yin_4 = Y_3^2 (k+3) / \{(Y_0(k+1)\} \tag{16}$$

Hence Y_{4in} can be suitably adjusted by selecting Y3 and k. Y4 it should be small so as to prevent the power from leaking out from any one arm into the three arms of the power Divider.

4. ANALYSIS OF POWER DIVIDER

The Power divider of Fig.2. is analyzed by assuming voltage and current waves in lines 1, 2 and 3 as shown. Equating the voltages and the currents at the nodes the following equations are obtained.

$$V_1 \quad = \quad V_1^+ + V_1^- = Vg_1 - 4 \, Ig \, Zg_1 \tag{17}$$
$$Ig \quad = \quad (V_1^+ - V_1^-)/Z_1 \tag{18}$$
$$V_2 \quad = \quad V_2^+ + V_2^- = V_1^+ e^{-j\theta} + V_1^{-ej\theta} \tag{19}$$
$$I_2 \quad = \quad V_2/Zg_2 = \{V_1^+ e^{-j\theta} + V_1^{-ej\theta}\} / Z_1 - \{V_2^+ - V_2^-\} / Z_2 \tag{19b}$$
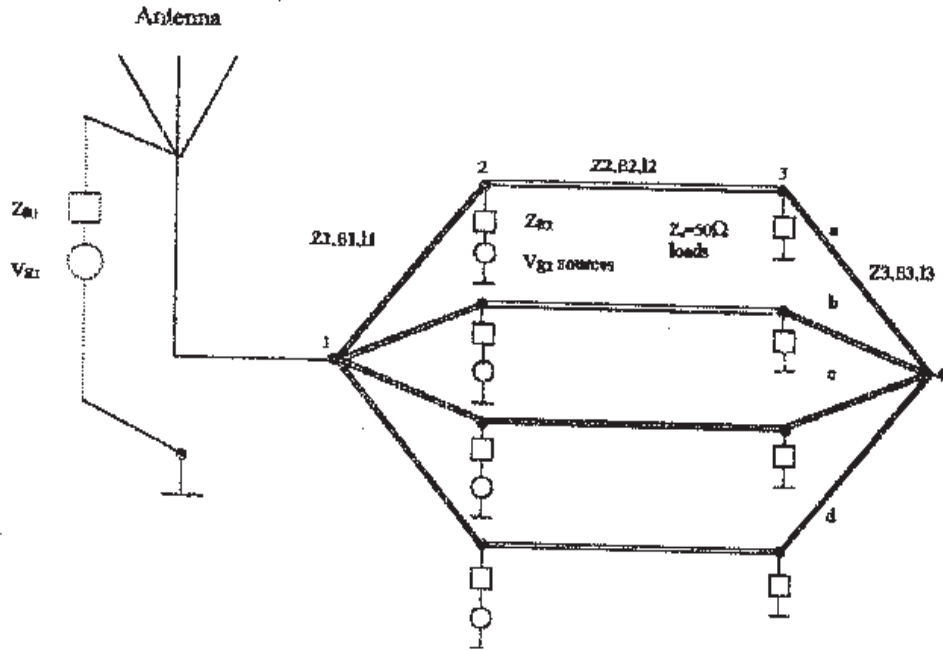
Fig.1. Power Divider-cum-combiner

$$V_3 = V_3^+ + V_3^- \quad = \quad V_2^+ e^{-j\phi} + V_2^- e^{-j\phi} \quad (20a)$$

$$I_3 = \quad V_3/Z_0 \quad = \quad \{ V_2^+ e^{-j\phi} - V_2^- e^{-j\phi}\} / Z_2 - \{V_3^+ - V_3^-\} / Z_3 \qquad (20b)$$

(i) Determination of V_1^+ and V_1^-

From (17) and (18).

$$Zin = V1/Ig = 4Zg1 = 4Zg_1 = Z_1\{V_1^+ + V_1^-\}/\{V_1^+ - V_1^-\}$$

$$\text{Or } V_1^-/V_1^+ = \{4Zg_1 - Z_1\} / \{4Zg_1 + Z_1\} \qquad (21)$$

On eliminating Ig, we get $Vg_1 = V_1^+ + V_1^-\}/\{V_1^+ - V_1^-\} / Z_1$

Using (21), $Vg_1 = 16Zg_1 \, V_1^+ - / \{4Zg_1 + Z_1\}$

Therefore, $\quad V_1^+ \quad = \quad Vg_1 \{4Zg_1 + Z_1\} / \{16Zg_1\} \qquad (22a)$

$\qquad\qquad\quad V_1^- \quad = \quad Vg_1 \{4Zg_1 - Z_1\} / \{16Zg_1\} \qquad (22b)$

(ii) Power dissipated in Zg2 :

From (19a) and (22)

$$V_2 = V_1^+ e^{-j\phi} + V_1^- e^{-j\phi} = Vg1\{4Zg1 \cos^{\phi - jz, \sin\phi\} / \{8zg)} \qquad (23)$$

At centre frequency $\phi = \Pi / 2$ and $V2 = -jZ1 \, Vg1 / (8Zg1)$

Power dissipated in Zg_2 (assumed to be real)

$$P2 = Z_1^2 \, Vg_1^2 / \{128 \, Zg_1^2 \, Zg_2\} \qquad (24a)$$
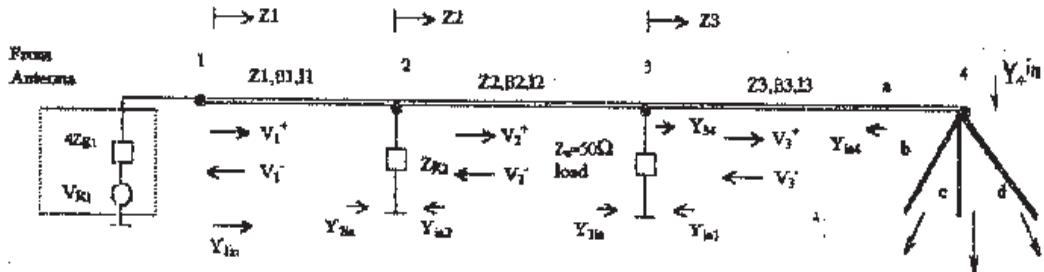
Fig.2. Power Divider

(iii) Power output in the load Z0 :

From (19) V_2^+ and V_2^- can be obtained in terms of V_1^+ and V_1^-

$$V_2^+ = \frac{V_1^+ e^{-j\phi}(1+Z_2/Z_1 - Z_2/Zg_2) + V_1^{-ej\phi}(1-Z_2/Z_1 - Z_2/Zg_2)}{2} \qquad (25a)$$

$$V_2^+ = \frac{V_1^+ e^{-j\phi}(1-Z_2/Z_1 + Z_2/Zg_2) + V_1^{-ej\phi}(1+Z_2/Z_1 + Z_2/Zg_2)}{2} \qquad (25b)$$

Substituting in 20(a)

$$V_3 = V_1^+ e^{-j\phi}(\cos\phi + j(Z_2/Zg_2 - Z_1)\sin\phi\} + V_1^{-ej\phi}(\cos\phi + j(Z_2/Zg_2 + Z_2/Z_1)\sin\phi)$$

$$= V_1^+(Z_2/Zg_2 - Z_1) - V_1(Z_2/Zg_2 + Z_2/Z_1), \phi = \Pi/2$$

Substituting for V1+ and V1- from (22)

$$V_3 = Vg_1 Z_2 \{Z_1/(Zg_1, Zg_2,) - 4/Z_1\}/8 \qquad (26)$$

Power in the load Z_0,

$$P_3 = Vg_1^2 Z_2^2 \{Z_1/Zg_1 Zg_2) - 4/Z_1\}^2 / (128 Z_0) \qquad (27a)$$

Substituting for Z_1 and Z_2 from (13) and (14) into (24a) and (27a)

$$P_3 = \frac{Vg_1^2 k(k+3)}{64 Zg_1 (k+1)(k+2)} \qquad (27b)$$

$$P_2 = Vg_1^2 / \{32Zg_1 (k+1)\} \qquad (24b)$$

And $P_3 / P_2 = k(k+3) / \{2(k+2)\}$ \qquad (28)

As k takes values 1, 2, 3 P_3 / P_2 becomes 0.66, 1.25 and 1.8, i.e. the desired load power P_3 can be increased relative to the isolated power P_2 by increasing k. For k unity, P_3 is less than P_2. The transmission line characteristic admittances, Y_1 and Y_2 can then be determined for a given value of k from (13) and (14).
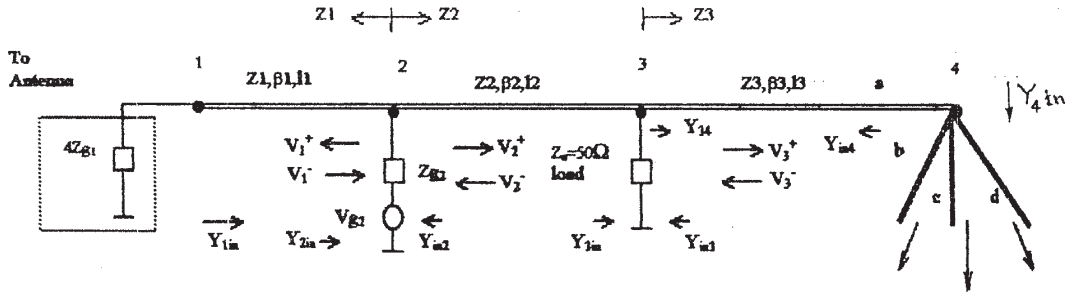
Fig.3. Power Combiner Circuit

5. ANALYSIS OF POWER COMBINER

Fig. 3 shows the Power Combiner circuit with assumed voltage and current waves. The voltages and currents at the nodes are :-

$$V_1 \quad = \quad V_1^+ e^{-j\phi} + V_1^+ e^{-j\phi} \tag{29(a)}$$

$$I_1 \quad = \quad \{V_1^+ e^{-j\phi} - V_1^- e^{-j\phi}\} / Z1 = \{V_1^+ e^{-j\phi} + V_1^+ e^{-j\phi}) / (4Zg_1) \tag{29b}$$

$$V_2 \quad = \quad V_1^+ + V_1^- = V_2^+ + V_2^- = Vg_2 - V_2^- \tag{30a}$$

$$I_2 \quad = \quad \{V_1^+ e^{-j\phi} - V_1^- e^{-j\phi}\} / Z1 = \{V_1^+ e^{-j\phi} + V_1^+ e^{-j\phi}) / (4Zg_1) \tag{30b}$$

$$V_3 \quad = \quad I_3 Z_0 = V_3^+ + V_3^- \quad = \quad V_2^+ e^{-j\phi} + V_2^- e^{-j\phi} \tag{31a}$$

$$I_3 \quad = \quad \{V2^+ e^{-j\phi} - V2^- e^{-j\phi}\} / Z2 - \{V_3^+ - V_3^-\} / Z_3$$

From (29b)

$$V_1^- = \{(4Zg_1 - Z_1) / 4Zg_1 + Z_1)\} V_1^+ e^{-2j\phi} \tag{32}$$

Substituting for V_1^- in (30a)

$$V_1^+ + V_1^- = V_1^+ [1 + \{(4Zg_1 - Z_1) / (4Zg_1 + Z_1)\} e^{-2j\phi}] = V_2$$

or $\quad V_1^+ = V2 / [1 + \{(4Zg_1 - Z_1) / (4Zg_1 + Z_1)\} e^{-2j\phi}] \tag{33}$

From (31a) and (31b)

$$V_2^+ e^{-j\phi} = I_3 (Z_0 + Z_2) / 2 + Z_2 (V_3^+ - V_3^-) / (2Z_3) \tag{34a}$$

$$V_2^+ e^{-j\phi} = I_3 (Z_0 + Z_2) / 2 + Z_2 (V_3^+ - V_3^-) / (2Z_3) \tag{34b}$$

Then (30) becomes

$$V_2 = V_2^+ + V_2^- = I_3 (Z_0 \cos\phi + jZ_2 \sin\phi) + jZ_2 (V_3^+ - V_3^-) \sin\phi / 2(Z_3) \tag{35a}$$

$$V_2^+ - V_2^- = I_3 (Z_2 \cos\phi + jZ_0 \sin\phi) + Z_2 (V_3^+ - V_3^-) \sin\phi / (2Z_3) \tag{35b}$$

From Fig. 3 $\quad I_{34} / I_3 = Y_{34} / Y_0 = (V_3^+ - V_3^-) Z_0 / [(V_3^+ + V_3^-) Z_3] \tag{36}$

Substituting for Y_{34} From (6)

$$\frac{(V_1^{'} - V_1^{-})}{Z_3} = \frac{I_3 Y_3}{Y_0} \frac{(3Yin_4 + jY_3 \tan \emptyset)}{(Y_3 + j3Yin_4 \tan \emptyset)} = \frac{I_3 Y_3^2}{3Y_0 Yin_4}, \quad \emptyset = \pi/2 \tag{37}$$

Substituting for Yin_4 From (15) into (37)

$$(V_3^{-} - V_t) / Z_3 = (k+1) \, I_3 / (k+3), \quad \emptyset = \pi/2 \tag{38}$$

Substituting (38) into (35)

$$V_2 = V_2^{+} + V_2^{-} = jZ_2 \, I_3 \, (3k+7) / [2 \, (k+3)] \tag{39a}$$

$$V_2^{+} - V_2 = jZ_0 \, I_3 \tag{39b}$$

Substituting (39a) into (33)

$$V_1^{-} = \frac{jZ_2 \, I_3 \, (3k+7) \, (4Zg_1 + Z_1)}{4Z_1 \, (k+3)} \tag{40a}$$

From (32)

$$V_1^{-} = \frac{-jZ_2 \, I_3 \, (3k+7) \, (4Zg_1 - Z_1)}{4Z_1 \, (k+3)} \tag{40b}$$

From (29b)

$$I_1 = \frac{jZ_2 \, I_3 \, (3k+7) \, (Z_1 \cos\emptyset - j4 \, Zg_1 \sin \emptyset)}{8Z_1 \, Zg_1 \, (k+3)} \tag{41a}$$

$$= Z_2 \, I_3 \, (3k+7) / [2Z_1(k+3)], \quad \emptyset = \pi/2 \tag{41b}$$

Power fed to the antenna from a single source Vg_2 (in one arm)

$$P_1 = I_1^2 \cdot 4Zg_1 = \frac{Zg_1 \, [Z_2 \, (3k+7) \, I_3]^2}{[Z_1 \, (k+3)]^2} \tag{42a}$$

Isolated Power in load Z_0 (in one arm)

$$P_J = I_3^2 \cdot Z_0 \tag{42b}$$

where I_3 is obtained by substituting (35a) and (35b) into (30b)

$$I_3 = \frac{-jVg_2}{\dfrac{Z_0 Zg_2}{Z_2} + \dfrac{(3k+7)Z_2}{2(k+3)} \left[1 + \dfrac{4Zg_1 Zg_2}{Z_1^2}\right]} \tag{43}$$

And

$$\frac{P_1}{P_3} = \frac{Zg_1 [Z_2 (3k+7)]^2}{Z_0 [Z_1 (k+3)]^2} = \frac{(k+1) \, (3k+7)^2}{8k \, (k+2) \, (k+3)} \tag{44}$$

where Z_1 and Z_2 have been taken from (13) and (14).

For k taking values 1,2,3 P_1 / P_3 becomes 2.04, 1.58 and 1.42, i.e. by increasing k the desired power P_1 fed to the antenna decreases. So a compromise in choosing the value of k is necessary.

6. CONCLUSION

A 4-way Power Divider-cum-Combiner using transmission lines has been analyzed. In the analysis the lines were assumed to be a quarter wavelength long at the centre frequency of the Power Divider-cum-Combiner. For the power divider, a ratio k:1 between the powers in the coupled and isolated arms as been assumed, where k is greater than unity. As k is increased, it was found that the coupled power increased in the power divider but decreased in the power combiner. Hence a compromise value of k is required. Once k is selected, the characteristic impedances of the respective transmission lines can then be determined.

REFERENCES

1.   R.E. Collin, Foundations for Microwave Engineering, Mc. Grew Hill, 1992.

2.   PA Rizzy, Microwave Engineering - Passive circuits, Prentice Hall, 1988.

MICROPROCESSOR BASED pH MEASURING SYSTEM

B.T. Jadhav[a]*, Y.S. Shinde[a], B.B. Godabale[b] and S.R. Sawant[c]

[a]*Department of Electronics, Yashwantrao Chavan Institute of Science, Satara-415 001 (M. S.)*
[b]*Department of Electro nics, K. B. Patil College of Engineering & Polyte.,
Satara-415 001(M.S.)*
[c]*Department of Electronics, Shivaji University, Kolhapur - 416 004 (M.S.)*

ABSTRACT

In many processes accurate measurement of pH value and its control is the important phase. To measure the desired level of pH different techniques are in use, designed for specific type of electrode and signal conditioning. Here we design and develop the microprocessor based pH measuring system which has good acquisition time and accuracy.

1. INTRODUCTION

The pH quantity pH = -log (Hl, shows the hydrogen (Hl ion concentration, indicates whether given solution is acidic, neutral or basic. The pH is an important parameter in various chemical and electrochemical processes. In many industries it becomes necessary to measure and control accurately the value of pH. For e.g. In Sugar industry at the clarification processes the measurement and control of pH of cane juice is very important. There are so many references on the developments of pH meters. So many of them are based on the analog as well as digital circuits using microprocessor, micro controllers and personal computers. Some instruments cannot prescribe correct value of pH and also there are variations in the readings [1]. We design and develop a simple laboratory purpose microprocessor-based pH measuring system.

2. MEASURING TECHNIQUE

The Fig.1. Shows the complete block diagram of microprocessor-based pH measuring System. The buffer solution having pH values 0 to 14 is used for testing and calibration purpose, in practice it may be any chemical. The combined electrode (consists of pH glass and reference electrode in a single entity) converts the H^+ ion concentration into the corresponding voltage. The isolator cum follower circuit follows the mV output from the sensor; the MOS-FET IC CA 3140 acts as a follower. The mV output is amplified and temperature compensated using the inverting stage of the OP-AMP IC 741 and signal is set at desired value. To convert analog signal in to the digital (ADC) form, IC 0809 is used and IC LF 398
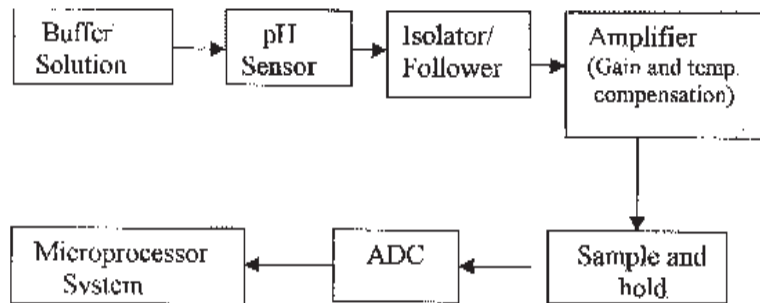
Fig.1. Block diagram of microprocessor based pH measuring System
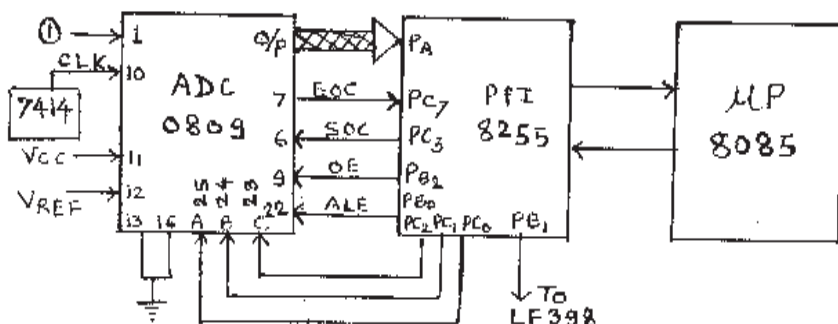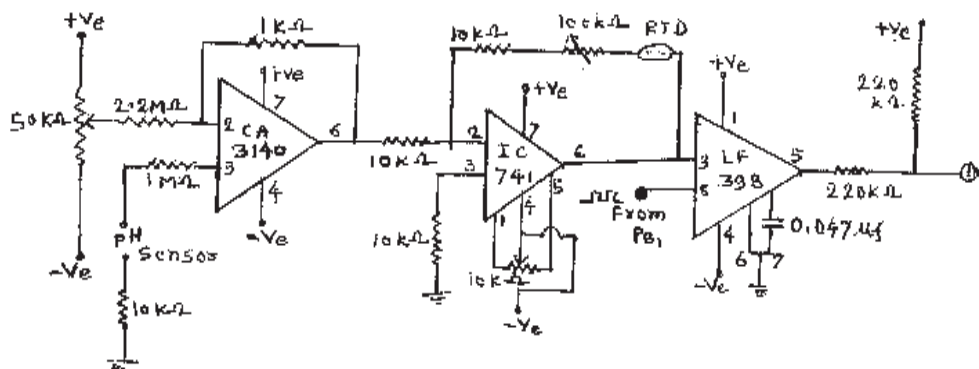
*Fig.2. Circuit Diagram*

provides the sample and hold facility. By utilizing the one of the port of IC 8255, the microprocessor 8085 collects the pH values in the digital form and stored in the memory. The pH reading is displayed on the microprocessor display by proper calibration of digital data and initialization of IC 8279. With proper logic and software support a pH measuring is achieved.

3. HARDWARE

3.1 Sensor

We used the combined Electrode as a pH sensor because it is very easy to manipulate and process it as well as it is possible to fill the reference chemical again and again hence it is cost effective [2]. Sensor generates the voltage at its output terminals in mV range, which is proportional to the concentration of the H^+ ion in the solution. The output of sensor depends on the temperature of solution in which it is dipped and the variation in the output voltage is 0.019V/pH/degree Celsius (^oC). For unit change of the pH value it's output changes by 49 m V at room temperature (25°C). The output of sensor is 0 mV at 7 pH & it gives +ve output voltage for pH values less than 7 and -ve output for pH values greater than 7. The total voltage variation range is +343 mV, 0mV and -343 mV for pH values 0, 7 and 14 respectively. The variation in output voltage is almost linear up to 100°C so it is easy for calibration but at higher temperature variations increases. Initially this sensor is tested in the Elico based pH meter.

3.2 Isolator/follower

As the pH sensor does not have any current driving capacity, it requires the voltage controlled or voltage operated device, which will not draw any current from the sensor, and hence loading of sensor is avoided. The only remedy for this is use of isolated gate FET or MOS FET IC, which acts as a follower [3].

As it was required to follow the sensor output, it is needed to use amplifier with unit gain so we use the easily available MOS FET IC CA 3140 that is pin compatible to the normal OP-AMP. The IC CA 3140 have very high input impedance about 1.5 Tera ohm and bias current is also very low about 1 Pico Ampere, hence it avoids any loading on sensor. Practically CA 3140 has better current driving capacity and acts as an insulator at the input stage; its speed of operation is also very high because of the FET'S used in it.

A follower is used in the non-inverting mode so its gain is 1 + Rf/Ri, which approximately equals to the unity because the input resistance Ri is very high as compare to Rf. The offset null is achieved by feeding the appropriate voltage at the inverting terminal. Thus this stage so follow the same voltage that is fed to it by the pH sensor.

3.3. Amplifier

The output from follower stage is fed to inverting amplifier IC 741 and its gain is adjusted by varying feedback resistor for proper calibration. The OP-AMP IC 741 has very wide bandwidth and starts from zero frequency. The gain of inverting amplifier is Rf/Ri and is adjusted by varying the 100K-ohm potentiometer connected in series with the l0K resistor that is same as input resistance (to ensure that the amplifier will work at least with unit gain). The offset null is achieved by connecting the 10K ohm preset in 1,4,5 pin's of the OP-AMP. At 25^oC temperature 100K is adjusted to obtain the proper gain of the amplifier. For other temperature values the RTD has been used in the feed back path for temperature compensation and WOK works as a temperature calibration knob. The output of this amplifier is fed to the sample and hold circuit [4,5].

3.4. Sample and hold

As the analog output from the sensor is not constant, the ADC can't tolerate it to convert it in proper digital equivalent. When ADC is reading the input, it needs of constant value during the conversion time. The sample and hold circuitry will hold the signal at constant level when ADC is converting it in the digital form. Using the IC LF 398 with proper choice of hold capacitor and acquisition time does this. Acquisition time is the time required to charge the hold capacitor to the new value ftom its previous hold voltage level after logic is made high. It is 40 microseconds for the hold capacitor of 0.047 micro fared. When the logic input is high it samples the signal and charges the hold capacitor to the certain value and when the logic input is low then the input of IC is tri-stated using internal FET. The charged capacitor act's as an input source to the internal MOS OP-AMP, which does not derive any current ftom the capacitor. The capacitor has no any leakage current so that its voltage remains constant and followed at olp of slh circuit until the logic is low. Afterward when logic is high, capacitor charges to the new value and same process followed to have constant output.

3.5. Analog to Digital Converter (ADC)

As the analog data cannot be processed or handled and stored using microprocessor, which can handle the large data with very high processing speed, it is required to converts into digital equivalent form. This is done with the monolithic package IC 0809 using successive approximation technique. It has 8-bit data bus and is connected to the one of the port of the 8255. The data can be stored and processed using μp 8085 and the proper software. The ADC 0809 is provided with additional circuit at its input stage to have its working in bipolar rage of input voltage. The Clock applied to ADC may vary from 10KHz to 1.2 MHz. For clock ftequency of 640 KHz the conversion time is 100 microseconds and the error of conversion is ± 1 LSB. Care should be taken that the +Ve reference voltage should not exceed the +Vcc and -Ve reference should not be less than the -Vcc (or ground).

Out of eight input channels input is accepted from one & is selected by sending the proper address of the channel followed by address latch signal. The start of conversion (SOC) pulse is sent to start the conversion and end of conversion (EOC) pulse is checked. If EOC is received, output buffer is enabled and digital data is read in the one of the port of 8255, lastly output buffer is disabled.

3.5.1 Dual range working for the ADC

As the sensor and amplified voltages are bipolar (+Ve as well -V e), the ADC should handle these voltages properly [6,7]. It can be achieved by using both +Ve and -Ve reference levels but the other channels may not have any need of working in the bipolar range. The external voltage divider network is used and the input given to the channel should remain +Ve for the maximum -Ve input voltage of the divider. If the +Vcc is the + Ve reference voltage & zero (or Ground) is the -V e reference voltage then first the input voltage is made of its half and it is then clamped at V cc/2 so that the range of the input that can be given to the voltage divider is +/- Vcc, hence the ADC can be used in the dual range. Table I shows actual voltages applied, the voltage at the channel and its converted hex equivalent.

Input votlages	Voltages at the channel	Hex Equivalent
-5	0	00
0	2.5	80
+5	5	FF

Table I : Voltages applied and converted Hex equivalent

3.6 Microprocessor

The 8085-microprocessor kit manufactured by Anshuman is used. Its working frequency is 3 MHz. It has facility of reading & writing and has 8- digit seven segment LED displays, which can be controlled by using the keyboard and display interface, using the supporting ICs 8255 (PPI) and 8279 respectively.

4. CALIBRATION

ADC converts the analog data to the digital equivalent and is stored in the memory in the hex form but user can't estimate correct value of pH accurately. So it is required to convert this data into its equivalent value of pH that is understandable to the user directly without any need of conversion. The calibration is done with the help of proper software programming in such a way that it will represent the equivalent pH directly and display it [7].

4.1 Logic for gain adjustment of the amplifier

The ADC is used in the dual range, we can apply any voltage between +5V to -5V, and the total voltage accepted by it is 10 V in magnitude. The ADC has 8-bit resolution so it makes the 2^8 i.e. 256 different output combinations; hence it makes 255 parts of the 10V. The voltage corresponding to single part is 10 V / 255 = 0.0392 V. As we need the accuracy of 0.1 in pH, the output of the follower changes by 0.049 V for change of 1 pH at the sensor hence for 0.1 variations in the pH value the follower output will changes by 0.0049 V. Hence the output of amplifier changes by value A * 0.0049 V, where A is the gain of the amplifier. The ADC will be able to differentiate this change in the voltage if it is equal to the voltage required for changing its output by one LSB.

Mathematically: Gain A * 0.0049 = 0.03921, A = 0.03921/0.0049, A = 8.003, A~ = 8. To have proper calibration, the gain of amplifier is adjusted to 8 so that the ADC will change its output by one LSB for 0.1 changes in pH at the sensor.

5. DATA AND RESPECTIVE VALUE OF pH

At the 7 pH, the output of sensor is 0.000V hence the output of amplifier is 0V and due to dual range working the data corresponding to 7 pH (0.00 V) is 1000,0000 = 80 H. Hence the microprocessor will read the value as 80 H. As the maximum variation in the pH value is from 0 to 14, the ADC will give 70 different successive outputs above and bellow the value 80 H for total specified range of input. So the total data corresponding to the specified values of pH will changes from 3A H to C6 H. The corresponding data to the 0 pH (+ 0.343 V

output of follower and -2.744 V output of amplifier) and the 14 pH (-0.343 V o/p of follower and +2.744 V o/p of the amplifier) are 3AH and C6H respectively. Some data samples are shown in the Table II.

pH	Hex data	pH	Hex data	pH	Hex data	pH	Hex data
0	3A	6.4	7A	7.1	81	8	8A
1	44	6.5	7B	7.2	82	9	94
2	4E	6.6	7C	7.3	83	10	9E
3	58	6.7	7D	7.4	84	11	A8
4	62	6.8	7E	7.5	85	12	B2
5	6C	6.9	7F	7.6	86	13	BC
6	76	7	80	7.8	87	14	C6

Table 2 : Data samples

5.1 Conversion in real pH value

The data corresponding to particular pH is available in the HEX form should be converted into the real pH value and displayed using the 8279 chip on the microprocessor display. For this conversion simple logic is used.

We know that the data 3A H corresponds to the 0 pH value. Now if the available data is 'm' then the one register (accumulator) is loaded with data 39 H, it is incremented by 0A H each time and compared with 'm' (for increment of pH by unit value the output of the ADC will jump (OA H) i.e. 10 places forward). Then it is found that how many times OA H should be added to the value 39 H to make it greater than 'm'. The number of times is supposing 'j'; this 'j' is measured using the counter register. Then j-l = 't', that '1' gives the integer part of pH. To get the tractional part of the pH, 'm' is subtracted from the data 39 H * j * 0A H which is available in incremented register (accumulator). Suppose the answer of this is 'k'. This 'k' is subtracted from the 09 H. Let the answer be 'n' which gives the tractional value (digit). Finally our real pH value is "t* n" and is stored in one of the register pair.

In this way any data is converted to its equivalent pH value. But the data allowed to display is 0 pH to 14 pH and if hex data goes out of the range 3A H to C6 H then "ERROR" message is displayed on the display.

6. SOFTWARE

The algorithm developed for pH measurement using microprocessor is given:

- Read the data from the ADC.

- Convert the data in to the corresponding pH equivalent and store integer part in the D register and tractional part in the E register.

- Use of 8279 by sending different control words check the data received.

Table 3 : Assembly Language program

HEX ADDRESS	LOOP	MNEMONICS		OP-CODE	COMMENTS
1. Read	*the*	*Data from the*		*ADC using*	*Sample & Hold*
6FDA	Start:	MVI	A 98	3E,98	Control word
6FDC		OUT	0B	D3, OB	
6FDE		MVI	1\ 02	3E,02	Send logic high
6FEO		OUT 09	D3, 09		
6FE2		MVI	D,03	16,03	
6FE4	DO:	DCR	D	15	Adjust delay for logic
6FE5		JNZ	DO	C2, E4, 6F	Make logic low
6FE8		MVI	1\ 00	3E, 00	
6FEA		OUT	09	D3, 09	Select channel 3
6FEC		MVI	A, 03	3E, 03	
6FEE		OUT	OA	D3, OA	ALE high
6FFO		MVI	A, 04	3E, 04	
6FF2		OUT	09	D3,09	Delay
6FF4		MVI	C,FF	OE,FF	
6FF6	Dl:	DCR	C	OD	
6FF7		JNZ		C2,F6,6F	ALE low
6FFA		MVI	A, 00	3E,00	
6FFC		OUT	09	D3, 09	Send SOC high
6FFE		MVI	A, OB	3E, OB	
7000		Nap		00	
7001		OUT	OA	D3,OA	Delay
7003		MVI	C,FF	0E,FF	
7005	Loop:	DCR	C	OD	
7006		JNZ	Loop:	C2, 05,70	Send SOC low
7009		MVI	1\ 03	3E, 03	
700B		OUT	OA	D3, OA	
700D	EOC:	IN	OA	DB,OA	Check EOC
700F		RAL		17	
7010		JNC		D2, OD, 70	
7013		MVI	A, 08	3E,08	Send OE high
7015		OUT	09	D3, 09	
7017		MVI	C,FF	OE,FF	Delay
7019	D2:	DCR	C	OD	
701A		JNZ		C2, 19, 70	
701D		IN	08	DB, 08	Read data and store at 2800
701F		STA	2800	32,00,28	H
7022		MVI	A, 00	3E,00	Make OE low
7024		OUT	09	D3, 09	
7026		LDA	2800	3A, 00, 28	

	2.	**Convert Data in the**	**Corresponding**	**pH equivalent and Store it**
7029		MVI H, 00	26,00	Get data in reg. E
702B		MOV E,A	5F	
702C		MVI A, 39	3E,39	Load acc. With 39H.
702E	ADD:	INR H	24	How many times 10
702F		ADI OA	C6, OA	Should be added to the 39H to
7031		CMP E	BB	make it greater than the data
7032		JZ NEXT:	CA, 38, 70	received.
7035		JC ADD:	DA, 2E, 70	
7038	NEXT:	SUB E	93	This gives ffractional part of pH.
7039		MOV B, A	47	
703 A		MVI A, 09	3E, 09	
703C		SUB B	90	
703D		MOV L, A	6F	Number of times -1.
703E		DCR H	25	Ifno. of times required to make
703F		MOV A, H	7C	39 greater are more than 09
7040		CPI 0A	FE,OA	(i.e.A, OB,etc) then this is
7042		JC DEC:	DA, 47, 70	converted to decimal equivalent
7045		ADI 06	C6,06	by adding 6 to it.
7047	DEC:	MOV H, A	67	Get converted data in DE.
7048		XCHG	EB	

	3.	***Use***	***Of 8279 hv***	***Sendinff different***	***Control Words.***
7049		MYI A,D3	3E,D3		
704B		OUT 15	D3, 15		
704D	D3:	MVI C, FF	0E, FF	Delay	
704F		DCR C	0D		
7050		JNZ D3:	C2,4F, 70		
7053		MVI A, 00	3E,00	Out various control words	
7055		OUT 15	D3, 15		
7057		MVI A, 32	3E, 32		
7059		OUT 15	D3, 15		
705B		MVI A, 90	3E, 90		
7050		OUT 15	D3, 15		

	4.	***The equivalent***	***Seven segment***	***Codes for the contents of the***
	Sending			***registers D and E***
705F		MVI C, 08	0E,08	Go to the subroutine if the
7061		MVI H, 21	26,21	accepted data is in range or not
7063		JMP Check:	C3, 50, 71	
7066	CONT:	MOV L,D	6A	
7067		MOV A,D	7A	Check data in D is greater than
7068		CPI OA	FE,OA	9 or not.
706A		JC NEXT 1:	DA, 78, 70	
706D		MOV A,D	7A	
706E		SBI 10	DE, 10	If the data is greater than 9, then
707D		MOV B,A	47	first digit is displayed as 1

7071		MVI	L,OI	2E,01	directly and data is stored in L
7073		MOV	A,M	7E	now.
7074		OUT	14	D3, 14	
7076	NEXT1:	DCR	C	OD	
7077		MOV	L,B	68	
7078		MOV	A,M	1£	
7079		OUT	14	D3, 14	Second bit of 2 digit or first bit
707B		DCR	C	OD	of 1 digit data is displayed.
707C		MVI	L,OA	2E, OA	
707E		MOV	A,M	7E	
707F		OUT	14	D3, 14	
7081		DCR	C	OD	
7082		MOV	L,E	6B	
7083		MOV	A,M	7E	Display point.
7084		OUT	14	D3, 14	
7086	DEND:	DCR	C	OD	
7087		MVI	L,OB	2E, OB	
7089		MOV	A,M	1£	Display fractional part, which is
708A		OUT	14	D3,14	in register E.
708C		INR	L	2C	
708D		DCR	C	OD	
708E	D4:	JNZ		C2,89, 70	
7091		LXIHFF, FF		21, FF, FF	
7094		DCX	H	2B	
7095		MOV	A,L	7C	Delay
7096		ORA	L	B5	
7097		JNZ D4:	C2,94, 70		
709A		JMP START:		C3, DA, 6F	
	5.	**Subroutine**		**To check the data**	**received is within the defined Ranee or not (<3A or > C6).**
7150	CHECK	LDA	2800	3A, 00, 28	
7153		CPI	3A	FE, 3A	Data less than 3 A H
7155		JC Error:		DA, 00, 72	
7158		CPI	C6	FE,C6	Data greater than C6 H
715A		JNC Error:		D2, 00,72	
715D		JMP CONT:		C3, 66,70	
	6.	**Subroutine**		**to send the messaee "Error" to the disolav when data is out of ranee.**	
7200	Error:	MVI	L,20	2E, 20	
7202	DEND1:	MOV	A, M	7E	
7203		OUT	14	D3, 14	
7205		INX	H	23	
7206		DCR	C	OD	
7207		JNZ DENDI:		C2,02, 72	
720A		LXIH, FF, FF		21, FF, FF	
720D	D5:	DCX	H	2B	
720E		MOV A, H		7C	Delay
720F		ORA	L	B5	
7210		JNZ	D5:	C2, OD, 72	
7213		JMP	L1:	C3, DA, 6F	

7.   Display

Memory location	Seven segment equivalent	Seven segment equivalent code of the data
2100	3F	0
2101	06	1
2102	5B	2
2103	4F	3
2104	66	4
2105	6D	5
2106	7D	6
2107	07	7
2108	7F	8
2109	6F	9
210A	80	Point (.)
210B	00	Blank
210C	40	Dash (-)
210D	73	p
210E	76	H
210F	00	Blank
2110	00	
2111	00	
2112	00	
2113	00	
2114	00	
2115	00	
2116	00	
2117	00	
2118	00	
2119	00	
211A	00	
211B	00	
211C	00	
211D	00	
211E	00	
211F	00	
2120	79	E
2121	50	r
2122	50	r
2123	5C	o
2124	50	r
2125	00	
2126	00	
2127	00	
2128	00	
2129	00	
212A	00	
212B	00	

- Sending the equivalent seven-segment code of the contents of registers D and E.

- Subroutine to check the data received is within the defined range or not.

- Subroutine to send the message "Error" to the display when data is out of range.

- Seven segment equivalent codes for the pH values of 0 to 9, point (.), blank, dash (-), p, H, blank spaces, Error and blank spaces.

The assembly language program developed for this system is given in the Table III.

7. RESULTS AND CONCLUSION

The sample results generated by this system are given in the Table IV. The results are comparable with the pH measured by the laboratory meter. By corresponding changes in the software the system is able to measure the pH in the two decimal digit forms. Such type of system is suitable for laboratory applications to measure the pH of a solutions having fixed temperature. By adding the extra circuitry and proper tuning of the parameters we utilize this system for pH controlling applications. Further improvement is that we are going to utilize the micro controller in place of the microprocessor.

Sr. No.	pH indicated by std. Meter	pH indicated by this system
1	7.01	7.0
2	4.96	5.0
3	8.55	8.4
4	10.15	10.0
5	11.00	10.9

Table IV : Sample results

REFERENCES:

1. N U Nayak, R H Suresh Bapu, Nalini Tondiraj and Y Mahadev Iyer, "PC CONTROLLED ON LINE pH MEASUREMENT AND CONTROL SYSTEM USING INDIGENOUS pH TRANSMITTER", 1. Instrument Society of India, 31 (2), p-150- 154.

2. Yadagiri, P., Thyagarajan, T., Panda, R.C., Rao, P.G., "Advances in modeling and analysis B: Signals, Information's, Patterns, Data acquisition, Transmission, Processing, Classification", 43(3), p-41-63.

3. Gopal, M., Kumar, S., et al, "Synthesis of a robust pH controller using QFT", Proceedings of IEEE TENCON' 1998. IEEE USA, p- 214-217 Vol. 1.

4. M N Aoutade, "Improved techniques for measurement of ph", unit 5, Ph. D. Thesis submitted to Pune University, p-99-114.

5. National semiconductor Data manual, P-7-105.

6. D. Patranabis, "Principles of Industrial Instrumentation", Tata McGraw-Hill Publishing Company Limited, p-475 - 481.

7. B. Ram, "Microprocessor...", PHI Publishing Company Limited, New Delhi.

DESIGN AND IMPLEMENTATION OF REMOTE DATA ACQUISITION SYSTEM FOR METEOROLOGY

S. Meenatchisundaram, S. Dwaragha Arumugham and K. Venugopal
*Department of Instrumentation and Control Engineering, Regional Engineering College
Tiruchirappalli, Tamilnadu

ABSTRACT

This paper deals with the design and development of wireless data acquisition system for meteorological variables. Two variables namely solar intensity and wind speed are measured and their outputs are conditioned. The Remote Data Acquisition System is designed using a micro-controller and its output is fed to the FSK modulator. A cordless circuit is 'used to transmit and receive the modulated signal. The received signal is demodulated and fed to the Pc. The values are displayed in a user-friendly format. The designed system is tested in the laboratory for a range of 100m.

I. INTRODUCTION

1.1 Meteorology

Meteorology is the science of the earth's atmosphere and its changes, used especially in forecasting the weather. Continuous monitoring of atmospheric parameters is an essential aspect for this. Wind speed and wind direction are measured using a wind anemograph or cup anemometer. Solar intensity or Sunshine is measured by concentrating the beam of sunlight by a convex lens on to a strip with markings on it. Due to the heat the strip turns brownish and the level of brownish area based on markings can be related to solar intensity. From the meteorological instruments, the readings are taken manually, processed and then sent to the Central Meteorological Center by the meteorological observer. Usually readings are taken at the interval of 3 hrs, which make up to 8 observations a day.

1.2. Wireless Data Acquisition System

To overcome the difficulty of measuring the meteorological variables manually, a wireless data acquisition system is designed and implemented as shown in *figure* 1. Two variables namely solar intensity and atmospheric wind speed are chosen as variables.

The Solar Intensity and Wind speed are measured using Solar Intensity Sensor (LDR) and Wind Speed Sensor (Alternator) respectively. The measured signals are fed to the micro-controller, then transmitted and received using FSK modulation.
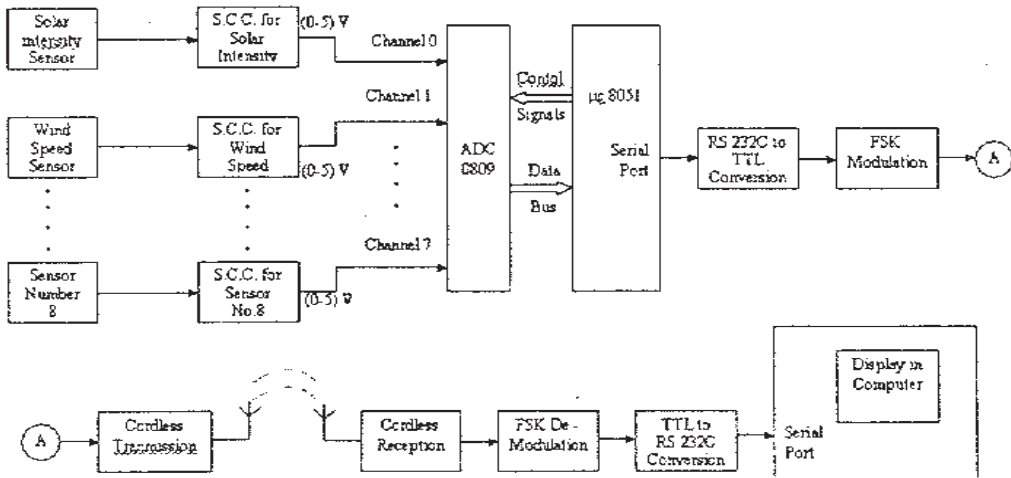
Fig.1. Block diagram of the wireless data acquisition system

2. SENSORS

2.1. Solar Intensity Sensor

LDR is used as the sensor. Its input output characteristics are determined with the help of a pyranometer[1]. Pyranometer has the thermal detector, which responds to the total power absorbed and theoretically it is non - selective to the spectral distribution of radiation. This implies that the naked thermal detector is also sensitive to long wave IR radiation from environment. The radiation energy is absorbed by a black painted disk present in it. The heat generated flows through a thermal resistance to the heat sink (the pyranometer body). The temperature difference across the thermal resistance of the disk is converted to a voltage and given as output. The irradiation or the solar intensity is equal to the ratio of the output of pyranometer (in μV) and the sensitivity of the pyranometer (in mV / W m^{-2}). The sensitivity of the pyranometer used is 5.11 μV / W m^{-2}. The resistance variation with intensity of light for a full 24 hr day are measured. A data logger is used to record the pyranometer output and resistance of LDR. Each value of pyranometer output (in mY) recorded for a day is converted into solar intensity. A chart is drawn showing the Input - Output characteristic of the chosen LDR with the help of recorded readings[2] as shown in *figure* 2.
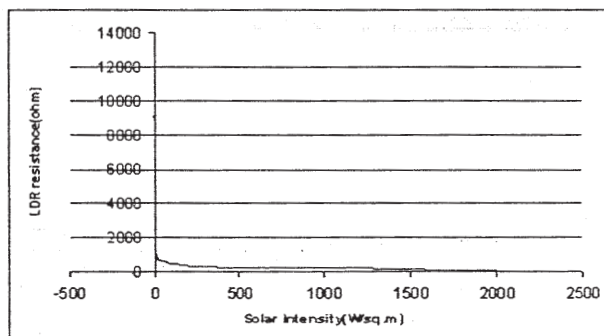
Fig.2. Input - output characteristics of LDR

2.2. Atmospheric Wind Speed Sensor :

An alternator with rotating blades on its rotor is chosen as a sensor as in the *figure 3*. The output of the transducer is 0 - 12 V ac.

(a) Side View   (b) Front View
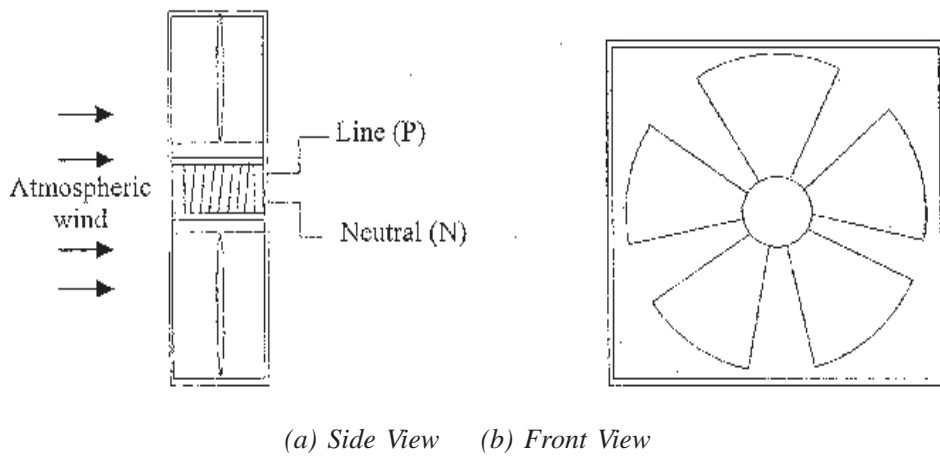
Fig. 3. Layout of the atmospheric wind speed sensor

By placing a hot - wire anemometer[3] near the chosen transducer, the Input - Output characteristics are determined as shown in *figure 4*.
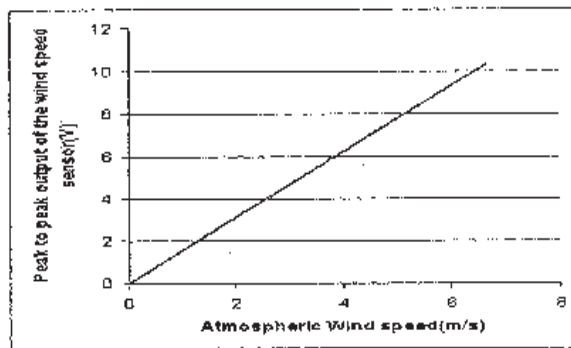
Fig. 4. Input - output chracteristics of wind speed sensor

3. SIGNAL CONDITIONING

3.1. *Signal Conditioning for Solar Intensity Sensor*

The resistance of the LDR is 12KΩ at near darkness. The bridge is designed to have an output voltage range of 0 - 2.5 V. Differential amplifier and clipper circuits are used to amplify the bridge output to 0 - 5 V and to restrict the output within 0 - 5 V respectively.
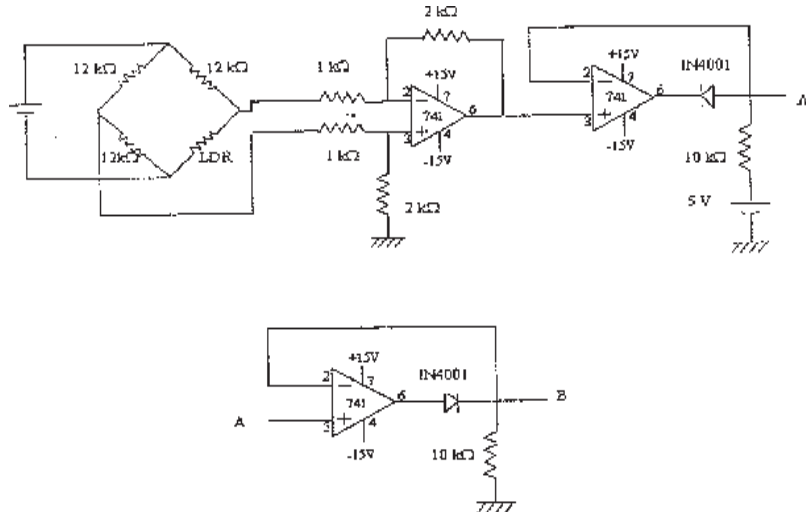
Fig. 5. Signal Conditioning for Solar Intensity sensor

3.2 Signal Conditioning for Wind Speed Signal

The precision rectifier circuit is designed to convert the alternating voltage signal to varying DC signal. A peak detector circuit is used to convert varying DC signal to constant DC signal. Clipper circuits are used to restrict the output within 0 - 5 V.

4. MICROCONTROLLER PROGRAMMING

4.1 Programming ADC 0809[4]

The program uses 8255A, programmable peripheral interface into share control signals and data signals with ADC 0809. Initially 8255 is configured in input/output mode with port A as input port, port B as output port, port C upper as input port and port C lower as output port. Port A is used for receiving analog to digital converted signal. Port B is used to send channel to be selected for conversion. Port C is used for control signaling. ALE and SOC signals are given as a pulse through the port C lower, in order to initiate the analog to digital conversion process. Port C. 7 is checked for EOC. The digital data is received through port A and stored in register Rl.

4.2 Transmission Programming:

The data that is received and stored in register R1 of micro controller is sent out serially though the on-chip serial ports, at a baud rate of 1200. 8051 has a serial data communication circuit that uses register SBUF to hold data. Register SCON controls data communication register, and baud rate is determined by the mode chosen and by initializing the timer with required count for baud rate. Typically, timer l is used in timer mode 2 as an auto load 8-bit timer. Transmission of serial data bits begins anytime data is written to SBUF. The flag TI in SCON is set to a 1 when the data has been transmitted and signifies that SBUF is empty. So the program waits for the TI flag before transmitting next data. Each data byte is sent with a frame that has 2 start bytes, channel number corresponding to the data byte and data byte.
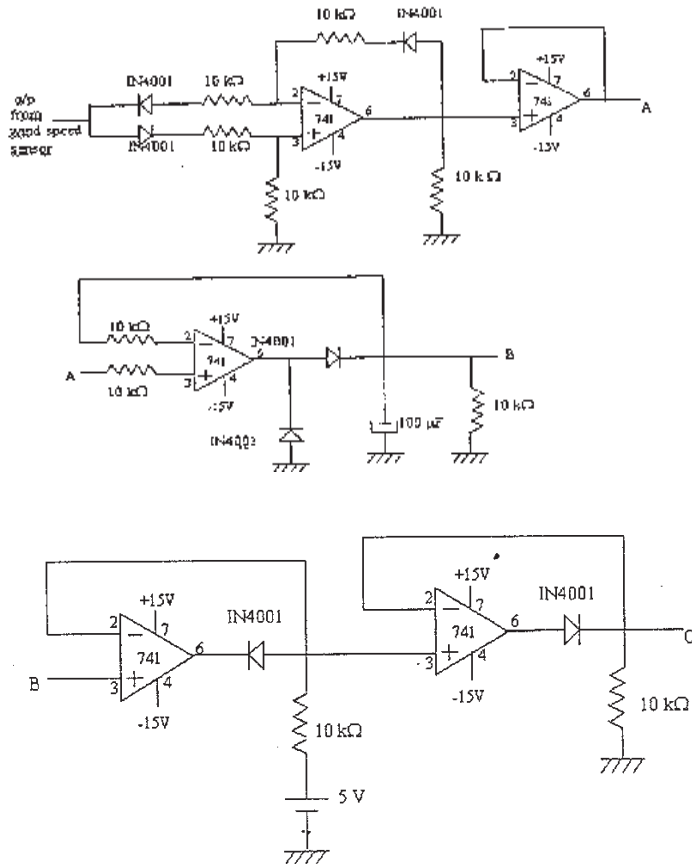
Fig. 6. Signal Conditioning for Wind Speed Sensor

A delay of 6.5ms is included between the transmissions of 2 individual bytes. The output of serial ports is given to the FSK modulator after passing through a RS232C - TTL level converter.

5. COMMUNICATION CIRCUITS

5.1 FSK MODEM:

The Frequency Shifting Keying (FSK) is employed in modulation / demodulation of digital information using an XR2206[5] and XR2211 respectively. In this technique the logic 0 and 1 are transmitted using two different frequencies (2200Hz and 1200Hz) called (preset) carrier frequencies. The signal that is sent out serially from the micro-controller is taken to the FSK modulator via the RS232-C Interface. The signal amplitude is converted from RS232 to TTL level using MC1489.

5.2. Cordless Transmitter and Receiver:

FM transmitter of handset of cordless phone is used to transmit the FSK signal and the base is used to receive the FM signal[6]. To perform the operation, the following modifications are made in the cordless. phone. Dialing section is removed / bypassed in both base and handset so that the cordless phone operates as if it were an intercom.

Telephone line interface is disconnected. Power to handset is supplied with direct variable voltage source and battery is removed. Mike in handset is removed and FSK signal is given to the nodes. The output signal is given as input to the FSK Demodulator instead of giving it to speaker and the speaker is removed.

The FSK demodulated signal and the ground signal are connected to the 2nd and 5th pin of the pin connector of the RS 232C interface of the computer. A code in C language is written to display the measurement values in the computer. The code first initializes the baud rate, number of bits per character, number of stop bits.

6. CONCLUSIONS

The Remote Data Acquisition System is designed and implemented for the meteorological variables Solar Intensity and Wind Speed. The performance of the system is tested in the laboratory for a distance of 100m. The recorded display obtained during the laboratory test is 14:30:54 The Solar Intensity is 1200 w/sq.m. 14:30:54 and the atmospheric wind speed is 0.86 m/s.

REFERENCES

1. Pyranometer CM 11/14 Instruction Manual, Kipp & Zonen, UK.

2. DELTA - T DL2e LOGGER User Manual, Version - 2.02, Delta - T Devices Ltd, 128 Low Road, Burwell, Cambridge, CBl OEl, UK.

3. Hot-wire Anemometer Testo 490 Manual, Testo Instruments, UK.

4. Micro 51 EB Technical Reference, Version - 1.0, Vi Microsystems Pvt. Ltd., Plot No.75, Electronics Estate, Perungude, Chennai - 96.

5. XR 2206 and XR 2211 Datasheets (www.exar.com)

6. Manahor Lotia, "Modem Telephone & Cordless Circuits", Volume - 1, BPB Publications, New Delhi, First Edition.(1997).

7. National Data Acquisition Data book, National Semiconductor, Germany (1995) for ADC 0809.

MODELING OF MIDDLE PRODUCT OF A DISTILLATION COLUMN USING AKAIKE INFORMATION CRITERIA

A. Vimala Juliet[1] and S. Renganathan[2]

[1]*Department of Instmmentation and Control Engineering, S.R.M. Engineering College, Kattankulathur 603203, Tamil Nadu, India*
[2]*Bharath Institute of Science & Technology, Salaiyur, Tambaram, Chennai, India,*

ABSTRACT

We present an approach that uses Canonical Variate Analysis and Akaike Information Criteria for system identification and reduction in order of a Distillation Column model. The optimal model stmcture of distillation column is found using Akaike Information Criteria. In the method proposed, the statistically significant values are first obtained using Canonical Variate Analysis approach, thus providing a mathematical basis for the model. The open loop response data are collected from a distillation column. Ten manipulated variables are reduced to two, which in turn is used for calculation in another refined model.

1. INTRODUCTION

There are about hundreds of variables related with distillation process, out of which five variables are taken as Control Variables and ten are taken as Manipulated Variables. In fact, a distillation column presents the following characteristics: it is a non-linear process; it is multi variable with strong interactions, and it exhibits pure time delays between its input and output variables [1]. Consequently, the application of Canonical Variate Analysis (CVA) and Akaike Information Information Criteria (AIC) for modeling will be a real and challenging one[2]. Determining a model using a conventional method is difficult, because it needs complete understanding of the process; even if it is found, it would be with higher dynamics, obviously very complicated. It would be difficult to determine the appropriate model structure, particularly in the presence of unknown feedback. Additionally, the parameter estimation requires nonlinear iterative parameter optimization that encounters convergence problems, especially for multi variable systems. The Canonical Variate Analysis provides an alternative method for finding state space or equivalent ARMAX models using a computation ally efficient and stable algorithm. Once model of this process is developed, then the refined model selection can be determined using Akaike Information Criteria. In Section 2, we discuss the working of the Distillation Column. The State space model along with Canonical Variate Analysis is briefly discussed in Sections 3.

2. PROCESS DESCRIPTION

The physical separation of mixtures can be achieved by various methods like filters, extraction, etc. But Distillation Column method is most suitable in Petrochemical industries. It separates based on the volatility of the components present in the crude oil. The Distillation tower at Chennai Petroleum Corporation Ltd., Tamil Nadu, India is 40.3m tall vertical column with 4.5m diameter in the fractionating section. The detailed model of the distillation column dynamics is not available. Data for the present work, collected from the open loop response of the column is shown in Table 1 and graphically shown in Figs l (a-j). The ten Manipulated Variables and five Control Variables and their ranges are shown in Tables 2 and 3.

The fractionation as practiced in refineries involves heating the crude to a temperature high enough to effect product separation and heating cost of crude is significant. So in order to reduce the fuel cost, crude is preheated in heat exchangers with products and pump around streams of unit so that maximum heat is recovered. Crude distillation column has two sections. The bottom section known as stripping section has 6 trays and the upper section known as fractionating section has 34 trays. The vaporized portion of the feed, strip out vapours from stripping section and steam emanate from the bottom section rises up the column. In order to condense the vapours into various distillate fractions at appropriate zones, it is necessary to maintain a temperature gradient across the tower. This is maintained by three pump around circuits in the column. The Top Pump Around (TPA) liquid stream is drawn from 37th tray at a temperature of $219^{O}C$ through a pump. This (TPA) returns to the tower at tray 39 only. The cooled TPA returns to tower at a temperature of $94°C$. The Middle Pump Around (MPA) and kerosene distillate product share the same tray 20. The cooled MP A at a temperature of $165°c$ returns to the tower at tray 25 only. The Bottom Pump around (BPA) and diesel product share the same draw tray 12 BPA drawn at $311°C$. The cooled BPA returns to the column at a temperature of $250°C$ to the tray 14. Thus TPA, MPA & BPA heat duties have been used to reduce vapour load in the column for the revamped capacity. The Process flow diagram of a distillation column is shown in Fig. 2.

The middle product temperatures are tabulated for various manipulated variables, by giving step changes. The operating point is taken as zero, and changes taking place in the variables, are scaled with respect to the operating point. For example, if the operating point of the manipulated variable (top pressure) is 2.7 kg/cm^2, and a step change is given to this manipulated variable, the changes in the controlled variable (middle product temperature) decreases from $219°C$ to $217.476°C$. Here $219°C$ corresponds to 0 and $219.476°C$ would corresponds to -1.524, as recorded in Tables.

3. STATE SPACE MODEL AND CANONICAL VARIATE ANALYSIS

Data collected from the petroleum industry are the time series data, which consist of output variables *(Y_t)* and input variables *(U_t)* as shown in Table 1. The first step in statistical procedure is to fit the ARX model using these input and output variables to find parameters like past lags, p and degree, d, as described later, in this section. This past lags and degree are used in canonical variate analysis to determine the order, K of the system[3]. Then the State Space model for the Distillation column is fitted using Markov's process[4].

A. Vimala Juliet and S. Renganathan

Table 1

Open loop response data

TP	TRF	NDR	KDR	DDR	TPAR	MPAR	BPAR	KSSS	BSS
0.000	0.000	-0.003	-0.001	0.002	0.000	0.000	-0.001	0.105	0.070
0.000	0.004	-0.001	-0.003	0.008	0.001	-0.002	-0.002	0.461	0.251
0.000	0.004	0.015	-0.006	0.013	0.001	-0.005	-0.005	0.796	0.489
0.000	-0.001	0.035	-0.007	0.017	0.001	-0.009	-0.006	0.942	0.782
-0.084	-0.013	0.057	-0.007	0.020	0.001	-0.013	-0.007	0.565	0.963
-0.202	-0.034	0.073	-0.006	0.022	0.000	-0.015	-0.008	-0.209	1.103
-0.370	-0.056	0.083	-0.004	0.024	-0.001	-0.017	-0.008	-1.173	1.201
-0.551	-0.080	0.092	-0.003	0.025	-0.001	-0.017	-0.008	-2.073	1.340
-0.761	-0.103	0.098	-0.001	0.026	-0.002	-0.017	-0.008	-3.288	1.480
-1.620	-0.188	0.131	0.004	0.035	-0.004	-0.015	-0.007	-4.775	1.857
-1.710	-0.200	0.137	0.005	0.037	-0.004	-0.015	-0.007	-4.921	1.913
-1.773	-0.211	0.144	0.005	0.039	-0.004	-0.015	-0.007	-5.047	1.969
-1.822	-0.221	0.150	0.006	0.041	-0.005	-0.015	-0.007	-5.131	1.997
-1.934	-0.264	0.180	0.007	0.041	-0.006	-0.015	-0.006	-5.382	2.220
-1.941	-0.271	0.184	0.007	0.040	-0.006	-0.015	-0.005	-5.382	2.276
-1.955	-0.279	0.188	0.007	0.039	-0.007	-0.015	-0.005	-5.424	2.360
-1.962	-0.288	0.192	0.007	0.039	-0.007	-0.015	-0.005	-5.403	2.415
-1.962	-0.296	0.196	0.007	0.038	-0.007	-0.015	-0.005	-5.445	2.513
-1.962	-0.300	0.199	0.007	0.038	-0.007	-0.015	-0.004	-5.445	2.597
-1.969	-0.309	0.202	0.007	0.038	-0.007	-0.015	-0.004	-5.445	2.681
-1.969	-0.314	0.203	0.007	0.038	-0.007	-0.015	-0.004	-5.445	2.778
-1.969	-0.321	0.207	0.007	0.038	-0.007	-0.015	-0.004	-5.466	2.848
-1.969	-0.327	0.208	0.007	0.038	-0.007	-0.015	-0.004	-5.466	2.960
-1.969	-0.331	0.211	0.007	0.038	-0.007	-0.015	-0.004	-5.487	3.058
-1.969	-0.338	0.212	0.007	0.038	-0.007	-0.015	-0.004	-5.487	3.141
-1.969	-0.341	0.213	0.007	0.038	-0.007	-0.015	-0.003	-5.487	3.211
-1.969	-0.348	0.214	0.007	0.038	-0.007	-0.015	-0.003	5.487	3.295
-1.969	-0.352	0.218	0.008	0.038	-0.007	-0.015	-0.003	-5.487	3.351
-1.969	-0.356	0.218	0.008	0.038	-0.007	-0.015	-0.003	-5.487	3.421
-1.969	-0.360	0.219	0.008	0.038	-0.007	-0.015	-0.003	-5.487	3.490
-1.969	-0.362	0.220	0.008	0.038	-0.007	-0.015	-0.003	-5.487	3.546
-1.969	-0.364	0.221	0.008	0.038	-0.007	-0.015	-0.003	-5.487	3.574
-1.969	-0.369	0.221	0.008	0.038	-0.007	-0.015	-0.003	-5.487	3.602

TP-Top pressure, TRF-Top Reflux flow, NDR-Naphtha draw rate
KDR-Kerosene draw rate, DDR-Diesel draw rate ,TPAR-Top pump around rate, MPAR-Middle
pump around rate, BPAR-Bottom pump around rate, KSSS-Kerosene stripper stripping steam.
BSS-Bottom stripping steam
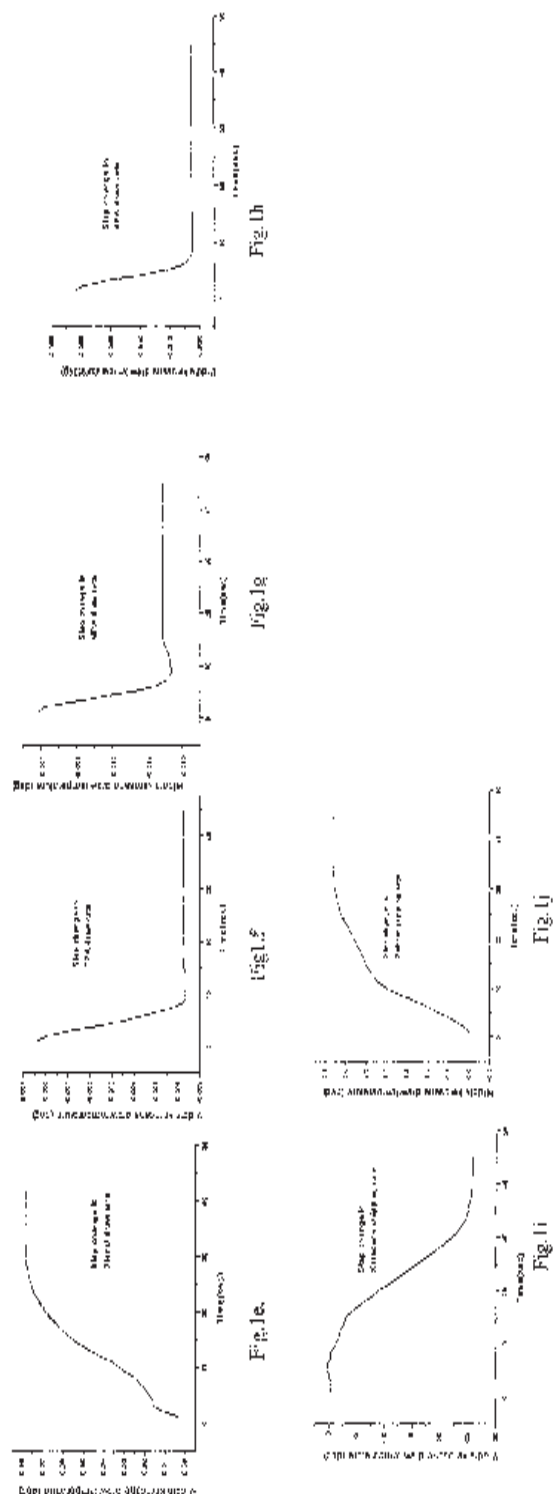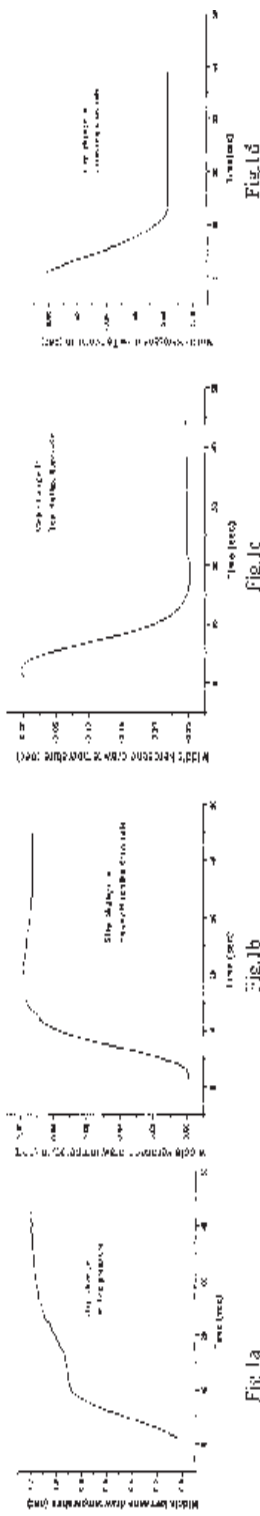
Fig.1(a–j)The open loop response of the kerosene draw temperature step change in 10 manipulated variables. In all figures, X-axis represents Time scale and Middle kerosene draw temperature is along the Y-axis.

S.No	Manipulated Variables	Range	Operating point	Unit
1	Top pressure	0-5	2.7	Kg/cm^2
2	Top reflux flow rate	0-180	112	M^3/hr
3	Heavy naphtha draw rate	0-73	25	M^3/hr
4	Kero draw rate	0-260	92	M^3/hr
5	Diesel draw rate	0-200	82	M^3/hr
6	Top pump around draw rate	0-500	375	M^3/hr
7	middle pump around draw rate	0-700	583	M^3/hr
8	Bottom pump around draw rate	0-500	445	M^3/hr
9	Kerosene stripper stripping rate	1-2	1.25	Ton /hr
10	Bottom stripping rate	0-6	4	Ton/hr

Table 2 : List of Manipulated Variables and their units

S.No	Control Variables	Range	Operating point	Unit
1	Top product temp	0-200	130	^oC
2	Heavy Naphtha draw temp	0-300	175	^oC
3	MPA(kerosene) draw temp	0-300	219	^oC
4	BPA (diesel)draw temp	0-400	361	^oC
5	Bottom level	0-100%	50	%

Table 3 : List of Control Variables and their units

Lag, *p* is determined by fitting Auto Regressive models with eXogenous inputs (ARX) as given in Eq. (1)

$$Y_i = \sum_{i=0}^{p} \alpha_i Y_i - i + \sum_{i=0}^{p} \beta_i U_{t-i} + \sum_{j=I}^{d} \eta_j{}^t j \qquad (1)$$

where *p* is the past lag and *d* is the polynomial degree and are determined by fitting procedure.

α, β and η are the estimated coefficients.

$$\alpha_i = [\alpha_i, \alpha_2, \alpha_3 ....\alpha_p] \qquad (2)$$

$$\beta_i = [\beta_i, \beta_2, \beta_3...........\beta_p] \qquad (3)$$

$$\eta_i = [\eta_i, \eta_2, \eta_3...........\eta_p] \qquad (4)$$

In CVA computation the AIC for all state orders up to the maximum 12 is computed. The optimal order, k is the order for which AIC is minimum, which is the order of the true simulation model.
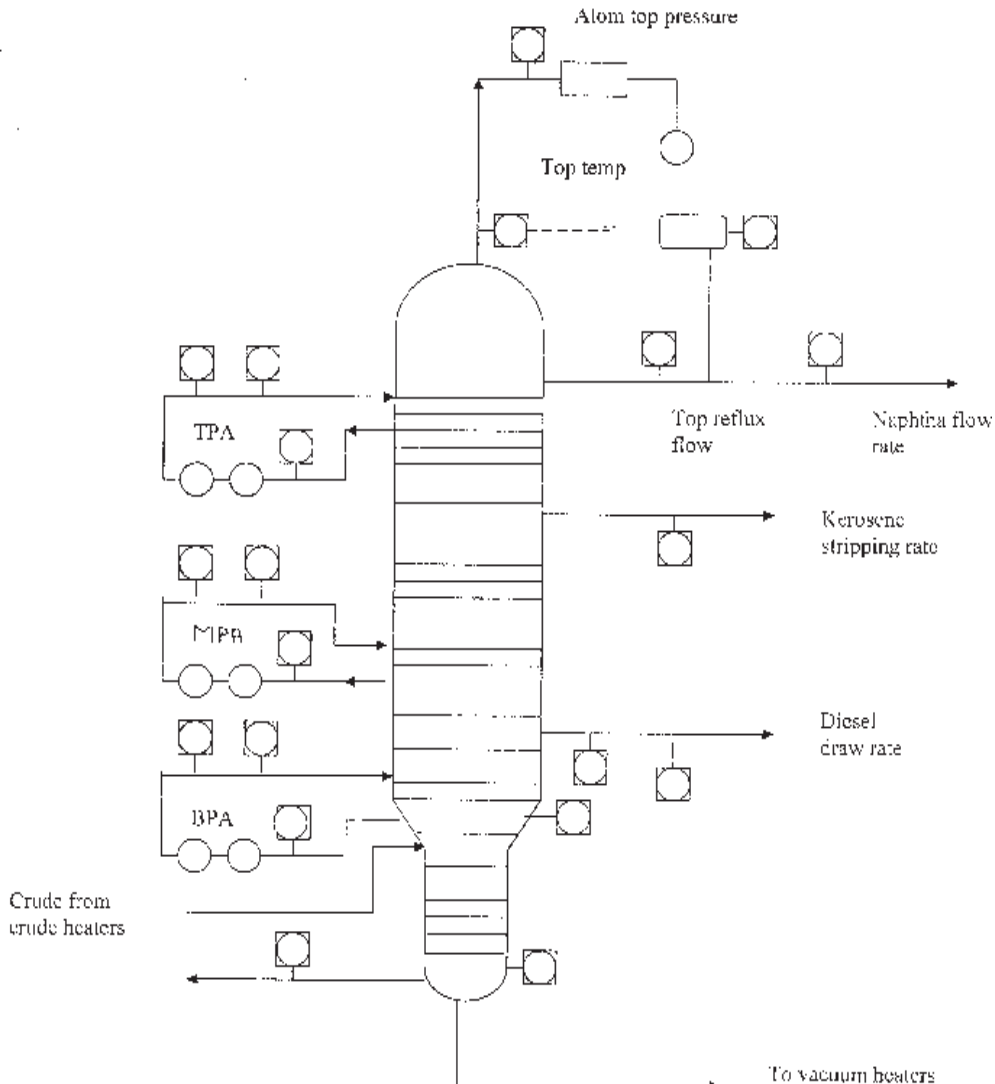
Fig.2. Process flow diagram Atmosphere tower

The AIC is calculated [5] using the expression as given in eq.(5),

$$AIC(k) = -2\log p(Y^N, U^N; \theta_k) + 2M_k \tag{5}$$

where p is the lag and M_k is the number of parameters in the state space model given by,

$$M_k = k(2n+m)+mn+n(n+1)/2 \tag{6}$$

Here, k is the number of states, n, the number of outputs, and m is the number of inputs to the system.[6]. The optimal state, order is used to compute the state space model of the form

$$X_{t+1} = \phi X_t + G U_t + W_t \qquad\qquad (7)$$

and the output eg. is given by

$$Y_l = H X_t + A U_t + B W_t + V_t \qquad\qquad (8)$$

where X_t is the Markov state order, W_t and V_l are white noise processes that are independent with covariance matrices Q and R. ϕ, G, H, A and B are coefficient matrices and their optimal estimates are found by CVA procedure [7].

4. RESULTS AND DISCUSSION

In the present work, we have taken the middle product temperature of the distillation column as the control variable. The middle product is accurately maintained at 219°C. It is trivial to note that all the ten manipulated variables mentioned in Table 1, would affect the process. In order to determine the variables that would affect the system most significantly, when disturbed, detailed statistical analysis has to be performed.

From the time series data, obtained from the open loop response (Table 1), the mean and standard deviation for all the variables are calculated and results shown in Table 4. As the table shows, the kerosene stripping rate and bottom stripping rate has got the most significant values. The variables which have large magnitude affects the process more significantly as pointed by Larimore [8, 9]. Hence the middle product temperature is most affected, when changes are made in these two manipulated variables. To build a mathematical model, these two variables are used as manipulated variables.

	TP	TRF	NDR	KDR	DDR	TPAR	MPAR	BPAR	KSSS	BSS
Mean	-1.524	-0.237	0.159	0.0043	0.033	-0.005	-0.015	-0.005	-4.284	2.323
Std. Dev.	0.705	0.124	0.066	0.005	0.009	0.003	0.004	0.002	2.08	0.99

Table 4. List of Manipulated Variables and their Statistical parameters

The Canonical Yariate Analysis uses singular value decomposition technique on the selected memory length and the rank of the matrix is found, which is nothing but the order of the model. This order is further used in Markov's process to predict the future values based on the past values, to fit the state space model for the middle portion of the distillation column. Thus the reduced order is found and refined model is selected using AIC.

AIC's for various lags and polynomial degrees are calculated by fitting data in the ARX model [10,11]. The calculated values, for degree 1, is shown in Table 5. The past lag is the one corresponding to the minimum value of AlC, which in this case is 5. Using singular value decomposition in CVA, the number of nonsingular elements is the rank of the matrix. This rank is the order of the model, which in the case of middle product turns out to be 4.

The calculated AlC values for various orders and parameters are shown in Table 6. The AIC is minimised and its corresponding values gives the optimal state order and the number of parameters.

Lags	AIC for Degree 1
0	850.2
1	-6519.6
2	-7526.8
3	-7659.3
4	-7708.4
5	-7727.0
6	-7724.7
7	-7711.5
8	-7694.0
9	-7675.2
10	-7657.4

Table 5. The Optimal selection of LAGP for CVA computations is one larger than the Lags of MIN.

Order	Parameters	AIC
0	11	1355.6549
1	17	−2592.9602
2	23	−8002.8793
3	29	−8997.5000
4	35	−9388.6610
5	41	−9375.6655
6	47	−9362.4771
7	53	−9349.0839
8	59	−9335.5594
9	65	−9321.8160
10	71	−9307.8988
11	77	−9293.8078
12	83	−9279.5387

Table 6. The Optimal order chosen minimizes the AIC.

5. CONCLUSIONS

The computation of the nonlinear Canonical Variate Analysis and Akaike Information Criteria has been performed to determine State variables. State transitions have been obtained by computing the nonlinear regression. The Canonical variate analysis has been used to determine the state of a distillation column directly from the data, without making any assumptions about the functional form of the nonlinear dynamics. Akaike Information Criteria has been used to find an appropriate model order. Thus the Canonical Variate Analysis has yielded satisfactory results when state space form of the model proposed by Larimore has been used.

REFERENCES

1. Peter Eserin et al., Application of CVA to the Dynamical Modeling & Control of Drum level in an Boiler, Proc., ACC, 1999, p1163.

2. Charles D. Schaper, et al., Identification of Chemical Processes using Canonical Variate Analysis, Proc. 29th Conference on Decision and Control, Hawaii, Dec. 1990, p605.

3. Akaike. H. "A. New look at Statistical model identification", IEEE Trans. Auto. Con. Dec. vol.19(6), 1974, p716.

4. Wallace E.Larimore. "Automated multi variable system Identification: Short Course", University of California, Santa Barbara, p1

5. Dale E. Seborg et al. "Identification of the Tennesse Eastman challenge process with subspace methods", pl06

6. Wallace. E. Larimore "Identification of co-linear and co-integrated multi variable system using canonical variate analysis", IFAC SYSID 1999, Santa Barbara, Jun, 2000, pI.

7. Wallace. E. Larimore, "Automated multivariable system identification and industrial identification" ACC Proc. 1999, p.1148.

8. Wallace. E. Larimore, "Optimal order selection and efficiency of canonical variate analysis system identification", Proc. 13 IFAC World Conference, vol. I, p.151.

9. Wallace. E. Larimore, "System identification of feedback and casuality structure using canonical variate analysis", IFAC SYSID, 1997, Fukuoka, Japan, July 8-11, 1997, p.1.

10. Wallace. E. Larimore et Al. "The ADAPTx software for Automated multivariate system identification", IFACSYSID 1999, Santa Barbara, p.1.

11. Peter J Diggle, "Time series, A Bio statistical Introduction", Oxford science publications, 1990, p.21.

DESIGN OF AT89C52 MICROCONTROLLER BASED SYSTEM FOR THE MEASUREMENT OF TEMPERATURE AND CONTROL

A. Rajendran and P. Neelamegam*

*Research & PG Department of Applied Physics, Nehru Memorial College, Puthanampatti,
Tiruchirappalli, Tamil Nadu - 621 007.*
**Research & PG Department of Physics, A YYM Sri Pushpam College, Poondi, Thanjavur,
Tamil Nadu - 613 503.*

ABSTRACT

An AT89C52 microcontroller based system is developed to measure and to control temperature for conductivity studies of liquids. The system improves the accuracy of recorded data, eliminates varying degrees of human participation, and saves operator time. Software programs developed in this system are simple to use and provide versatility in programming temperature ranges and timing processes.

1. INTRODUCTION

The measurement of temperature is important in, medicine, ecology, industry and plant science research. Accurate measurements are required with close attention to the sensitivity of the instrument used over the whole measured range in order to achieve reliable results. Conventionally, these measurements were performed byvarying the temperature manually in steps, are recorded either manually or on the chart. The main aim of this paper is to describe a data acquisition system for measurement of temperature and control the system based on a microcontroller that has been designed and developed using PID algorithm. Electronic temperature controllers are commercially available and some of them have been reported in literature [1-2]. The continuous and tedious attention required for manual adjustment is eliminated. Typical applications of this system are melting point studies and the cyclic annealing - of semiconductor devices, water bath temperature control, conductivity measurement system, thermoluminescence measurement system and also suitable for general use.

2. SYSTEM DESCRIPTION

The block diagram of temperature measurement and control set up is shown in figure. 1. The system hardware consists of a k-type thermocouple, instrumentation amplifier (IC714), 12-bit analog to digital converter, solid-state power controller and AT89C52 microcontroller. A two-row 16 characters LCD display from Hitachi is interfaced with microcontroller to allow user communications and to display the results.
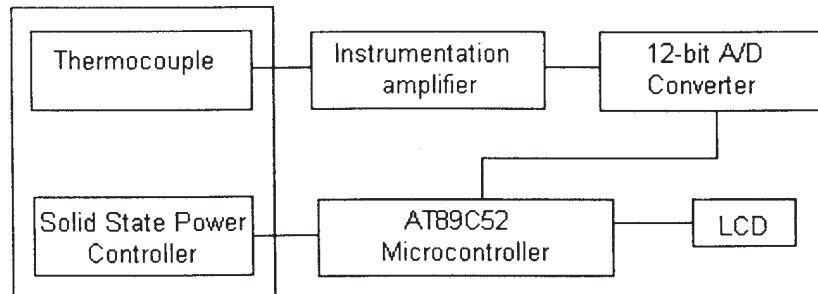
Fig.1. Block diagram of temperature measurement and control

3. HARDWARE SYSTEM

3.1. A T89C52 Microcontroller and A/D converter

Figure 2 shows AT89C52 microcontroller and 12-bit A/D converter (IC7109). The AT89C52 microcontroller is a low power, high performance CMOS 8-bit microcontroller with 8 KB of flash programmable and erasable memory and 256 bytes of RAM. It has 16-bit timer/counters, a full duplex serial port, on-chip oscillator, clock circuitry and low power idle and power down modes and it has the facility of three level program memory lock. Port 0 of the microcontroller is interfaced with 12-bit A/D converter (IC 7109). The 7109 A/D converter is a high performance, low power integrating device which provides the used with high accuracy, low noise, low drift, versatile and economical A/D converter of the dual slope,

Fig.2. AT89C52 microcontroller and 12-bit A/D converter
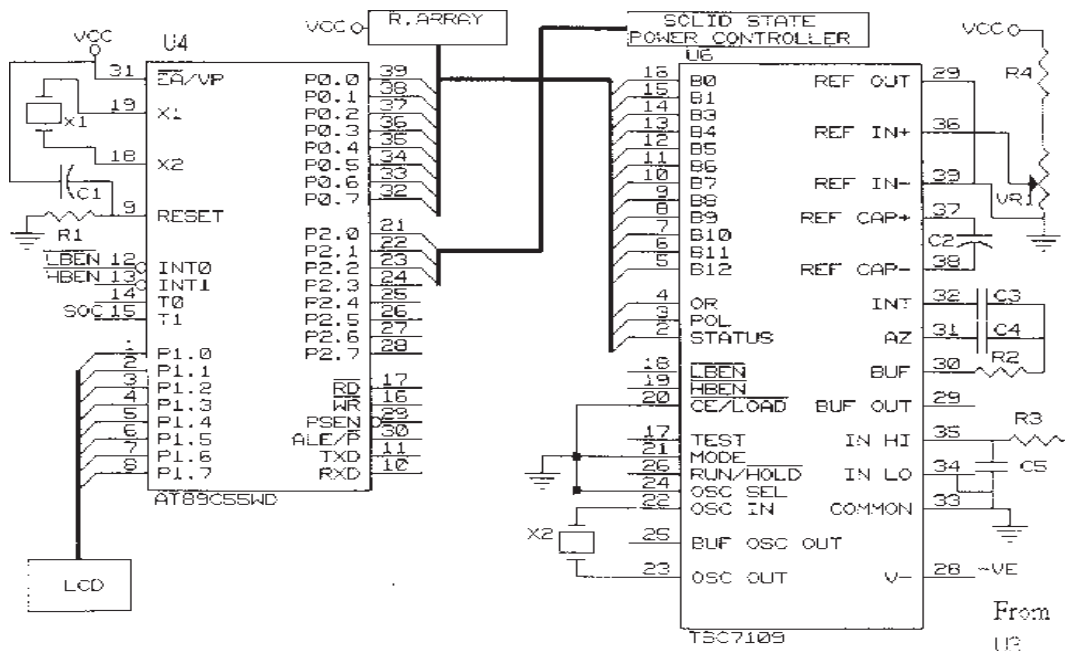
integrating 12-bit A/D converter which can make 30 conversions per second. It is used to convert the analog temperature into digital values. B_0 to B_7 and B_8 to B_{11} (12 bit), sign and overflow signal of ADC 7109 are connected through port 0. A 4MHz crystal is connected in between the pins 22 and 23. The LBEN and HBEN signals are used for reading lower byte and higher byte of digital word of ADC [3]. In the higher byte we get the four bits of the most significant data on D_0-D_3 and also the polarity and over range indication on bits D_4 and D_5. The pin 29 generates the internal reference voltage. As recommended by the data sheet a preset of 25K is connected between pin 29 and +5V. A tap from reset is given to pin 36, the reference input pin. Pins 30-32 are for auto zero circuit components. This IC uses +5V and -5V power supply. The output signal from the thermocouple after amplification is connected to the pin 35 of AOC 7109 through 1 MΩ resistance to convert analogue signals to digital value.
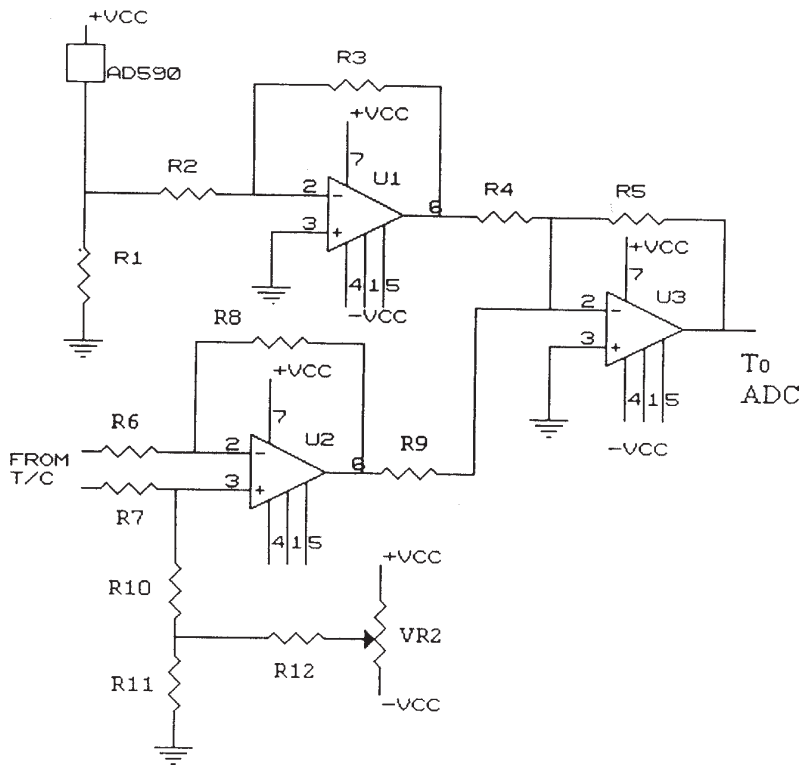
Fig.3. Circuit for temperature measurement

3.2. Temperature Measurement

The signal generated by the thermocouple junction due to thermal changes is fed to an amplifier circuit is shown in figure.3. The output signal is amplified to a suitable level by using a instrumentation amplifier read by the microcontroller through AID Converter. A semiconductor temperature sensor A0590 is used in the circuit to simulate a reference junction.
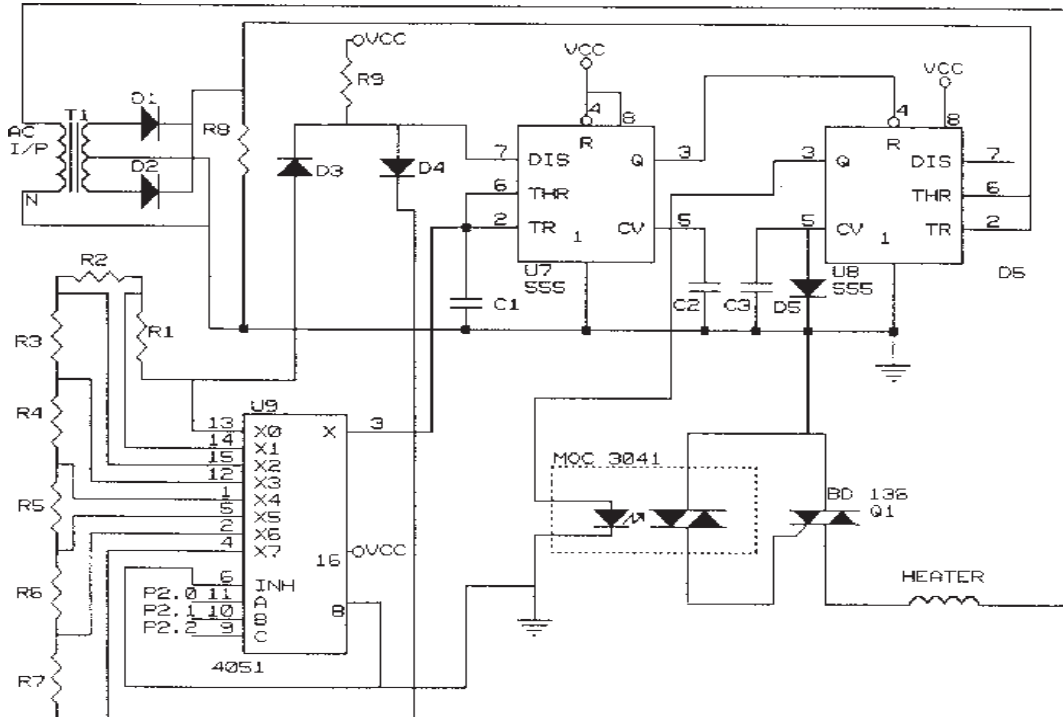
Fig.4. Circuit for solid state power controller

3.3. Solid state power controller

Figure 4 shows solid-state power controller, which is used to control the power to the heater. The power controller is establishing a variable duty cycle switch with zero cross over switching. The circuit is built around IC 555 timers, triac driver (MOC 3041), triac (BD136). U7 wired as a variable duty cycle oscillator with a constant time period of around 0.1 second. Duty cycle can be varied from 0 to 100% using the resistance R1 to R7, which are selected by the multiplexer (4051). The duty cycle can be changed by proper words from the microcontroller to pin 9, 10 and 11 of 4051. U8 wired as comparator with hysteresis (i.e.) schmitt trigger. The transformer Tl with rectifying diodes 01 and 02 delivers unidirectional. The low AC voltage is given to pin 2 and 6 of U8. The output of U8 from pin3 is connected to pin2 of triac driver as shown in the figure. MOC 304]. which incorporates a zero voltage crossing bilateral triac driver providing low power dc control of power triac, is used to drive the triac. By outputting 0 to 7 to port 2 of microcontroller the duty cycle of oscillator of an U7 can be changed and hence the power to the heater can be varied.

4. SOFTWARE SYSTEM

When the temperature is being measured, a set temperature is read to compute the error. The proportional, integral and derivative constant of the error are computed individually and their sum the Proportional+Integral+Derivative (PID) constant is then calculated and the

computed data is sent to 4051. By this the firing angle of the triac can be changed to the desired value and hence the power of the heater.

Software is developed in assembly language to initialize LCD display, to start AQC conversion, to check end of conversion, to read higher and lower bytes of ADC by enabling LBEN and HBEN signal, measure the temperature of the sample, indication of over range and sign of data, data computation for acquired data, storage of data for temperature. Flowchart for temperature measurement and control system using PID algorithm is shown in figure.5.
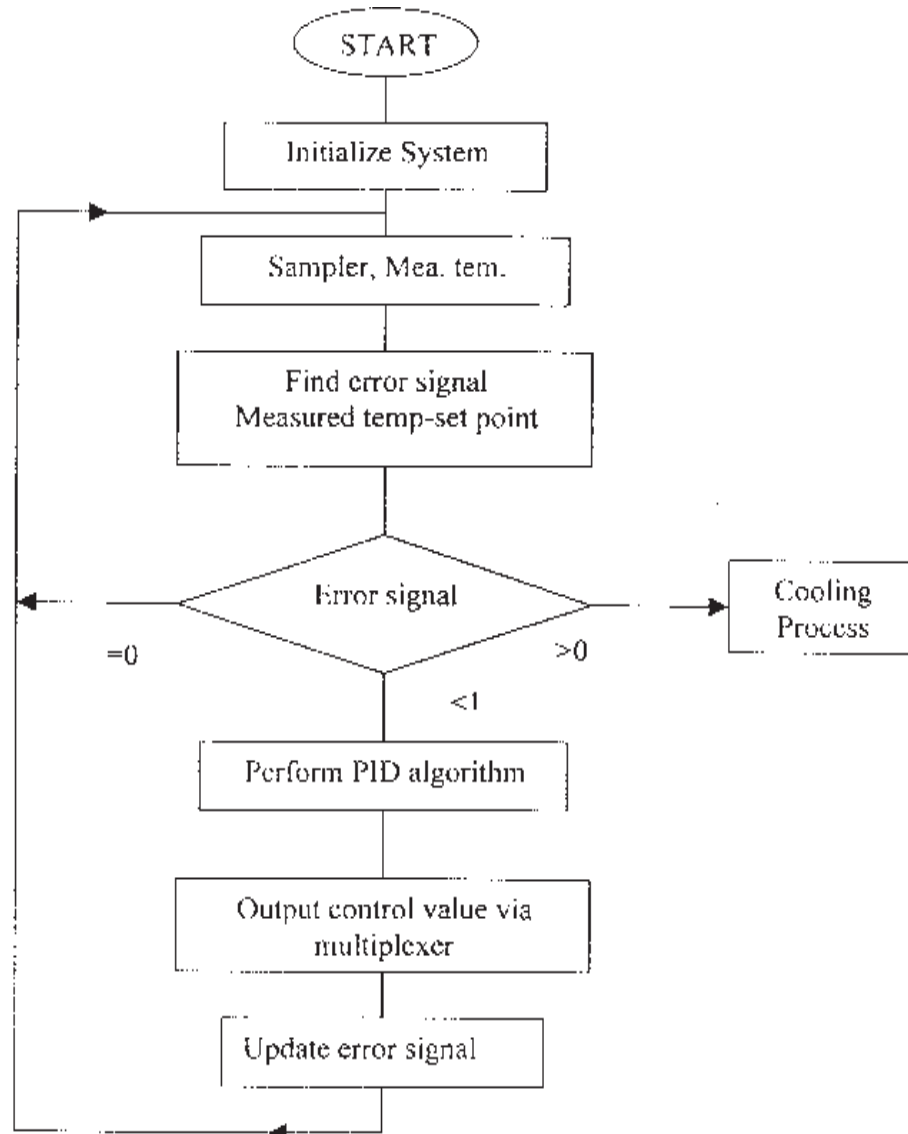
Fig. 5a. Flowchart for temperature measurement and control using PID algorithm
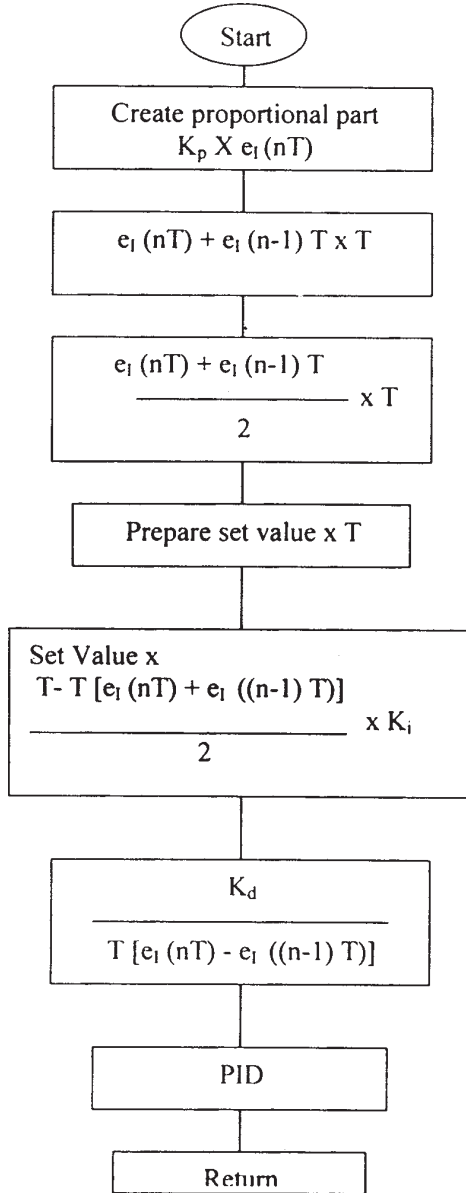
Fig. 5b. Flowchart for temperature measurement and control using PID algorithm

5. RESULTS AND DISCUSSION

During the development stages, the various circuit units of the hardware system were evaluated individually and as an integrated unit. All the software systems were enhanced to achieve optimum operation. In addition, for different samples, the experiment was run under different environments in the completely automated mode to illustrate the capabilities of the system. The instrument was tested by measuring temperatures in a wide range 30 to 500°C.

The performance of the instrument is compared with the electrx digital temperature controller to check accuracy of the instrument. Using this instrument the conductivity of KCL solution at various temperatures is measured and it is shown in figure.6.
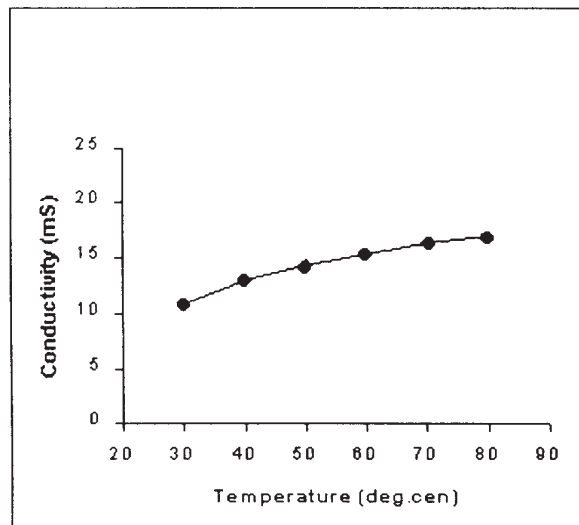
Fig.6. Conductivity of Kcl solution at various temperatures

REFERENCES

1. J.R. Engstrom and W.H. Weinberg, "Design and construction of a digital temperature controller for use in surface studies", Rev. Sci. Instrum. Yo1.55, pp.404, 1984.

2. J.E. Maclennan, M.R. Meadows, M.A. Handschy and N.A.Clark, Persollal computer based programmable temperature controller for general laboratory applications," Rev.Sci. Instrum., vol.56, pp 775, 1985.

3. P. Neelamegam, K. Padmanabhan and S. Selvasekarapandian Automated Thermoluminescence measurements using 6502 microcomputer board Meas. Sci. Technol. 3 1992 pp 581-587.

DEVELOPMENT OF A THERMAL CONTACT CONDUCTANCE TEST FACILITY

V. Vasudeva Rao, R. Raghukulender and M.V. Krishna Murthy*

Department of Mechanical Engineering, Sreenidhi Institute of Science and Technology
Hyderabad - 501 301

*Department of Mechanical Engineering, Indian Institute of Science,
Bangalore - 560 012

ABSTRACT

This paper presents the details of a test facility developed to measure thermal contact resistance across metallic contacts. The construction and instrumentation is such that, contacts of various geometry (nominally flat, hemisphere to flat, cone to flat contacts) can be investigated. Heat flow through the contact can be measured over a wide range of contact pressures (0.1 to 40MPa) and mean interface temperatures (0 to 250°C). The associated thermal potential differences required for calculation of thermal contact resistance can be measured. The use and the reliability of this apparatus are established by the measurements made on nominally flat contacts of 88-304. An additional and more important feature is that the direction of heat flow can be reversed without disturbing the contact under investigation. The apparatus also facilitates measurement of thermal conductivity. Using this test facility Thermal contact conductance across 88-304 test specimens is measured with and with out copper foils as interstitial materials in the contact pressure range of 0.1 to 2 MPa. The results showed that in the presence of copper metallic foils the contact conductance increased rapidly with increase in contact pressure when compared to the bare joint under the same set of conditions. The results are presented in graphical form.

1. INTRODUCTION

When two solid surfaces are brought in contact with each other for the purpose of transmitting energy in the form of heat or electricity, the interface formed between them is known as *contact.* When conduction heat transfer takes place across the interface, an extra resistance known as *thermal contact resistance* exists at the interface. The importance of thermal contact conductance has been recognised in the late 30's. Thermal contact resistance plays an important role in aerospace, electrical and electronic equipment when heat transfer from or to the equipment is very critical. Earlier investigators observed that the thermal contact resistance/conductance is influenced by 1) contact pressure 2) mean interface temperature 3) ambient pressure and temperature 4) interstitial material 5) heat flow direction 6) external magnetic field 7) vibration 8) surface roughness 9) waviness 10) thermal conductivity of the contacts and 11) micro-hardness. Each of these parameters will have its influence on thermal

contact conductance. It is due to this reason that the mathematical modeling of contact resistance problem is not fully successful and remains a research topic till today. Therefore, the designer of heat transfer equipment still depends on experimental results rather than the predicted values for a particular set of operating conditions for more reliability. Keeping this in view, several investigators developed test facilities to measure thermal contact conductance. However, each of these facilities that are developed in the past has their own advantages and limitations. Hence, to investigate the influence of each of these parameters on the thermal contact resistance a test facility is designed and developed which facilitates varying one parameter at a time keeping all other parameters constant throughout the experiment irrespective of the other operating conditions.

2. LITERATURE REVIEW

Fletcher[1] and Madhusudana and Fletcher 2 presented excellent reviews on the developments in contact heat transfer, its importance and applications in various fields. Fletcher[3] presented various experimental techniques for thermal contact resistance measurements and test facilities developed by different investigators. O'Callaghan and Probert[4] suggested certain specific modifications to take care of transverse losses in the test column. O'Callaghan and Probert[5] developed an improved test facility by duly incorporating the suggestions of O'Callaghan and Probert[4]. Snaith et al[6] discussed several difficulties associated when accurate measurements of thermal contact conductance are to be made. The accuracy of measurement depends on specimen geometry, form ratio, transverse heat losses, the apparatus design, heat metering, temperature measurement, and measurement procedures. The authors recommended a number of special criteria for thermal contact conductance testing and analysis. However, there has been little serious consideration *or* implementation of these recommendations. The apparatus design, which is the most important one among all the above mentioned factors, can suffice all the other requirements. From the published literature it is known that there are no test facilities designed duly implementing the recommendations of Snaith et al[6]. Precisely it is the purpose of this paper to design and develop a test facility in the light of the recommendations of Snaith et al.[6]

3. METHODOLOGY / MEASUREMENT PRINCIPLE

Thermal contact resistance is defined as a ratio of the temperature drop across the interface to the average heat flow rate through the interface. Mathematically it is expressed as the following

$Rc = \Delta T / Q, \ hc = 1/ Aa \ Rc$;

Thermal contact conductance *(hc)* is the reciprocal of the product of the nominal contact area *(Aa)* and contact resistance *(Rc)*. To estimate thermal contact resistance or contact conductance, the knowledge of ΔT and Q are required. The average heat flow rate Q is determined from an arithmetic average of heat flow rates Q_1 and Q_2 passing through the upper and lower heat flux meters. The heat flow rates Q_1 and Q_2 are estimated from the least-square fits of the measured temperatures along each heat flux meter shown in Fig.I.

$Q_1 = - k_1. \ Aa. \ (dT/dx)_1; \ Q_2 = - k_2.Aa.(dT/dx)_2;$

Where k_1 and k_2 are the known thermal conductivities of the heat flux meters and $(dT/dx)_1$ and $(dT/dx)_2$ are the temperature gradients obtained using least-squares-fit of the measured temperatures by thermocouples. The interface temperature drop ΔT is determined by linear extrapolation of the temperature profiles to the interface of the test specimens.
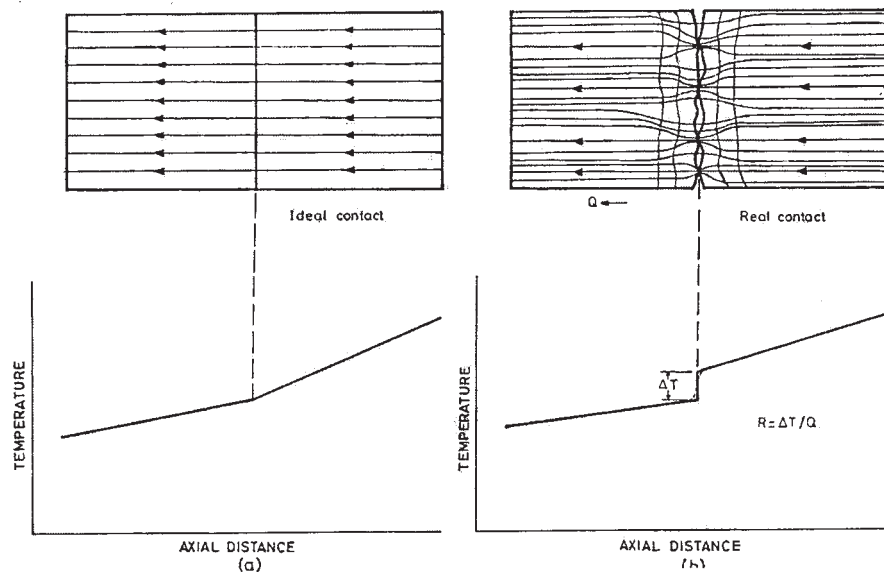

*Fig.1. Details of axial temperature profiles and heat flow across a joint*
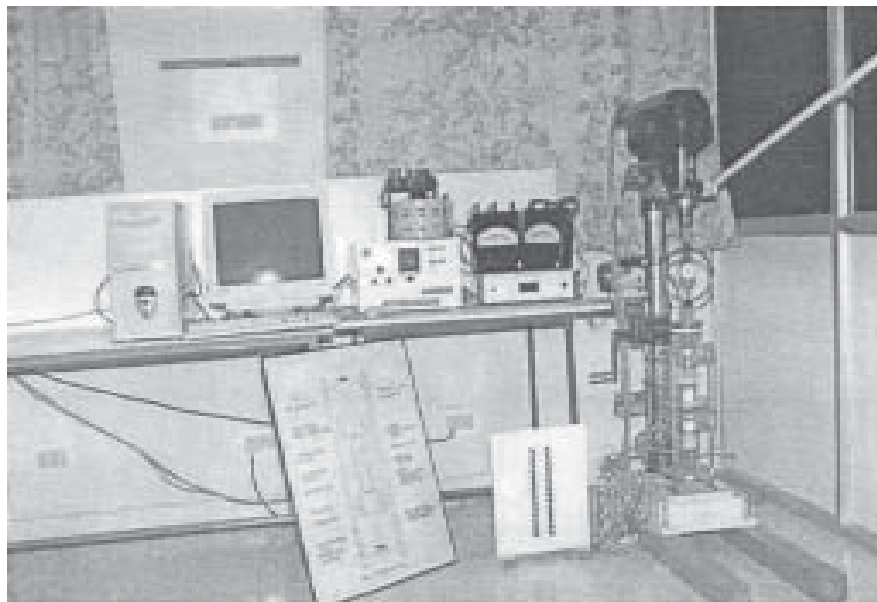
Fig.1a. Experimental Test Setup

The apparatus developed to meet the above requirements is shown in Fig. 1a. It consists of five sub-systems namely 1) Test column, 2) Mechanical loading system, 3) Heating circuit, 4) Cooling circuit and 5) Instrumentation. The system is capable of 1) operating between 0 to 250°C, 2) varying the contact pressure in the range of 0.1 MPa to 40MPa, 3) changing the direction of heat flow without disturbing the contact to study the directional effects, 4) accommodating different sizes (10 mm to 50mm diameter) of specimens in the test column.

4. TEST COLUMN

The test column consists of two heater-cooler blocks, two heat flux meters, two test specimens, two pairs of ball and conical seating arrangement stacked one over the other as shown in Fig.2.
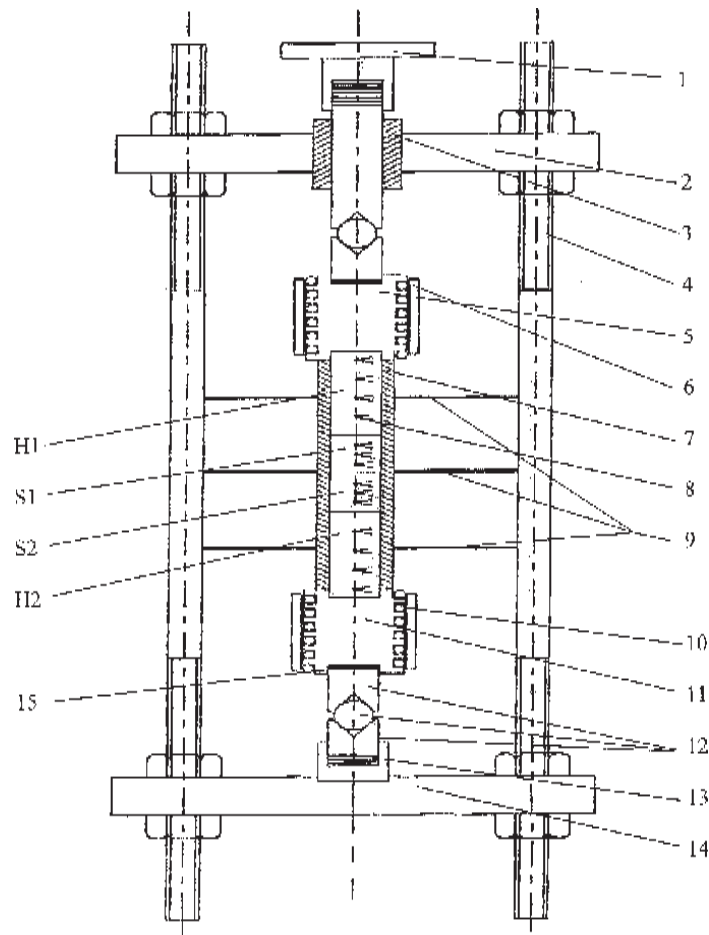
Fig.2. Test Column Details

1) Loading pin 2) Upper end plate 3) M.S. Bush 4) Tie rod 5) Heater - Cooler Block 6) Heater coil 7) Teflon insulation 8) Thermocouple 9) Aluminium radiation shields 10) Copper cooling Tube 11) Heater - Cooler Block 12) Ball and conical seating arrangement 13) Stack of SS-304 washers 14) Lower end plate 15) SS-304 washer.

H1) Heat flux meter (Top) H2) Heat flux meter (Bottom), S1) SS-304 specimen (Top), S2) SS-304 specimen (Bottom).

5. MECHANICAL LOADING SYSTEM

The mechanical loading system consists of a C-frame that grips the test column with a spindle above the loading pin and a base plate at the bottom of the test column. The applied pressure is transmitted along the axial direction of the test column. This is ensured by the two pairs of ball and conical seating arrangement, one at the top and other at the bottom of the test column. The load on the test column is varied by adding the dead weights to the lever attached to the C-frame. Proving ring that is attached to the spindle of the frame senses the load that is transmitted to the test column and the load indicator displays the load in kN. The C-frame described earlier takes care of the reactive forces developed during loading.

6. HEATING CIRCUIT

The heating circuit consists of a servo stabiliser of 3 k V A rating, single phase dimmerstats of 0 to 250V range with 8Amps rating, analog Watt meters of 0 to 600W range. The heat generation in the heaters is by simple ohmic heating. The source temperature can be varied from room temperature to 250°C by changing the input voltage to the heater element by regulating the dimmerstats. 3 kV A continuously varying servo stabiliser incorporated in the heating circuit maintains the output voltage at 230V with a variation of less than I Volt. This resulted in a constant heat generation and thereby a stable temperature of the heater-cooler block. Analog Watt meter connected in series indicates the power dissipated in the heater.

7. COOLING CIRCUIT

A closed loop cooling circuit, consisting of a constant temperature bath, a centrifugal pump, cooling coils embedded in the heater- cooler blocks is used. The temperature of the heater-cooler block can be varied in the range of -195°C to 150°C and maintained with in ±1°C by choosing an appropriate coolant. When the temperatures are to be varied between -30°C to 0°c ethylene glycol may be replaced for distilled water and Methyl cyclohexane may be replaced to reach -85°C. Liquid Nitrogen may be used as a coolant to go down to -195°C. LN_2 can be circulated in the coils by pressurising the LN_2 dewar with compressed Nitrogen and can be let out to the atmosphere after it boils off.

8. INSTRUMENTATION

The basic measurements involved in contact conductance and thermal conductivity tests are temperature measurements. The instrumentation in the present test facility consists of temperature sensors (T-Type thermocouples), constant temperature reference bath, and a precession multimeter. SWG 24 gauge thermocouple wire is drawn from a single spool and cut to required lengths. The measuring junctions of the thermocouples are formed by fme soldering. The beads so formed are shining bright and their diameter measured slightly over 1 mm. The wires are insulated by a layer of thin Teflon tape and are wrapped on the individual wires. With all this the thermocouple junction measured 1.1 mm and tightly fits in to the drilled holes of 1.2 mm diameter in the heat flux meters and test specimens. The total stretch of thermocouple wires from measuring junction to the cold junction is continuous and uninterrupted. Fourteen thermocouples are used to measure the temperature in the test column and one thermocouple to measure the reference bath temperature. Thermocouple extension cables are used to connect the cold junctions to the measuring instrument. The cold junction of the thermocouple is maintained at O°C using a reference bath that contains melting ice in

distilled water. The reference bath is capable of maintaining the temperature with in ±0.05°C. The output from the temperature sensors is read through a precession multimeter. The output e.m.f is converted into the corresponding temperature using the calibration curve of the thermocouples. The temperature measurement accuracy of the system is ±l°C.

9. EXPERIMENTAL PROCEDURE

To start the experiment, the heat flux meters and the test specimens are installed in the test column in accordance with the arrangement shown in the Fig.2. The holes that are meant for installing the thermocouples are filled with silicon heat sink compound with a syringe and thermocouples are installed. The radiation shields are installed in position and this completes the test column assembly. The loading pin is lowered gently so as to align the test column properly. All the thermocouple circuits are checked for continuity and proper functioning. The top heater is switched on and the cooling water is circulated to the bottom cooling coils. Adjusting the input voltage to the heater coil through a dimmerstat and constant temperature bath sets the mean interface temperature. Adding the dead weights to the end of the lever sets the contact pressure. The tests can be conducted by varying the contact pressure (in the range of 0.1 to 40 MPa) with increments of 0.1 MPa approximately and maintaining the mean interface temperature constant. Then the contact pressure can be decreased in steps of 0.1 MPa. This completes one load cycle, *i.e.* one loading and one unloading at a constant mean interface temperature. The mean interface temperature is set to the next higher value by increasing the input voltage to the heater coil. The loading and unloading processes are repeated in the same manner at each value of the mean interface temperature. Similarly, tests can be conducted by varying the mean interface temperature and maintaining the contact pressure constant. It is also possible to change the direction of heat flow in the test column without disturbing the test specimens. In this manner the contact conductance can be measured as a function of contact pressure, mean interface temperature and direction of heat flow.

10. SYSTEM RESPONSE

The output from the developed system is in the form of temperature data. The input to the system is in the form of externally controlled parameters. In the present context the system response basically means that, how the system responds in the form of a change in the contact conductance (output) for a known change in the externally controlled parameters (input). To show the system response, typical experimental data are presented in which one parameter, namely contact pressure is varied keeping all the other parameters constant.

10. a. System Response for a Change in Contact Pressure

Fig.3 shows the variation of thermal contact conductance in the test column when the contact pressure (load on the test column) is increased in steps, as and when the system attained steady state conditions according to a pre-set condition. The object of the experiment is to determine the effect of contact pressure on thermal contact conductance at constant electrical power (64W) input to the top heater in atmospheric environment of 1 atm. pressure. In this experiment top-heating with bottom-cooling configuration is used. The experiments were also conducted to determine the effect of 100μm thickness copper foil on thermal contact conductance when compared to bare joints under the same test conditions.

Stainless Steel-304 test specimens used in the present investigation are with RMS surface roughness of 2.56μm for the top specimen and 1.01μm for the bottom specimen. The results indicate that the thermal contact conductance for the bare joint is higher than the contact conductance of the joint with copper foil of 100J. 1m thickness as interstitial material for a given set of conditions. This undesirable trend is due to the dominating bulk thermal resistance offered by the thick copper foil than the plastic flow of deformed foil to fill the voids and reduce Thermal Contact Resistance. With this it is predicted that the enhancement in the contact conductance takes place with the foil of lesser thickness that conforms to the surface texture of the contacting surfaces with the application of pressure.
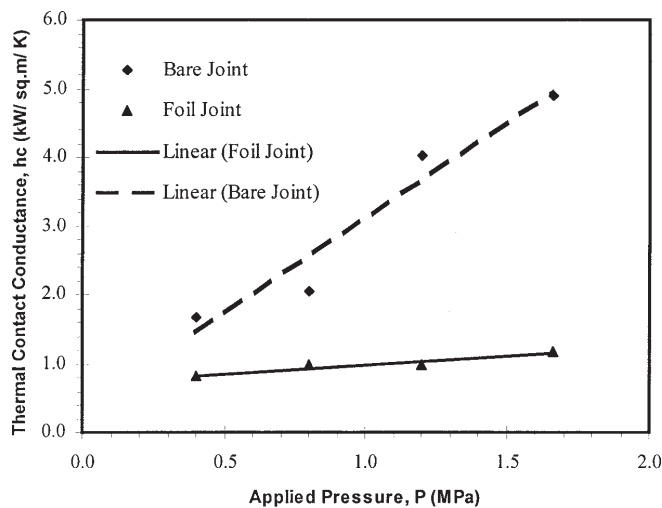
Fig.3. Comparison of Thermal Contact Conductance Vs Applied Pressure for Bare and Foil Joint

11. CONCLUSIONS

The developed test facility to measure thermal contact conductance across metal-metal contacts is proven to be effective, in terms of measured thermal conductivity of the specimens. The maximum error in the measured value of thermal conductivity is found to be +6.86% and a minimum of -0.78%, when compare to the ASM metals hand book of thermal conductivity, for a given constant heat input. Proving tests are conducted and the experimental setup is free from directional bias when compared to the earlier test facilities.

ACKNOWLEDGEMENTS

REFERENCES

1. Fletcher. L.S., "Recent developments in contact conductance", Transactions of the ASME Journal of Heat Transfer., Vol-110, pp 1059-1070, 1988.

2. Madhusudana. C.V., and Fletcher. L.S., "Contact Heat Transfer - The Last Decade", AIAA Journal. Vol.-24, No-3, pp 510-523, 1986.

3. Fletcher. L. S., "Experimental Techniques for Thermal Contact Resistance Measurements", Experimental Heat Transfer, Fluid Mechanics and Thermodynamics. M. D. Kelleher et al. (Editors). Elsevier Publishers., pp 195-206, 1993.

4. O'Callaghan. P. W., and Probert. S. D., "The Effects of Transverse Heat losses on Longitudinal Heat Transport Observations", Transactions of the Institute of Measurement and Control. Vol.-4, No-3, pp 25-T34, 1971.

5. O'Callaghan. P. W., and Probert. S. D., "An Improved Thermal Contact Resistance Rig", Transactions of the Institute of Measurement and Control. Vol.-5, No-8, pp 311-315., 1972.

6. Snaith. B., O'Callaghan. P.W., and Probert. S.D., "Can Standards Be Set for Reliable Measurements of Thermal Contact Conductance", AlAA-83-0533., AIAA 21st Aerospace Science Meeting, January 10-13, Reno, Nevada, 1983.

EFFECT OF Al METALLIC FOILS ON THERMAL CONTACT CONDUCTANCE ACROSS CONTACTS OF STAINLESS STEEL - 304

**V. Vasudeva Rao, A. Kumara Swamy, R. Raghukulender
and M.V. Krishna Murthy**

**Department of Mechanical Engineering, Sreenidhi Institute of Science and Technology,
Hyderabad- 501 301.*
*Department of Mechanical Engineering, Indian Institute of Science, Bangalore - 560 012.

ABSTRACT

This paper presents the results of an experimental investigation conducted to determine the effect of Aluminium metallic foils on the thermal contact conductance between nominally flat contacts of 88-304. The contacting surfaces of the steel specimens are generated by turning on a precision, lathe and then characterized for surface parameters using a Taly-Surf surface roughness tester. A set of 8 pairs of specimens is included in the present investigation. A set of 4 pairs is tested with Aluminium foils of thickness 20µm and another set of 4 pairs is tested without a foil. In the present work, 56 data points are obtained and results are reported in graphical form.

Experiments are conducted to determine Thermal Contact Conductance in the pressure range of 0.1 to 10 MPa. The results of the present investigation revealed that the enhancement of contact conductance as a function of contact pressure is relatively high in the range of 0.1 to 4MPa when compared to that in the range of 4 to 10 MPa. This can be attributed to the transformation from plastic to elastic deformation mode due to work hardening of contacting asperities within the range of applied pressure. The measured contact conductance of bare joints is less when compared to the joint~ with metallic foils under the same set of conditions.

1. INTRODUCTION

Thermal Contact Resistance (TCR) is an interface resistance between two solid contacting surfaces at different temperatures and is defined as the ratio of temperature drop at the interface to the heat flux. Thermal contact Resistance plays a very important role in many engineering applications. But even today the estimation of contact resistance is very difficult and even questionable due to its dependence on many parameters (like contact pressure, mean interface temperature, material properties, surface parameters, interstitial medium etc.) that influence the contact heat transfer phenomenon. SS-304 is an engineering material that is used in many process equipment. It is inevitable to have joints and assemblies in the construction of any

heat transfer equipment. Bare joints offer much greater thermal resistance when compared to joints with sandwiched interstitial materials. The use of interstitial materials to improve thermal joint conductance is known for the last two decades. Due to the limitations associated with the mathematical predictions, experimental results are very much required when the role of contact conductance is very critical.

2. LITERATURE SURVEY

There are several theoretical and experimental investigations that involve the determination of the effect of interstitial materials on Thermal contact conductance (TCC). Some of the most important contributions in this area have been presented here to give the current state-of-the-art. Fried and Kelley[1] investigated the influence of aluminium vapour deposited coating on the Thermal Conduction of Metallic Contacts in a Vacuum environment. Mal'kov and Dobashin[2] considered soft sliver coating on SS contacts for enhancement of contact conductance in vacuum. Molgaard and Smeltzer[3] presented the results of Thermal Contact Resistance of Gold Foil Surfaces in the range of 30 to 500°C. Mikic and Carnaciali[4] studied the Effect of Thermal Conductivity of Plating Material in Thermal Contact Resistance and validated the solutions with experimental results. Fletcher[5] presented a Review of Thermal Control Materials for Metallic Junctions and introduced concept of non-dimensional conductance for thermal joints with interstitial materials. Fletcher and Shoup[6] proposed Optimum Design of Elastomeric Gaskets for Combined Thermal and Vibration Performance in a view to reduce both vibration transmission and thermal resistance. Veziroglu et.al.[7] analyzed Thermal Conductance of Contacts with Interstitial Plates and concluded that the TCC is a function of the properties of plate materials. O'Callaghan et.al[8] developed and demonstrated a theoretical optimization procedure to establish the appropriate interstitial filler material thickness for Minimum Thermal Contact Resistance. But their theory is based on the assumption of ideal plastic asperity deformation. Cook et.al[9] proposed a novel concept for reducing Thermal Contact Resistance by introducing interstitial materials whose melting temperature is slightly more than the room temperature. This interstitial material will be in liquid state when the joint reaches the actual working temperature. Antonetti and Yovanovich[10] developed a thermo-mechanical model that predicts the Thermal Contact Conductance of silver coated nominally flat contacting surfaces. Yovanovich[11] in his review on thermal management of electronic equipment, stated that the contact resistance problem require simultaneous solution of thermal, mechanical and metrological problems. Chung et. al[12] developed analytical expressions for TCC of cylindrical contact spots for phase mixed metallic coatings using plasma enhanced deposition on to a cold surface. Couedel et.al[13] used the experimental data on metallic foils (tin, lead and copper) available in the published literature and presented a correlation to determine TCC. But these models are successful only to a certain extent due to the assumptions they make. Therefore, in the present work it is proposed to experimentally determine the effect of Al Metallic foils on Thermal Contact Conductance across Contacts of Stainless Steel – 304.

3. EXPERIMENTAL INVESTIGATION

a. Specimen-Preparation:

The test specimens are fabricated as follows: Stainless Steel 304 rod of 28mm diameter is taken from a bar stock and machined to 25 mm dia. x 25mm length so that the from ratio

is 1:1. In order to measure the temperature gradients in the test specimens, temperature measurements are to be made along the axis of the test column with temperature sensors. To install the temperature sensors (Thermocouples in the present case) in the test specimens, 1.2 mm dia. holes are drilled up to the axis, i.e. to a depth of 12.5 mm such that the depth to hole diameter ratio is about to. In each test specimen, 3 such holes are drilled with an axial distance of 6.25mm. In the present investigation the test specimens are machined with varying surface roughness between one and 10μm. The contacting surfaces of the steel specimens are specifically designed and generated by turning on a precision lathe. The specimens are first cleaned with kerosene and then with soap solution to remove any traces of oil on the contacting surfaces. The contacting surfaces are then cleaned with acetone before they are characterized for surface parameters using a Taly-Surf surface roughness tester.

Test Column Assembly

The test column consists of two similar test specimens, a 20μm thick aluminium foil, two similar heat flux meters made of SS304, two heater-cooler blocks made of electrolytic
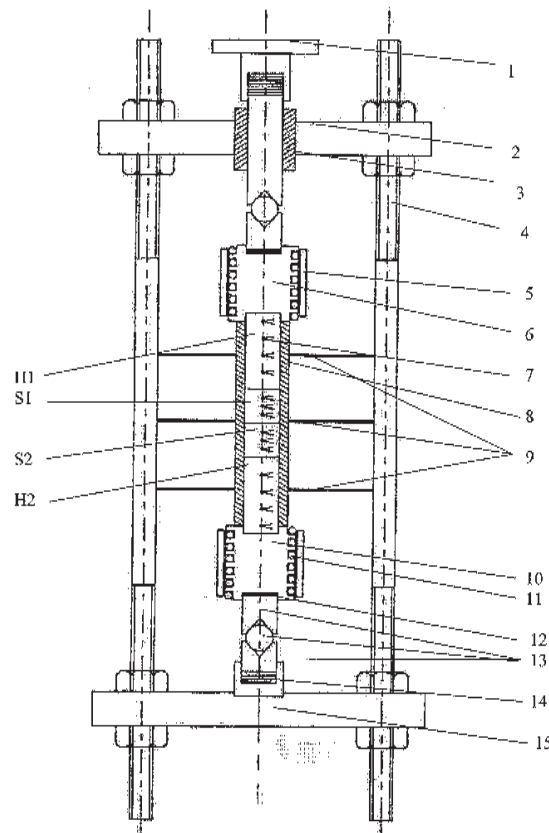
Fig.1. Test Column Details

1) Loading pin, 2) Upper end plate, 3) MS Bush, 4) Tie rod, 5) Heater Coil, 6) Heater-Cooler block, 7) Thermocouple, 8) Teflon insulation, 9) Radiation Shields 10) Heater-Cooler block, 11) Copper cooling coil, 12) SS-304 washer, 13) Ball and conical seating arrangement, 14) Stack of SS-304 washers, 15) Lower end plate. H1) Hop Heat Flux Meter, S1) Top Specimen, S2) Bottom Specimen, H2) Bottom Heat Flux Meter.

grade copper and two pairs of ball and conical seating. Aluminium foil is sandwiched between two test specimens. These are stacked as shown in the Fig.1, such that the test column is exactly symmetric about the interface formed between the test specimens. The test specimens and the heat flux meters are inserted in a 6mm thick Poly-Tetra-Fluoro-Ethane (PTFE) tube which has a vertical slit in its wall. The test column is then inserted between the heater and cooler blocks. All the interfaces thus formed, except the test interface, are smeared with a thin layer of silicon heat sink compound to reduce the thermal resistance at these interfaces to a minimum value. Then the ball and conical seating are kept in position along with the loading pin, three radiation shields as - shown in the Fig. 1. This completes the assembly of the test column.

c. Experimental Procedure

The test column is instrumented with calibrated thermocouples of T-type. The out put of the thermocouples, via. a zero degrees centigrade reference bath, is measured using a precision multi-meter. The loading of the test column is achieved by a lever and static hanging weights. Heating and cooling circuits are switched ON to set a temperature gradient. Temperature measurements are taken after the test column attaining the steady state conditions. The experiment is continued in a similar way after increasing the load to a next higher value.

4. RESULTS AND DISCUSSION

The results of the present experimental investigation are presented graphically in fig.2 through fig.7. Fig.2 shows the results of a thermal joint that has a surface roughness
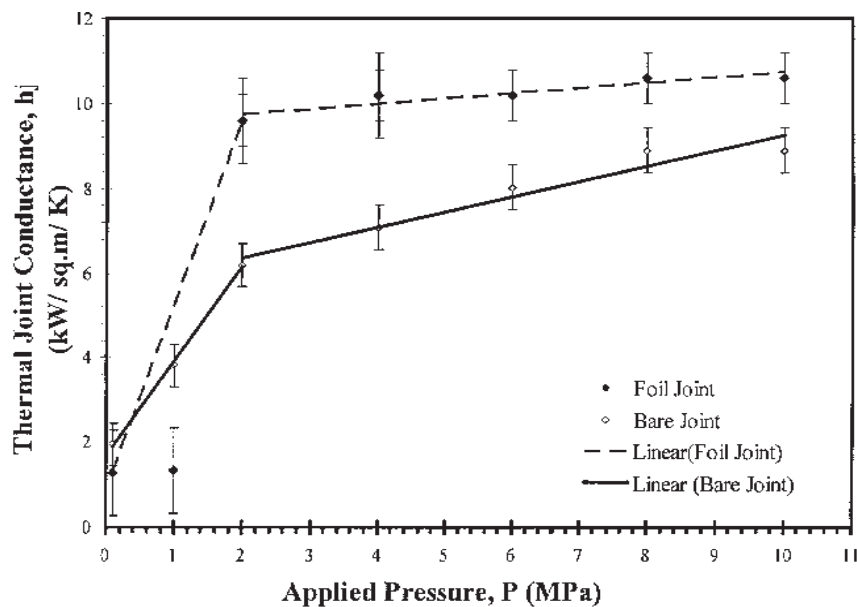

*Fig.2. Improvement in Thermal Joint Conductance due to A1 foil as Thermal Control Material
(Bare Joint - 1.20μm, Foil Joint - 1.28 μm)*
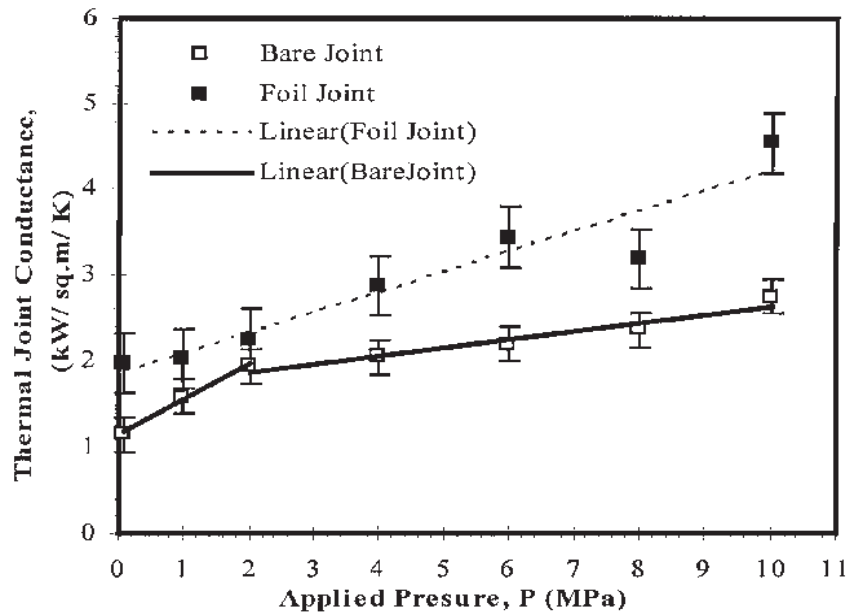
Fig.3. Improvement in Thermal Joint Conductance due to Al foil as Thermal Control Material
*(Bare Joint - 6.49μm, Foil Joint - 6.51 μm)*
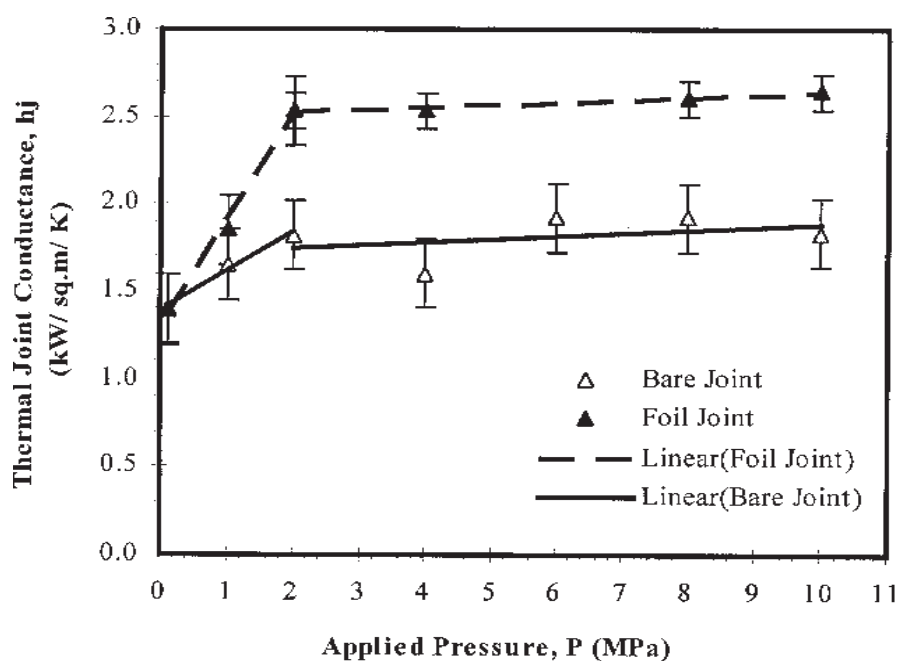
Fig.4. Improvement in Thermal Joint Conductance due to Al foil as Thermal Control Material
*(Bare Joint - 9.49μm, Foil Joint - 9.51 μm)*
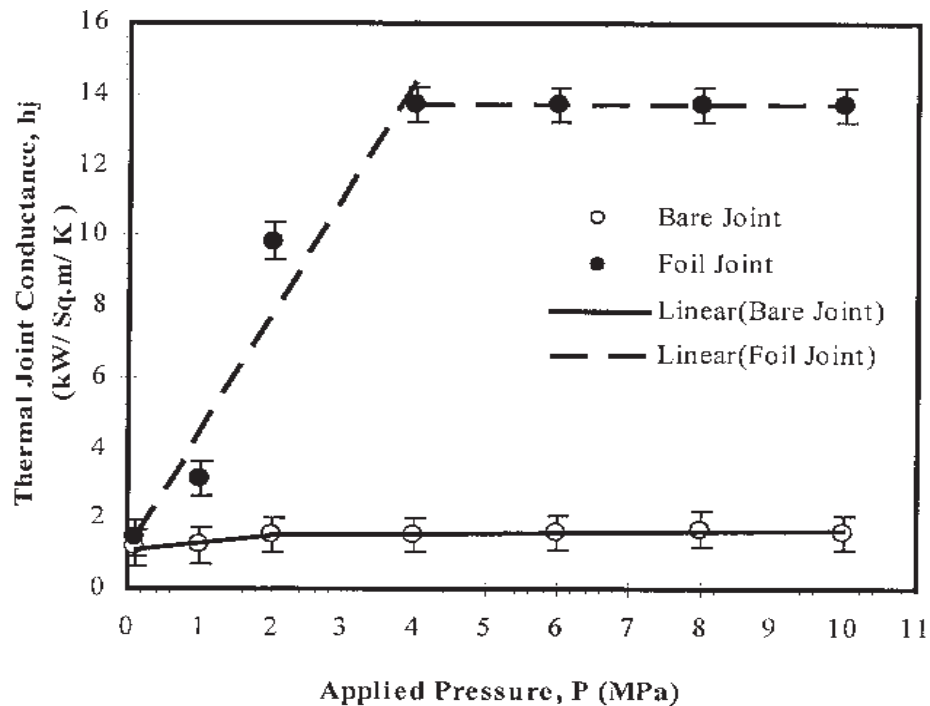
Fig.5. Improvement in Thermal Joint Conductance due to Al foil as Thermal Control Material
*(Bare Joint - 12.42μm, Foil Joint - 13.4 μm)*
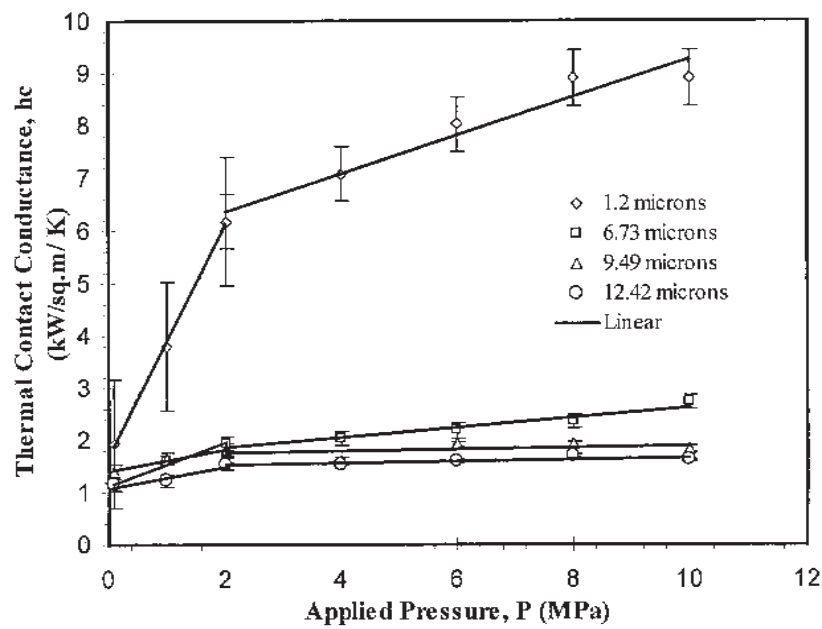
*Fig.6. Comparison of Contact Conductance Vs Applied Pressure for Bare Joints*
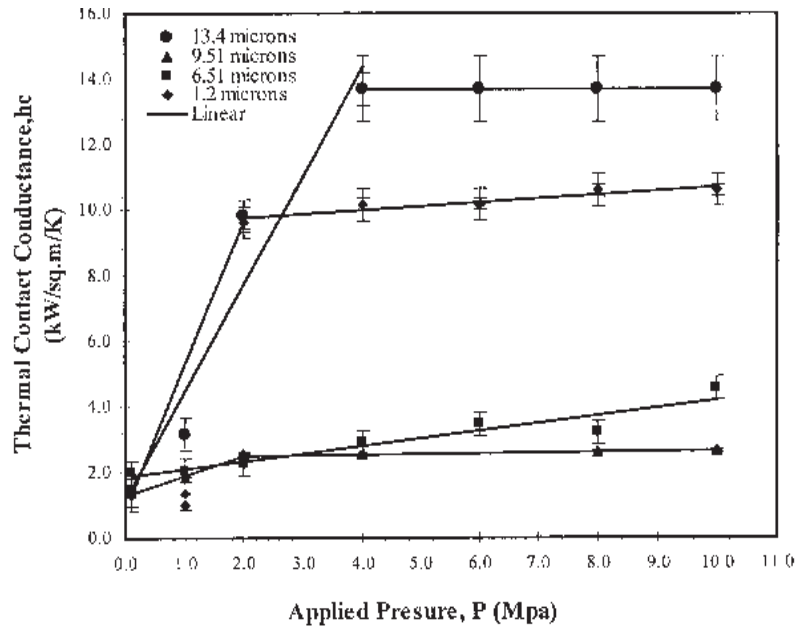
Fig.7. Comparison of Contact Conductance Vs Applied Pressure for Joints with Foil at the Interface

of 1.2μm. The two curves shown in fig.2 are one with an interstitial material (20/lm aluminium foil) and one with out interstitial material. It is observed that the insertion of aluminium metallic foil has enhanced the joint conductance. Similarly, Fig. 3 shows the results of a joint with equivalent RMS surface roughness 6.5μm. The joint conductance with a metallic foil is substantially high when compared to a bare joint. Fig.6 and Fig.7 represent the variation of contact conductance with applied pressure for all the data sets with 1.2, 6.5, 9.5 and 12.5μm as equivalent RMS surface roughness with and without an aluminium metallic foil. From these graphs it is evident that the use of interstitial material enhances the joint conductance. Also from fig. 4 and fig.5 it is observed that the rate of enhancement is high in the range of 0.1 to 4MPa when compared to that in the range of 4 to 10 MPa. This can be attributed to the transformation from plastic to elastic deformation mode due to work hardening of contacting asperities within the range of applied pressure.

5. CONCLUSIONS

In the present work, 56 data points are obtained and the results are reported in graphical form. A set of 8 pairs of specimens is included in the present investigation of which 4 pairs are tested with 20μm aluminium foils and 4 pairs without a foil. It is concluded from the results of the present investigation that the enhancement of contact conductance as a function of contact pressure is relatively high in the range of 0.1 to 4MPa when compared to that in the range of 4 to 10 MPa. This can be attributed to the transformation from plastic to elastic deformation mode due to work hardening of contacting asperities within the range of applied pressure. The measured contact conductance of bare joints is less when compared to the joints with metallic foils under the same set of conditions.

As the experimental results of the present investigation are encouraging, further experiments are planned and some are underway. The effect of other types of interstitial materials like coating, greases and gases are being investigated using the test facility. The results of these tests will be published in future. There is a scope for developing mathematical models as the experimental results are available for comparison.

ACKNOWLEDGEMENT

REFERENCES

1. E. Fried and M.J. Kelley, 'Thennal Conduction of Metallic Contacts in a Vacuum.' AIAA Paper No. 65-661 AIAA Thennophysics Specialists Conference., Monterey, Ca., USA., Sept.1965.

2. V. A Mal'kov and P. A. Dobashin, 'The Effect of Soft-Metal Coatings and Linings on Contact Thermal Resistance,' Inzhenemo-Fizicheskii Zhurnal, Vol. 17, No.5, pp 871-879. 1969.

3. J. Molgaard and Smeltzer, 'The Thennal Contact Resistance at Gold Foil Surfaces,' Int. J. Heat Mass Transfer, Vol. 13, pp. 1153-1161. 1970.

4. B. B. Mikic and G. Carnaciali, 'The Effect of Thennal Conductivity of Plating Material in Thennal Contact Resistance' Trans. ASME J.of Heat Transfer, Vol. 92, No.3, pp 475-482. 1970.

5. L. S. Fletcher, 'A Review of Thennal Control Materials for Metallic Junctions' J. of Spacecraft and Rockets, Vol. 9, pp 849-850. 1972.

6. L. S. Fletcher and T. E. Shoup, 'Optimum Design of Elastomeric Gaskets for Combined Thermal and Vibration Perfonnance,' 1. of Spacecraft and Rockets., V 01.11, No.5, p.p. 344-346., 1974.

7. T.N. Veziroglu, H. Yuneu and S. Kakac, 'Analysis of Thennal Conductance of Contacts with Interstitial Plates," Int. J. Heat Mass Transfer, Vol. 19, pp 959-966. 1976.

8. P.W. O'Callaghan, S.D. Probert, B. Snait, and F. R. AI-Astrabadi, 'Prediction of Interstitial filler Thickness for Minimum Thennal Contact Resistance,' AIAA Journal, vol. 21, No.9, pp. 1325-1330. 1983.

9. R.S. Cook, K.H. Token and R.L. Calkins, 'A Novel Concept for Reducing Thennal Contact Resistance,' J. of Spacecraft and Rocket, Vol. 21 No.1, pp.122-124.1984.

10. V.W. Antonetti and M.M. Yovanovich, 'Enhancement ofthennal Contact Conductance by Metallic Coatings: Theory and Experiment, Trans. ASME J. of Heat Transfer, Vol. 107, pp. 513- 519. 1985.

11. M.M. Yovanovich, 'Theory and Applications of Constriction and Spreading Resistance Concepts for Micro-Electronics thennal Management," Proceedings of the Int. Sym. on Cooling Technology for Electronic equipment, Pacific institute for Thennal Engineering, Honolulu. 1987.

12. K.C. Chung, J.W. Sheffield and H. J. Sauker, Jr., "Thennal Constriction Resistance of Phase Mixed Metallic Coatings," Trans. ASME Journal of Heat Transfer, Vol.114, pp. 811-818, 1992.

13. D. Couedel, L.S. Fletcher and G.P. Peterson, 'A correlation for the Thermal Contact Conductance of interstitial Metallic Foils, Proceedings of the 10th International Heat Transfer Conference, Brighton, U.K., Vol.6, pp. 337-341. 1994.